Engineering Ordered and Nonordered Porous Noble Metal Nanostructures: Synthesis, Assembly, and Their Applications in Electrochemistry

ARTICLE *in* CHEMICAL REVIEWS · JULY 2015

Impact Factor: 46.57 · DOI: 10.1021/acs.chemrev.5b00255 · Source: PubMed

4 AUTHORS:

Chengzhou Zhu
Washington State University
69 PUBLICATIONS **2,346** CITATIONS
SEE PROFILE

Dan Du
Washington State University
126 PUBLICATIONS **3,603** CITATIONS
SEE PROFILE

Alexander Eychmüller
Technische Universität Dresden
356 PUBLICATIONS **10,473** CITATIONS
SEE PROFILE

Yuehe Lin
Washington State University
361 PUBLICATIONS **20,705** CITATIONS
SEE PROFILE

CHEMICAL REVIEWS

Review

pubs.acs.org/CR

Engineering Ordered and Nonordered Porous Noble Metal Nanostructures: Synthesis, Assembly, and Their Applications in Electrochemistry

Chengzhou Zhu,[†] Dan Du,[†,⊥] Alexander Eychmüller,[‡] and Yuehe Lin*[,†,§]

[†]School of Mechanical and Materials Engineering, Washington State University, Pullman, Washington 99164-2920, United States

[⊥]Key Laboratory of Pesticide and Chemical Biology of the Ministry of Education, College of Chemistry, Central China Normal University, Wuhan 430079, P. R. China

[‡]Physical Chemistry, TU Dresden, Bergstrasse 66b, 01062 Dresden, Germany

[§]Pacific Northwest National Laboratory, Richland, Washington 99352, United States

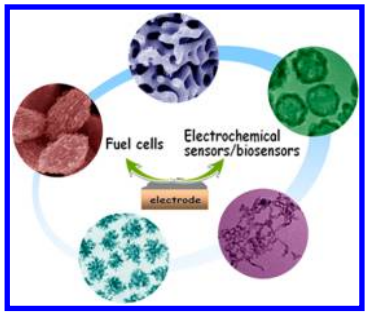

CONTENTS

1. INTRODUCTION

Novel self-assembled architectures have received significant interest in nanoscience and nanotechnology. A large variety of nanostructures involving optimized sizes, morphologies, and compositions are indeed playing major roles in the development of advanced functional materials for several emerging applications. However, the use of nanoparticles (NPs) as building blocks and their assembly into functional architectures is of special relevance for realistic development and represents a rapidly growing branch of research.[1−4] New features arise naturally during the assembly of these architectures, including the emergence of collective behavior due to the interactions between disparate electronic, magnetic, and chemical phenomena. These assembled architectures offer desirable combinations of high internal reactive surface areas and straightforward molecular transport through broad "highways" leading to their surfaces. Porous nanomaterials can be branched out into three different categories according to their pore size: microporous (pore size <2 nm), mesoporous (2 nm < pore size <50 nm), and macroporous (pore size >50 nm) systems. Abundant morphologies are also obtained in monoliths exhibiting

Received: April 28, 2015

DOI: 10.1021/acs.chemrev.5b00255
Chem. Rev. XXXX, XXX, XXX−XXX

hierarchical structures that combine micro-, meso-, and macropores. Micro- and mesopore provide high surface areas while macrospore guarantees accessibility to the surface.[5,6] To date, significant efforts have been made to design novel hierarchically porous nanostructures using intelligent approaches, which are of significant importance in achieving high-performance applications. For example, the past two decades have witnessed a remarkable drive for the development of ordered mesoporous silicas[7,8] and their derived ordered mesoporous carbons,[9,10] mesoporous metals,[11,12] mesoporous metals oxide,[13,14] and even polymer nanostructures,[15] most of them being obtained from nanocasting pathway. Of related interest are hierarchically porous nanostructures, both ordered and disordered, leading to a synergistic effect with advanced properties.[16−18] A typical example is that porous graphene materials have recently attracted vast interests due to their large surface areas, unique porous structures, diversified compositions, and excellent electronic conductivity. These unordinary features allow porous graphene materials to serve as advanced electrode materials in high-performance electrochemical energy storage and conversion devices.[19,20] Moreover, metal−organic frameworks consisting of ordered networks can be constructed from metal cations coordinated to organic molecules, which have recently emerged as a new class of crystalline porous materials.[21,22]

Among them, noble metal nanomaterials, such as Au, Ag, Pt, and Pd, as one of the most important materials, have received increasing research interest in recent decades because of their wide applications in catalysis, sensing, electrochemical energy storage, biomedical diagnosis, therapy, etc.[23−29] Recent advances demonstrated that rational adjusting the size, shape, composition, and structure provides new insight into design of innovative noble metal nanomaterials with exotic properties.[30−33] These key factors will furnish massive opportunities for tuning their properties and enhancing their application performances. Specifically, porous noble metal nanostructures (PNMNs) with highly ordered/disordered structures have been attracted considerate attentions for a branch number of catalytic applications.[34−37] Taking electrochemical catalysis as an example, most electrochemical systems consist of porous electrode materials. These 3D porous architectures are able to provide higher specific surface areas and larger pore volumes, not only maximizing the availability of electron transfer within nanosized electrocatalyst surface area but also providing better mass transport of reactants to the electrocatalyst. Fabricating interconnected mesoporous arrays/superstructures is critical to achieve both high surface area and fast mass transfer.

Considering the accumulated number of publications dedicated to noble metal-based porous architectures, we aim at providing an overview of the different kinds of PNMNs in this review, including ordered and nonordered porous nanostructures. From the perspective of their synthetic approaches, this review stresses on the recent progress for constructing ordered porous nanostructures and a series of nonordered architectures, such as aerogels, nanofoams, hollow structures and various highly branched nanomaterials (Figure 1). More importantly, the exploitation of the attractive and unique properties of theses PNMNs in electrochemical applications, such as fuel cells and electrochemical sensors/biosensors, are highlighted in this review. Furthermore, we will also discuss some key issues and future perspectives on the development of PNMNs. We do hope this review can inspire enormous interest from different fields and bring new vigor into nanomaterial and nanotechnology.

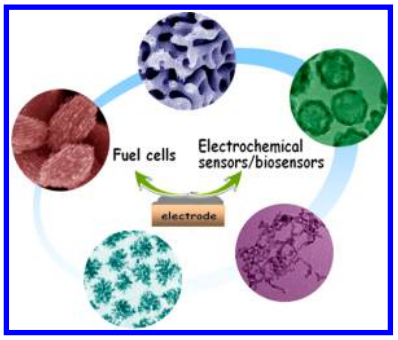

Figure 1. Rational design of various porous noble metal nanostructures and utilizing them as advanced catalysts in fuel cells and electrochemical sensors and biosensors.

2. ORDERED POROUS NOBLE METAL NANOSTRUCTURES

Replication methods using templates, including hard templates and soft templates, are considered the most effective protocols for the preparation of ordered porous nanostructures. The structures and properties of the templates have significant impacts on the properties of the replicated porous materials. In general, two kinds of templates, defined as hard and soft templates, have been described as molds for nanocasting processes. To date, hard templates including assembled colloidal crystals, mesoporous silica, zeolites, and alumina membranes, containing 3D interconnected mesopores, have been widely introduced for the synthesis of a series of ordered porous nanostructures composed of metals,[38,39] oxides,[40,41] carbon and other compositions,[42,43] with controlled structures and morphologies. By exploiting liquid crystal systems, nanocasting from soft templates was also developed. The use of diverse templates and deposition procedures contributes greatly to the synthesis of mesoporous metals with well-controlled structural characteristics.[44] In addition, the preparation of hierarchically ordered PNMNs can also be facilely realized using different templates, affording the integrated control of pore size and surface nanostructure.

2.1. Hard Template

Compared with other strategies, the hard-template process using ordered porous nanostructures as a hard template is considered the most general approach for preparing ordered meso/macrostructures consisting of metals, oxides and carbon, with well-tuned structures and morphologies.[45,46] Typically, as shown in Figure 2, three main steps are generally involved for this synthetic pathway: (1) the preparation of a sacrificial template with a specific ordered porous structure, (2) creation of a hybrid composed of the starting template and a target product through in situ deposition target precursors into the ordered pores, codeposition and assembly of core−shell nanostructures, and (3) removal of the original template, leaving behind a metal replica of the starting template. These ordered meso/macroporous materials were characterized by several fascinating properties, which make them extremely promising for use as candidate templates. High quality ordered meso/macroporous materials (e.g., MCM-48, MCM-41, KIT-6, and SBA-15) enable the creation of well-defined metal replicas that inherit their typical characteristics of a long-range periodic nanostructure. Carefully controlling template parameters,

DOI: 10.1021/acs.chemrev.5b00255
Chem. Rev. XXXX, XXX, XXX−XXX

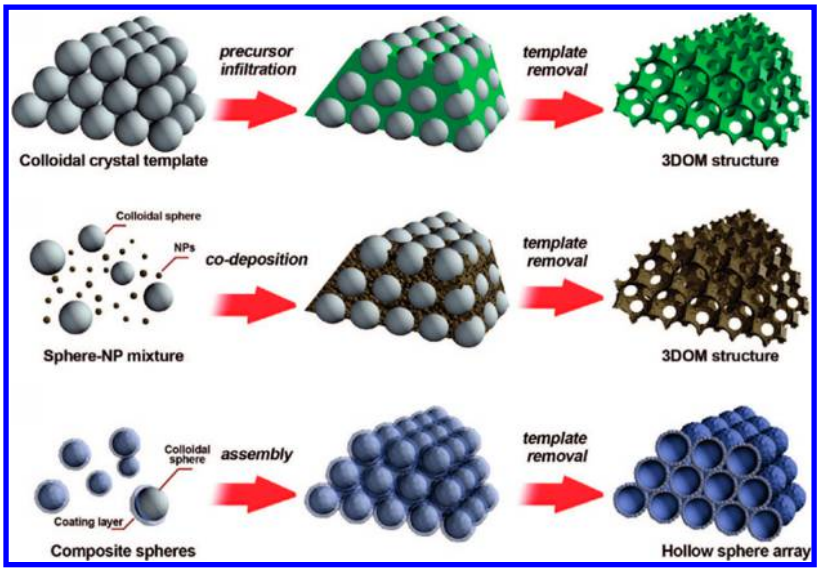

Figure 2. Three different approaches for synthesizing ordered macroporous structures using colloidal crystal templating. Reprinted with permission from ref 46. Copyright 2008 American Chemical Society.

including the pore size and surface functionality, facilitate the generation of ordered PNMNs with tunable properties. Moreover, several synthetic methods, including electroless deposition, electrochemical deposition, and hydrogen reduction of metal salt precipitation were adopted to prepare ordered porous nanostructures using hard templates.

2.1.1. Ordered Macroporous Nanostructures. Colloidal crystalline templates, such as silica and latex crystals, are 3D close-packed crystals of submicrometer spheres, whose long-ranged ordered structure is replicated in a solid matrix, yielding materials with ordered pores.[47−49] Assemblies of monodisperse silica colloidal crystal with 2D or 3D long-range ordered arrays were considered one of the most efficient templates for the construction of macroporous nanostructures. Silica colloidal crystals fabricated by the Stöber procedure are easy to acquire with controllable diameters ranging from tens of nanometers to several micrometers. Furthermore, different functional groups, such as $-NH_2$, −SH, and −COOH can be covalently grafted through silanol groups (−Si−OH) terminated on the surfaces of the silica colloidal crystals, enabling new functions for different purposes. Colvin and co-workers demonstrated a versatile route for synthesizing macroporous metal films using silica colloidal crystals.[50] In detail, colloidal crystals-based arrays were first fabricated on the surface of glass substrates by vertical deposition, which can adsorb Au NPs due to the modification of thiol of the surface of silica colloidal crystals. The tiny pores of the template matrix can be filled with Au NPs uniformly because of the strong penetration ability of small sized Au NPs. After heat treatment, metal formation in the pores readily occurs through electroless deposition. Finally, a free-standing porous metal film will be attainable after removal of the pristine template. Lu et al. reported a simple alternative procedure, which is based on the self-assembly of Au NPs followed by electroless plating, to incorporate larger Au NPs with diameters ranging from approximately 10 nm to approximately 60 nm into 3D ordered colloidal crystal films.[51] Using a similar protocol, ordered Au/Pt nanostructures with hierarchical porosity, such as macroporous nanostructures and ordered hollow nanospheres, can be selectively and conveniently synthesized (Figure 3).[52] The concentration of Au NPs used

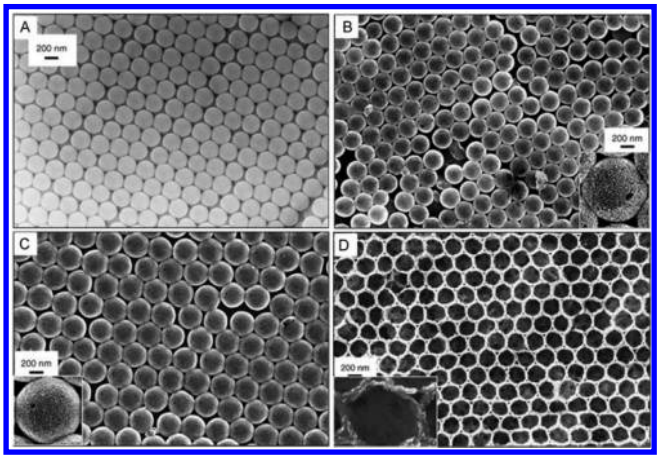

Figure 3. (A) SEM image of 267 nm silica particle-based template, and SEM images of the resulting ordered hollow nanostructures evolved using (B) 267 nm and (C) 300 nm silica colloidal crystals as templates, respectively. The insets show the high-magnification SEM image. (D) Typical SEM image of an ordered macroporous Au/Pt nanostructure. The insets show the high-magnification SEM image. Reprinted with permission from ref 52. Copyright 2005 Wiley-VCH.

and immersion time play a critical role in synthesizing these different porous nanostructures. Cage-type mesoporous Pt nanostructures with adjustable large mesopores and rough surfaces were fabricated via the deposition of Pt using a dual-template composed of a assembled silica arrays and block copolymer Pluronic P123.[53] In addition to colloidal silica, assembled latex microspheres were also used as templates for preparing porous Au films on flat substrates.[54] Concentrated Au NPs and latex microspheres were first mixed together and deposited on the substrate. The formation of thick multilayer latex crystals was achieved when the films dried, entrapping Au NPs in the interstitial spaces of the latex crystal and further assembling at the bottom of latex layers upon evaporation. Thus, ordered porous Au nanostructures immobilized on glass slides can be obtained after removing the latex templates.

2.1.2. Ordered Mesoporous Nanostructures. In addition to this crystalline colloid fabrication method, mesoporous

DOI: 10.1021/acs.chemrev.5b00255
Chem. Rev. XXXX, XXX, XXX−XXX

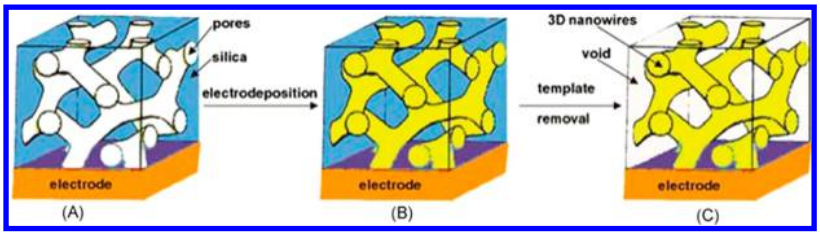

Figure 4. Schematic illustration of the synthesis of 3D continuous macroscopic metal or semiconductor nanowire networks by a template electrodeposition technique. Reprinted with permission from ref 66. Copyright 2004 Wiley-VCH.

silicas as hard templates for the design of porous nanostructures have received significant consideration. Various types of noble metal nanostructures, including NPs,[55,56] nanowires,[57,58] and nanoworms,[59] and ordered mesoporous nanostructures[39] were synthesized using mesoporous silicas as hard templates. The synthesis of asymmetrically mesostructural Pt networks replicated from MCM-48 silica was reported by Ryoo and co-workers. A Pt precursor was first impregnated into MCM-48, and the resultant mesostructured Pt networks can be easily obtained via H_2 reduction at specific temperatures.[60] The same method was also demonstrated for the synthesis of Pt[61] and bimetallic PtRu[62] mesoporous nanostructures. Considering the small size of the silica template, Kuroda et al. employed KIT-6 with different pore sizes as the template and investigated the effect of pore size on the mesoporous Pt replicas via vapor infiltration of a reductant.[63] A mesoporous Pt replica with relatively large mesopores (over 10 nm) was successfully deposited into one side pore of the *Iad* bicontinuous structure, favorable for the accessibility and diffusivity of large guest molecules from the outside.

Combined with the templating, electrochemical methods using external power sources provide facile and efficient routes for creating diverse nanomaterials with well-defined mesoporous nanostructures in a short time.[64,65] A variety of 3D noble metal nanowire networks have been successfully synthesized via mesoporous silica films with ordered porous nanostructures. Lu et al. developed a general synthetic route to 3D metal or semiconductor nanowire networks using an electrodeposition method (Figure 4).[66] The macroscopic connectedness of the networks resulted in a continuous, homogeneous surface morphology with ordered mesoporous structures. At the same time, this method can be easily extended to synthesize hierarchically porous nanostructures through the introduction of colloidal silica. Because the colloidal silica significantly affects the nucleation and growth of the silicate/surfactant assemblies, more complicated nanostructures, such as highly porous nanowire networks with sponge-like and grass-like morphologies, were prepared by varying the size and shape of the silica additives. Apart from the morphologies, the composition of the networks can be precisely controlled through electrodeposition. Similarly, 3D mesoporous Pt network-like nanostructure with double gyroid (DG) morphology was also reported previously.[67]

Despite the recent advances mentioned above, the morphologies of the resulting mesoporous metal nanostructure have been limited, most of them being powders with irregular morphologies or films on the surface of conductive substrates. The limitations of morphology and size control are associated with the requirement of novel synthetic procedure of the mesoporous metal nanostructures. It is noted that the shape and size distributions of the NPs play critical role in controlling their function and utilization in applications. Yamauchi's group developed a sophisticated chemical reduction for template preparation of mesoporous Pt-based NPs with controlled shape, size, and composition.[12,68,69] Typically, as shown in Figure 5A, mesoporous Pt NPs with different morphologies

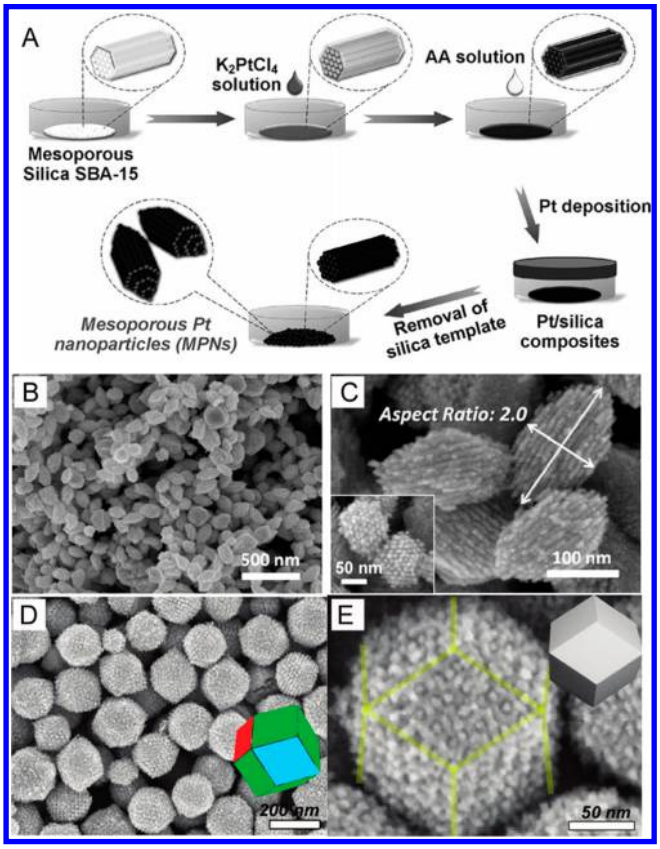

Figure 5. (A) Schematic representation of a synthetic procedure for preparation of olive-shaped mesoporous Pt NPs. (B, C) Typical SEM images of Pt NPs created from mesoporous silica (SBA-15) with a 12-h deposition time. The inset shows the honeycomb arrangement of the Pt nanowires. Reprinted with permission from ref 69. Copyright 2012 Wiley-VCH. (D, E) SEM images of the resulting mesoporous Pt NPs prepared with mesoporous silica KIT-6. Reprinted with permission from ref 12. Copyright 2011 American Chemical Society.

were successfully created using ascorbic acid (AA) as controlled reductant and 2D mesoporous silica (SBA-15) as well as 3D bicontinuous mesoporous silica (KIT-6) as hard templates. The particle size could be facilely tuned by varying the reduction time. Well-defined olive-shaped mesoporous Pt NPs could be produced when 2D SBA-15 was adopted as the template (Figure 5B,C).[69] The average particle size with wide range from 150 to 230 nm could be obtained through different deposition times. The single crystallinity of the Pt fcc structure was

DOI: 10.1021/acs.chemrev.5b00255
Chem. Rev. XXXX, XXX, XXX−XXX

observed to coherently extend over the entire particle. Using the same method, the Pt NPs created from KIT-6 displayed polyhedral morphology (Figure 5D,E).[12] Moreover, bimetallic PtRu mesoporous NPs were also produced using this concept.[68] It is a fact that replication of mesoporous templates with perfect retention of both the mesostructure and the morphology is extremely difficult, which results in the mesoporous noble metal nanostructures with different size distributions. For the most cases, this nonuniformity was attributed to the severe volume collapse when the metal precursor was reduced. To address this problem, Yang and co-workers first synthesized single-crystal-like MCM-48 nanospheres and used them as a unique hard template. Well-defined mesoporous Pt nanospheres possessing both the mesostructure and morphology of the silica template were facilely replicated using molten salt impregnation and the following H_2 reduction process.[70]

2.2. Soft Template

2.2.1. Lyotropic Liquid Crystals. Amphiphilic molecules, including surfactants and amphiphilic block copolymers, contain the hydrophilic and hydrophobic parts, which are covalently linked together. Spherical micellar structures are evolved spontaneously by self-assembly when the mixed solution is above the critical micelle concentration (CMC). The increase in surfactant concentration triggers the occurrence of lyotropic liquid crystals (LLCs) phases. The resulting LLCs phases show long-range spatially periodic nanostructures with lattice parameters in the range of 2−15 nm.[71] Attard and co-workers successfully fabricated mesoporous Pt NPs from LLCs made of highly concentrated surfactants for the first time.[72] Additionally, they developed a versatile route for the creation of mesoporous Pt nanostructures through electrodeposition from LLCs plating mixtures.[73] These pioneering works paved a new route to synthesize noble metal-based mesoporous nanomaterials. Since then, a wide array of mesoporous noble metal nanostructures, including Pt,[74] Ru,[75] and PtRu alloy[76−78] have been reported as functional materials.

Due to the high concentration of surfactants involved (normally more than 40 wt %), multiple process steps are usually necessary to obtained homogeneous LLCs with high viscosities. This approach is limited to the synthesis of mesoporous films and particles. Controlling the generation of porous noble metals within the confined void space of templates remains a significant challenge. In this context, Yamauchi's group proposed a LLCs formation process that involves solvent evaporation, i.e., evaporation-mediated direct templating (EDIT).[79−81] Because of the introduction of volatile solvent, such as ethanol[82] and tetrahydrofuran,[83] the diluted surfactant solution can be directly evolved into LLCs templating mixtures without heating-aging processes. For example, the syntheses of monometallic Pt[84] and bimetallic mesoporous Pt−Ru alloy fibers[80] by a dual-templating route were demonstrated using LLCs as mesostructural direct templates and porous anodic alumina membranes (PAAMs) as morphological direct templates. As shown in Figure 6A,B, Pt fibers with stacked donut-like mesospace fibers were observed. Combining LLCs templating with vapor reduction and PAAMs with a confined effect can lead to new mesoporous nanostructures.[84] They also the investigated the effect of reduced pressure on the morphological changes of LLCs and successfully prepared mesoporous Pt nanotubes with the assistance of PAAMs.[85] The detailed mechanism is attributed

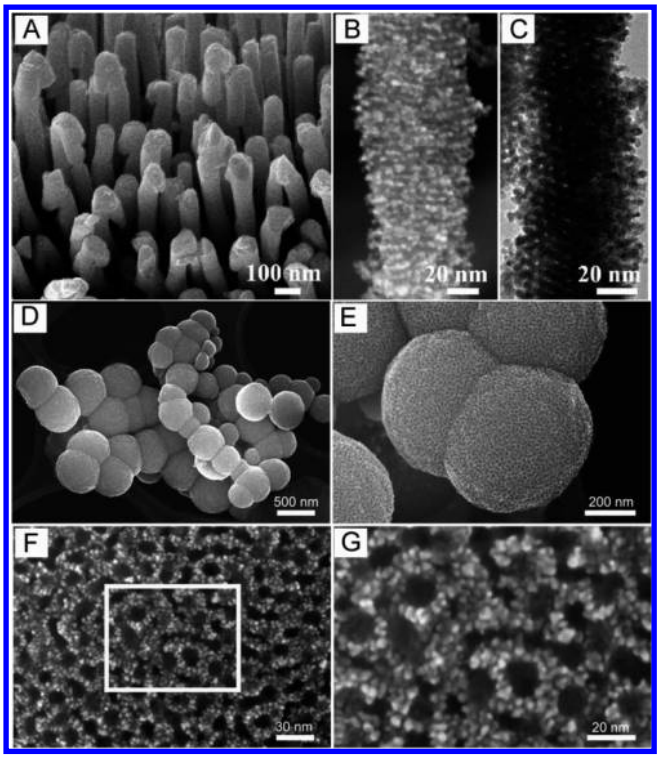

Figure 6. (A, B) SEM and (C) TEM images of the Pt fibers synthesized from the PAAMs with a pore diameter of 70−100 nm. Reprinted with permission from ref 84. Copyright 2008 American Chemical Society. (D, E) SEM images of mesoporous Pt particles with giant mesocages. (F, G) High-magnification SEM image of the surface of the particle, with (G) showing the square area in (F). Reprinted with permission from ref 83. Copyright 2008 Wiley-VCH.

to the volume change of the LLCs at reduced pressures. In addition to vapor infiltration of a reducing agent, other reduction methods, such as electrochemical and chemical deposition, have been widely adopted to construct mesoporous noble metal nanostructures. Most of the mesoporous metal nanostructures prepared by LLCs have been limited to 2D hexagonal nanostructures with mesopores less than 4 nm in diameter. LLCs are powerful soft templates for rationally designing mesoporous metal nanostructures with tunable pore size; this control is achieved by changing the surfactants or amphiphilic block copolymers. For example, using LLCs composed of diblock copolymers, mesoporous Pt particles with giant mesocages (approximately 15 nm) were synthesized via electrochemical deposition (Figure 6D−G).[83] Because of the adjustable molecular weight and composition, metal architectures with various mesostructures and pore sizes can be easily prepared where the effective movement of large guest species within the mesopores will be greatly accessible. Pt nanorods with cage-type mesopores were also reported using diblock copolymers in the PAAMs.[86]

2.2.2. Micelle Assembly. In contrast to the LLCs approach consisting of a high concentration of surfactants, micelle assembly in a low-concentration surfactant solution offers a more versatile and advantageous alternative to fabricate mesoporous metal nanostructures. On this basis, Yamauchi and co-workers recently demonstrated a new approach, i.e., electrochemical micelle assembly, for constructing mesoporous Pt-based films through potentiostatic deposition.[87−90] In this procedure, surfactant micelles can be effectively formed when

DOI: 10.1021/acs.chemrev.5b00255
Chem. Rev. XXXX, XXX, XXX−XXX

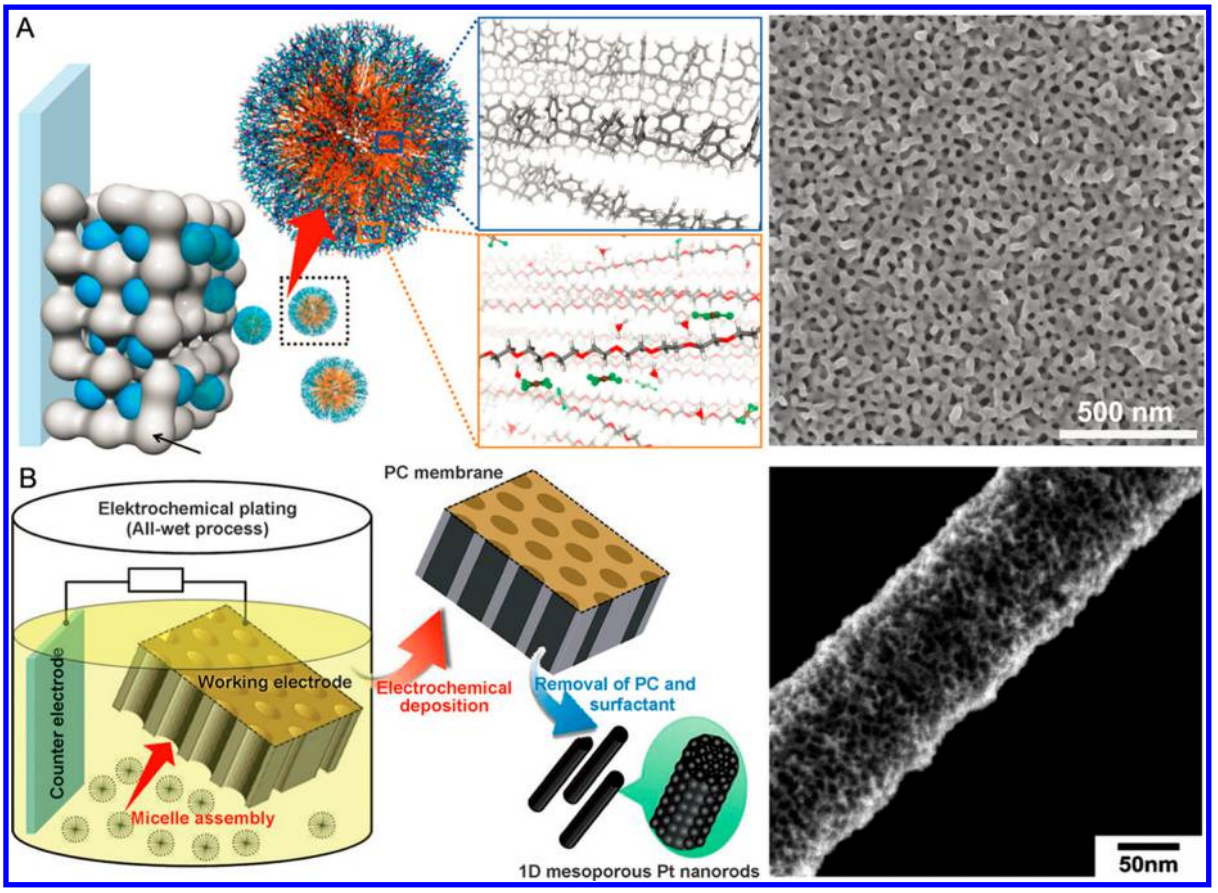

Figure 7. (A) Schematic demonstration of the synthesis of mesoporous Au films through micelle assembly and the corresponding SEM image of mesoporous Au film. Reprinted with permission from ref 91. Copyright 2015 Nature Publishing Group. (B) Electrochemical assembly of micelles in confined space for the design of 1D mesoporous Pt nanorods and the typical SEM image of the resulting product. Reprinted with permission from ref 95. Copyright 2013 Wiley-VCH.

the surfactant concentration added is above the CMC. Metal-aqua complexes, derived from the coordination between metal precursors and water, can usually interact with ethylene oxide groups of the surfactant micelles. Therefore, due to these structural directing agents, well-defined mesoporous films can be directly obtained on electrode surface via electrochemical deposition. These unique mesoporous structures with accessible pores and mesopore sizes can be well regulated by varying the surfactants. Moreover, in the presence of different precursors, bimetallic mesoporous films with composition-controlled nanostructures will be available to optimize their functional properties.[87] As shown in Figure 7A, Li et al. electrochemically deposited mesoporous Au films with controlled pores using diblock copolymers derived micelles as soft templates. In this process, Au crystal growth can be precisely tuned, benefiting the fabrication of the 3D uniformly mesoporous nanostructures for the first time.[91] In addition to the noble metals mentioned above, some nonprecious metal, such as Cu, can also be introduced into these Pt-based mesoporous film.[92,93] Furthermore, dealloying was adopted for further modification of mesopore walls, significantly improving the electrochemical performance.[93] On this basis, Pt/Pd bimetallic alternating multilayer mesoporous films were constructed using layer-by-layer (LBL) electrochemical deposition.[94] This novel mesoporous nanostructure featured a high surface area, heterometallic interfacial atomic contacts, and tunable thickness of each layer and exhibited enhanced electrochemical performance toward methanol electro-oxidation. Furthermore, the other advantage of this electrochemical micelle assembly method is that specific mesoporous nanostructures can be formed within confined spaces with the help of direct templates. As shown in Figure 7B, Li et al. successfully designed self-supported 1D mesoporous Pt nanorods with polycarbonate membrane using the confined effect. The resulting nanostructures characterized by 6−8 nm pore sizes and thin wall thickness were well formed within the entire Pt nanorods.[95] As an effective alternative to this electrochemical method, various reducing approaches, such as galvanic replacement[96] and solution-based reduction,[97,98] were also exploited to produce Pt-based mesoporous nanostructures using micelle assembly.

Different from the aforementioned mesoporous film, Li et al. presented a simple method to synthesize uniformly sized mesoporous Pd NPs with periodically ordered mesostructures using self-assembly of amphiphilic molecules.[99] In this process, Pd precursor was reduced by AA in the presence of cationic hexadecylpyridinium chloride (HPC) and triblock copolymers (Pluronic F127), which served as structure-directing agents and protective agents, respectively. Structural change in the HPC micelles from spheres to tubular structures was responsible for the formation of mesostructures inside the particles, while the addition of Pluronic F127 significantly suppressed the grain growth and therefore affects the particle size. This efficient design concept will be definitely expand the morphological diversity of the ordered PNMNs and find more applications.

DOI: 10.1021/acs.chemrev.5b00255
Chem. Rev. XXXX, XXX, XXX−XXX

2.2.3. Degradable Block Copolymers. Block copolymers (BCPs) are polymers that consist of two or more homopolymers, which are covalently linked and this linkage prevents macrophase separation. BCPs have received great interest due to their ability of self-assemble into a variety of periodic nanostructures, depending on their constituted polymer chains and molecular weights.[100] The advantages of the BCPs lie in the fact that the degradable characteristic of BCPs enables the facile production of nanoporous polymer materials with well-ordered nanostructures by selective removal of constituted components.[101,102] Similar with the traditional templates mentioned above, nanocasting approach using the resulting nanoporous polymers with well-ordered nanochannels as novel templates are also applied to create diversified nanostructures (e.g., metal, metal oxides).[103−106] As expected, such replication involves the selective removal of the specific polymer block for creating ordered porous nanostructures, backfilling of the porous structure with inorganic material, and subsequent removal of the remaining polymer template.[107] To date, various novel templates based on degradable BCPs have been designed and utilized to synthesize ordered PNMNs with different morphologies and compositions.[108,109]

Ho and co-workers reported the synthesis of well-defined multibranched Au from the seeding growth approach using a DG BCP template.[110] Self-assembly of degradable polystyrene-*b*-poly(L-lactide) (PS−PLLA) BCP was achieved and a DG phase composed of cocontinuous PLLA networks in a PS matrix was fabricated upon solution casting of the resultant PS−PLLA followed by quenching from the microphase-separated melt. After hydrolytic treatment, the PLLA networks can be selectively removed to yield a nanoporous gyroid PS matrix, which can serve as a template for the nucleation and growth of Au through the seeding growth approach. As shown in Figure 8, different kinds of Au nanostructures within the nanochannels of PS template can be obtained by adjusting the growth time of Au. After removal of the PS template using UV-ozonolysis or dissolution using tetrahydrofuran, a series of nanostructured Au, including Au NPs, branched Au, 3D ordered nanoporous Au (3DON Au) particle and nanoporous gyroid Au can be well inherited. Steiner and co-workers have also made great contributions to the replication of complex BCPs into the ordered PNMNs. For example, they proposed an efficient method for the creation of 3D ordered Au PNMNs based on degradable BCP.[111] An isoprene-*block*-styrene-*block*-ethylene oxide (ISO) BCP consisting of two chemically distinct, interpenetrating gyroid networks (I, O) of opposite chirality in a matrix of the third block served as precursors of template, the I gyroid network of which was then removed by selective UV and chemical etching. The resulting porous nanostructures were backfilled with Au by electrodeposition. As a result, a continuous, triply periodic Au network with the dimension of the full unit cell of 50 nm was attainable. In addition to single component nanostructures, the synthesis of multicomponent nanomaterials with complex yet well-controlled ordered PNMNs are also desirable. Appropriate orthogonally degradable BCPs have great potential for use as templates to fabricate such complex porous nanostructures. Toward this end, Steiner et al. reported the synthesis and self-assembly into cocontinuous network structures of polyisoprene-*block*-polystyrene-*block*-poly(propylene carbonate) where the polyisoprene and poly(propylene carbonate) blocks can be orthogonally removed from the polymer film.[112] Taking advantage of this unique property, sequential block etching and backfilling the resulting mesopores with different metals lead to the creation of periodically ordered porous nanostructures with two distinct metal networks (e.g., Au and Cu), having potential in a wide range of applications.

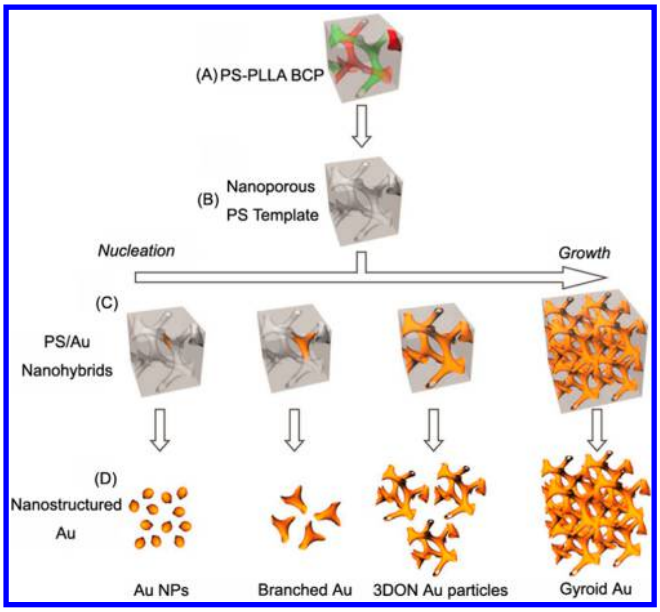

Figure 8. Schematic illustration for fabrication of various nanostructured Au from BCP template: (A) PS−PLLA DG phase (skeleton of DG structure with two identical networks (green and red)); (B) gyroid-forming nanoporous PS template after removal of PLLA network; (C) PS/Au nanohybrids from controlled nucleation and growth of Au within the BCP template via seeding growth approach; (D) nanostructured Au after removal of PS template. Reprinted with permission from ref 110. Copyright 2013 Wiley-VCH.

2.3. Self-Assembled Mesoporous Nanostructures

As an alternative route to both hard and soft template, the self-assembly of performed NPs with block copolymers seemed a viable pathway to prepare self-sustaining structures with mesopores.[113−116] Wiesner and co-workers ingeniously utilized the self-assembly between metal NPs and block copolymer to synthesize ordered mesoporous.[117,118] As shown in Figure 9,

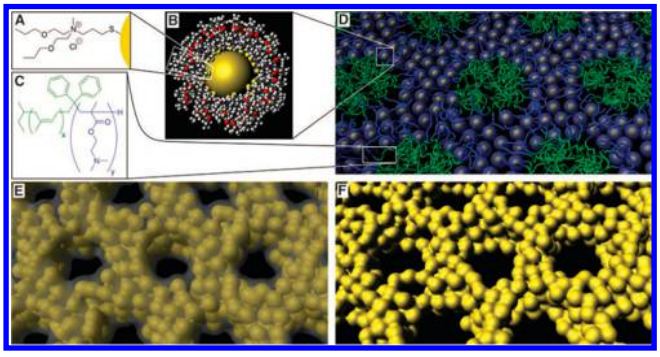

Figure 9. Illustration of CCM-Pt-6 produced after each stage of the synthesis. (A) A thiol-containing charged ligand was attached to (B) Pt NPs, which were mixed with PI-*b*-PDMAEMA (C) and cast into films that displayed a hexagonal mesostructure. (E) Pyrolysis of these films yielded a Pt−C composite with retention of the mesostructure. (F) The carbon film was removed by plasma treatment or acid etch to yield the bare mesoporous Pt film. Reprinted with permission from ref 117. Copyright 2008 American Association for the Advancement of Science.

DOI: 10.1021/acs.chemrev.5b00255
Chem. Rev. XXXX, XXX, XXX−XXX

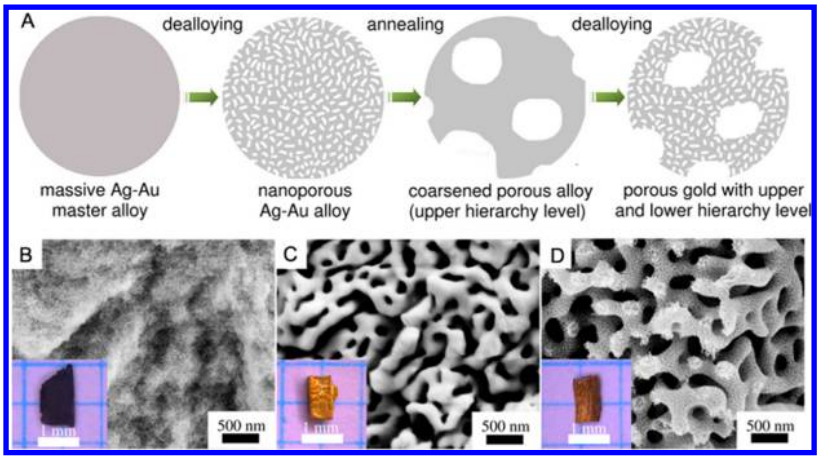

Figure 10. (A) Schematic illustration of the synthetic strategy toward hierarchical NPG. Overview SEM images showing microstructure evolution through the consecutive synthesis steps, i.e., (B) the first dealloying product $Au_{52}Ag_{48}$, (C) annealed sample with coarsened ligaments, and (D) formation of hierarchical nanostructure after second dealloying step. Reprinted with permission from ref 126. Copyright 2013 American Chemical Society.

The specific ligand-stabilized Pt NPs mixed with poly(isoprene)-*block*-poly(2-(dimethylamino)ethyl methacrylate) (PI-*b*-PDMAEMA) was first mixed together.[117] Film casting of the mixture afforded metal-rich mesostructured NPs−block copolymer hybrids with an inverse hexagonal morphology after solvent evaporation and subsequent annealing to 130 °C. Rapid pyrolysis process was carried out to convert the inverse hexagonal hybrid to an ordered mesoporous Pt−C composite. Further pyrolysis at 410 °C converted the obtained composites into an amorphous carbon scaffold, which allowed the retention of the hexagonal structure while fusing the Pt NPs when heating the sample to 550 °C. Finally, ordered porous Pt mesostructures can be produced through pyrolysis under an inert atmosphere followed by plasma or acid etching. In this system, the solubility and size of metal NPs metal volume fraction play significant roles in the resulting mesoporous nanostructures. Similarly, Pt and Pd hybrid thin films with high NPs loadings were obtained by spin-coating solutions of block copolymer with ligand-covered Pd or Pt NPs onto silicon substrates, which can be facilely transformed into Pt/Pd porous nanostructures by plasma cleaning.[118] These examples demonstrate the promise of this self-assembly approach for the preparation of novel ordered PNMNs.

In another report, Li et al. demonstrated the synthesis and analysis of highly ordered 3D single-network superstructures of single and binary metal NPs from triblock terpolymer/NP self-assembly.[119] Ordered PNMNs with monometal and bimetal can be well maintained upon plasma etching of these hybrids. They found that NP ligands were essential for the assembly between BCP and metal NPs. Ligand density and interactions with BCPs can realize the programmable control of the NP spatial arrangement due to owing the dominant effects on NP distribution. Experiment and theory analysis further provided insights into short- and long-range NP−NP correlations, and local and global contributions to structural chirality in an alternating gyroid domain. These examples demonstrate the promise of this self-assembly approach for the preparation of novel ordered PNMNs.

3. NONORDERED POROUS NOBLE METAL NANOSTRUCTURES

Compared with ordered porous nanostructures, nonordered counterparts are more ubiquitous in nature and form a variety of porous nanomaterials. Large specific surface areas and rapid mass transport pathways are considered the most important aspects in the materials design strategy. In this sense, tremendous efforts have been made for fabricating novel noble metal nanostructures featured by a type of hierarchical porous architecture to achieve higher catalytic performances and better noble metal utilization.[120]

3.1. Nanofoams/Nanosponges

3.1.1. Dealloying Derived Nanofoams. Dealloying refers to the selective etching of active component from an alloy in the bulk form or a thin film and triggers the evolution of a porous nanostructure with nanosized ligaments and pores.[121] Raney nickel is considered as a successful example of a porous structure, which is obtained by chemical dealloying.[122] A competition of two processes, i.e., dissolution of the active component (i.e., pore formation) and surface diffusion of the other component to aggregate into 2D clusters (i.e., surface passivation), is involved in the formation of the unique porous nanoarchitectures. Core−shell structures with conformal noble metal shells encasing alloy cores and porous noble-metal-rich NPs are usually produced, both of which have been reported to yield enhanced performances. The porous nanostructures can be prepared using electrochemical dealloying and chemical dealloying or both dealloying methods at the same time.

Among the different PNMNs, nanoporous gold (NPG) is of significant interest because of its exceptional mechanical, physical, and chemical properties associated with a 3D bicontinuous interpenetrating ligament-channel nanostructure.[123] Pioneering works reported on unsupported, nanostructured Au that was formed by selectively dissolving an active metal, such as Ag or Cu, from the corresponding gold alloy.[121] Ding et al. fabricated the thin and mesoporous membrane-NPG leaf by leaching Ag/Au leaf with concentrated nitric acid.[124] A continuous crystal lattice throughout the porous network was observed, while the adjustable pore size can also be fabricated via simple room-temperature post-processing. To precisely modulate the size and structure of the

DOI: 10.1021/acs.chemrev.5b00255
Chem. Rev. XXXX, XXX, XXX−XXX

NPG, they developed a facile two-step dealloying method to prepare free-standing metal membranes with hierarchical porous architecture with the help of Ag plating.[125] The resultant NPG exhibited a bimodal pore size distribution consisting of two different porosity channels, where both pore sizes can be tuned independently. In another report, hierarchical NPG can be easily made through a dealloying-annealing-dealloying step without Ag plating.[126] As shown in Figure 10, electrochemical dealloying of the bulk alloy yielded a nanoporous AgAu alloy as an intermediate product, which can be evolved into a porous alloy with ~200 nm pores at the upper hierarchy level after thermally coarsening. Then, the fine ligaments with ~15 nm lower hierarchy channels can be created after a second dealloying. This two-step dealloying strategy mentioned above can enable the fabrication of hierarchical porous structures in the bulk form with precise control over the bimodal pore size distribution. Moreover, to solve the key issue during corrosion, namely the large shrinkage of the sample and the formation of macrocracks, they also found that doping Pt in master alloy can effectively mitigate the evolution of macro-defects during the synthesis of NPG.[127] Additionally, a series of monometallic nanofoams, including Au,[128] Pd,[129] and Pt,[130] were fabricated using a dealloying approach for various applications.

Compared with monometallic systems, bimetallic nanostructures are of significant importance in many research areas due to their clearly altered properties. A wide range of compositions and morphologies (e.g., size, shape, surface structure and crystal facet) can be offered to sensitively control their surface properties and thus enhance their applied performances. Dealloying was approved as an efficient and versatile method for the construction of well-defined porous alloy nanomaterials using binary/ternary alloys as the master precursors because of their more active properties, low cost of nonprecious elements, and simple implementation. Strasser et al. fabricated Pt−Cu core−shell NPs by electrochemically dealloying carbon-supported Pt−Cu alloy NPs.[131,132] The exceptionally enhanced oxygen reduction reaction (ORR) activity was ascribed to the surface compressive strain resulting from a pure Pt skin and a Pt−Cu alloy core, shifting the electronic band structure of Pt and then weakening chemisorption of oxygenated species. Chen et al. also synthesized porous Pt−Cu bimetallic nanostructure characterized by a Pt skin and a Pt−Cu core, which could be synthesized by potential-controlled dealloying of bulk Pt−Cu binary alloy.[133] The mole ratio of the composition can be flexibly tailored over a wide composition range by only regulating the dealloying potential. Similarly, a Pd-enriched outer surface layer was also observed on PdCo and PdNi porous nanostructures fabricated via electrochemical and chemical dealloying.[134,135] To shed light on the structural evolution in these dealloyed systems, Oezaslan et al.[136] and Sieradzki et al.[137] respectively investigated the size−morphology−composition relationship on different dealloyed alloy NPs. As shown in Figure 11, three entirely different size-dependent morphology regions within the resulting particle ensembles were observed.[136] Single core−shell NPs are exclusively evolved by dealloying NPs below a typical diameter of 10−15 nm. Multiple core−shell NPs with irregular shapes dominate when the size of NPs are between 15 and 30 nm. Above the second critical diameter of approximately 30 nm, surface pits and nanopores next to multiple Co/Cu rich cores are presented in the dealloyed Pt−Co and Pt−Cu particles. It is also revealed that bimetallic nanostructures derived from the ternary

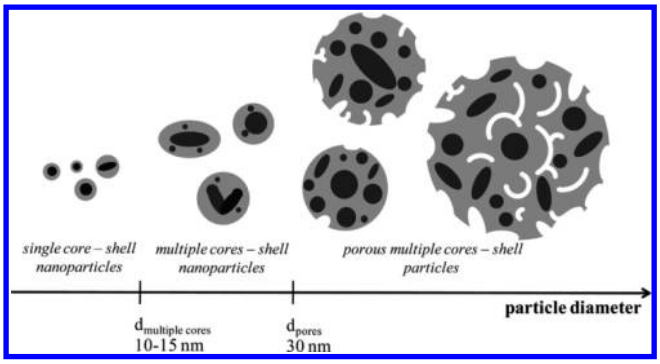

Figure 11. Illustration of the evolution in size-dependent morphology and composition of dealloyed Pt−Cu and Pt−Co particle electrocatalysts. Reprinted with permission from ref 136. Copyright 2011 American Chemical Society.

precursors have some obvious advantages, such as a large pore volume and small ligament size compared with binary precursors. The content of the resulting bimetallic nanostructures can be further dealloyed to fine-tailor the nanostructures with optimized pores and compositions, leading to the enhanced applied performances.[138] These results will contribute greatly to the understanding of the size−morphology−composition relationships associated with morphological evolution from different dimension levels, providing detailed information about the dealloyed NPs and the bulk porous materials. A large number of bimetallic materials with porous nanostructures, such as PdNi,[139] PdCu,[140] PdPd,[141] PtNi,[142] AuPt,[143] and PtAl,[144] were successfully synthesized by dealloying and used as advanced electrocatalysts in fuel cells.

The dealloyed nanostructures mentioned above are usually derived from bulk-like or film precursors. Combining with the dealloying approach, significant efforts were dedicated to prepare PNMNs with specific morphologies and sizes and construct more complex nanoarchitectures for various applications. Liu and co-workers synthesized porous Pt−Co nanowires with controllable morphologies and compositions by dealloying Pt_1Co_{99} nanowires in a mild acidic medium, which were previously electrodeposited within confined space of a porous anodic aluminum oxide (AAO) membrane (Figure 12).[145] Taking advantage of the compositional tunability, the as-synthesized porous Pt−Co alloy nanowires exhibited enhanced electrocatalytic activity toward methanol oxidation. Other 1D porous nanostructures, including AuAg nanotubes[146] and PdNi alloy nanowires,[135] were also reported based on well-defined template followed by dealloying. Inspired by this facile approach, Li and co-workers demonstrated a general approach for synthesizing Pt-based alloy nanoporous NPs by dealloying, utilizing monodisperse nanocrystalline intermetallics as precursors.[147] In addition to the good dispersity, the final product displays a small pore size (less than 5 nm) and a much higher surface area and is considered potential candidate as nanocatalysts. It is worth nothing that chemical etching is subjected to some intrinsic drawbacks. The etching process is so fierce that the surface atoms of the alloys are usually corroded at random sites. Better control over this etching process is greatly needed to control the morphological and compositional parameters of dealloyed products. Li et al. presented a controllable synthesis of concave PtNi alloys using a coordination assisted chemical-etching process, making this process moderate and controllable and leading to novel noble metal-based nanomaterials with special morphologies and

DOI: 10.1021/acs.chemrev.5b00255
Chem. Rev. XXXX, XXX, XXX−XXX

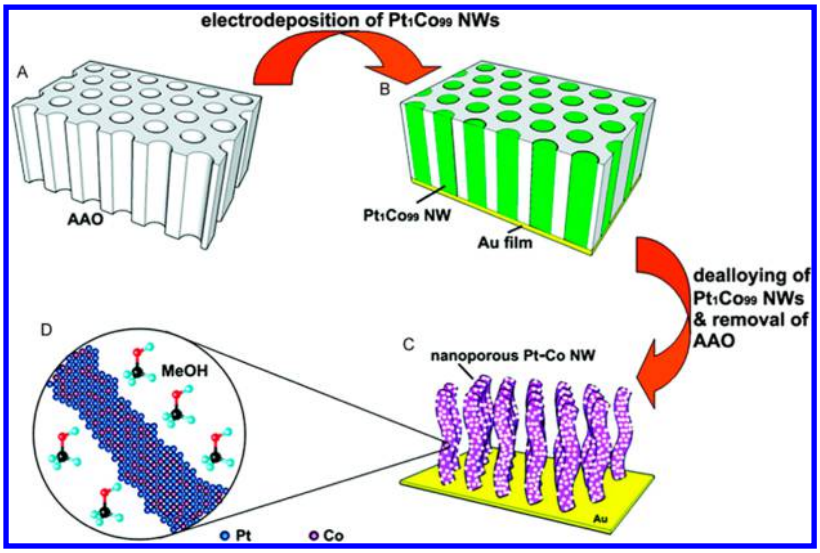

Figure 12. (A–C) Schematic illustration of the synthetic procedure of nanoporous Pt–Co alloy nanowires; (D) enlarged schematic of the core–shell-like structure of the ligaments. Reprinted with permission from ref 145. Copyright 2009 American Chemical Society.

structures.[148] The formation of the concave structure was attributed to the different etching priorities on specific sites. Thanks to the larger surface area and higher density of exposed atomic steps, concave PtNi alloys exhibited enhanced catalytic activity in comparison to the uncorroded precursors.

Based on the dealloyed nanofoams, other types of functional PNMNs were rationally designed via modification of their compositions and morphologies, aiming to create heterogeneous interfaces with enhanced performances. On the one hand, the porous nanostructures can be inherited due to the rigid 3D skeletons. On the other hand, several factors critical to catalysis, such as a heterogeneous interfaces, Pt skin layer, core–shell structure, and alloy effect, can also be realized, facilitating their catalytic activity. Xiao et al.[149] and Ding et al.[150] synthesized AuPt bimetallic porous nanocomposites via different reduction methods. In the first report, hierarchical nanoporous AuPt with heterogeneous interfaces were fabricated via chemical corrosion followed by electroless deposition. Using this method, island growth and deposition of high density of Pt NPs on the surface of the ultrathin NPG film in the free-standing state were successfully realized.[149] An unusual Pt growth mode of Pt with coherency between the Pt and the NPG was observed in the latter work, which used a vapor-phase reducing agent.[150] An atomically thin layer of Pt over a NPG core can be facilely created. Because of the unique structures of the resulting products, they both exhibited excellent electrocatalytic performance in fuel cells. Xu and colleagues proposed a versatile method for the synthesis of bimetallic catalysts (Pt/Cu and Pd/Cu) with nanotubular porous structures based on a convenient integration of dealloying process and galvanic replacement reaction.[151] This simple method can be facilely extended to other transition metals for the preparation of similar porous composites with hierarchically hollow nanostructures on a large scale, which have significant potential in heterogeneous catalysis and fuel cell technology. Furthermore, Shao et al. first fabricated porous/hollow Pd–Cu NPs using electrochemical dealloying and used them as substrate for constructing a core–shell nanocatalyst featured by a monolayered Pt shell.[152] The resulting electrocatalyst showed a 14-fold ORR activity improvement of Pt over commercial Pt/C nanocatalysts because of the Pt monolayer and synergistic effect from the core.

3.1.2. Aerogels. Self-assembly processes represent the most powerful strategy for the production of complex materials with unique structural and compositional sophistication.[2,153] Aerogels, a unique class of materials with low density, high porosity, and high surface area, are well-known for their extraordinary physical and chemical properties, which are usually associated with macroscale self-assembly.[154,155] Currently, the vast majority of work is dedicated to silica and other metal oxide-based aerogels and thus does not provide a large range of functionalities. Many preparation techniques were developed to incorporate other functional units, endowing the new functionalities of the composites aerogels.[156,157] The creation of a novel aerogel using semiconductor NPs as building blocks has aroused significant attention.[158–160] In spite of great contribution to this research area, aerogels created from only metal NPs have been less intensively investigated. As a pioneering work, Eychmüller and co-workers successfully realized the controlled destabilization of citrate-stabilized noble metal NPs in aqueous solution to fabricate monometallic and bimetallic hydrogels and aerogels, opening a new avenue to self-supported 3D PNMNs.[161–163] The as-prepared aerogels are network-like, very low-weight, highly porous, and macroscopic solids, which display fantastic structures on nanoscale. In comparison to other PNMNs, metallic aerogels indeed possess unprecedented properties in terms of the density/pore size parameter (Figure 13).[164] These metallic aerogel-based PNMNs combine the characteristic properties of metals with the superior properties of nanostructures, which involve high specific surface areas, very low densities, broad pore size distributions, high gas permeabilities, and high electrical conductivities. There are a wide range of potential applications in sensors and electrochemical energy conversion and storage.

The general principle of the evolution from colloidal NPs to aerogels is demonstrated in Figure 14A. First, the highly stable aqueous metal NPs (Au, Ag, and Pt) were concentrated. Efficient destabilization and hydrogel formation is initiated by the addition of ethanol or hydrogen peroxide to the concentrated colloids. The fusion of the initial NPs leads to a self-supporting network, i.e., a hydrogel, which forms a

DOI: 10.1021/acs.chemrev.5b00255
Chem. Rev. XXXX, XXX, XXX–XXX

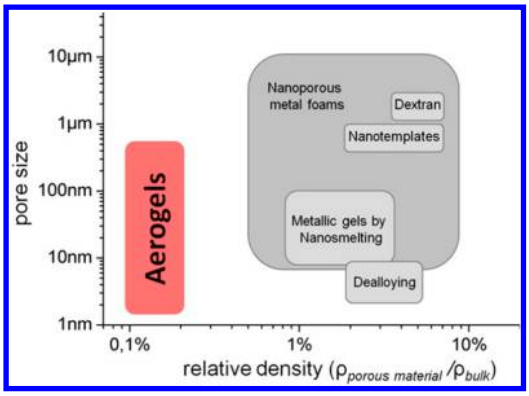

Figure 13. Density/pore size parameter space of aerogels. Reprinted with permission from ref 164. Copyright 2014 American Chemical Society.

monolith several millimeters in diameter. Supercritical drying with carbon dioxide is used to transform them into aerogels without destroying the fragile and complex structure of the nanoporous network, while the macroscopic sizes of the gels are well maintained. Using this method, Au, Pt, and Ag monometallic aerogels could be readily formed, as well as AuAg and PtAg bimetallic aerogels (Figure 14B–F).[161] Take PtAg bimetallic aerogel as an example, the resulting product did not show original single NPs with good dispersion but rather a fused nanowire-like structure. Furthermore, HRTEM revealed the multifaceted structure of the network. Distinctive differences between mono- and bimetallic gel formations can be found with respect to their effective destabilization agents and time scales of formation as well as their microscopic properties. Unlike Au and Ag aerogels, the Pt aerogel consisted of ultrathin networks with similar diameters to the starting NPs (4–5 nm), confirming the presumption that the Pt hydrogel formed directly from the pristine metal NPs without any NP preagglomeration. However, it should be pointed out that the formation of these assembled aerogels usually takes a long time (several weeks to months), which limits their large-scale manufacturing and practical applications. Based on this result, the synthetic procedure was significantly simplified and hydrogel formation was also remarkably accelerated by only increasing the reaction temperature in the absence of destabilizers.[164] A series of multimetallic hydrogels with tunable compositions could be completely formed within several hours. This general and facile approach significantly improves the reproducibility and favors their potential applications. It is interesting that the formation of AuPt aerogels is unavailable and still under investigation. In another work, Arachchige et al. also adopted this destabilization approach, i.e., oxidative removal of the surface thiolates of Ag nanoshell by tetranitromethane, for the fabrication of metallic Ag gel frameworks.[165] It is found that the tetranitromethane/thiolate molar ratio had the significant effect on the gelation kinetics, which is closely related to structures of the resulting Ag gel.

In another report, Arachchige and co-workers investigated the effects of the concentrations of bimetallic alloy nanoshells (Au/Ag, Pd/Ag, and Pt/Ag) on the evolution of the hydrogel and proposed a new synthetic procedure for metallic aerogels that involved the salt-mediated self-assembly.[166] They found that the concentrated colloids derived from the rotator evaporation can form hydrogels, while the centrifuge filtration was not applicable to form hydrogel spontaneously even after 2–3 months. Furthermore, the concentrated colloids prepared via the centrifuge filtration could be effectively evolved into hydrogel after intentional introduction of NaCl. The as-synthesized gel was comprised of an interconnected network of triangular or nearly spherical hollow particle building blocks, which show the similar diameter with pristine colloids. The

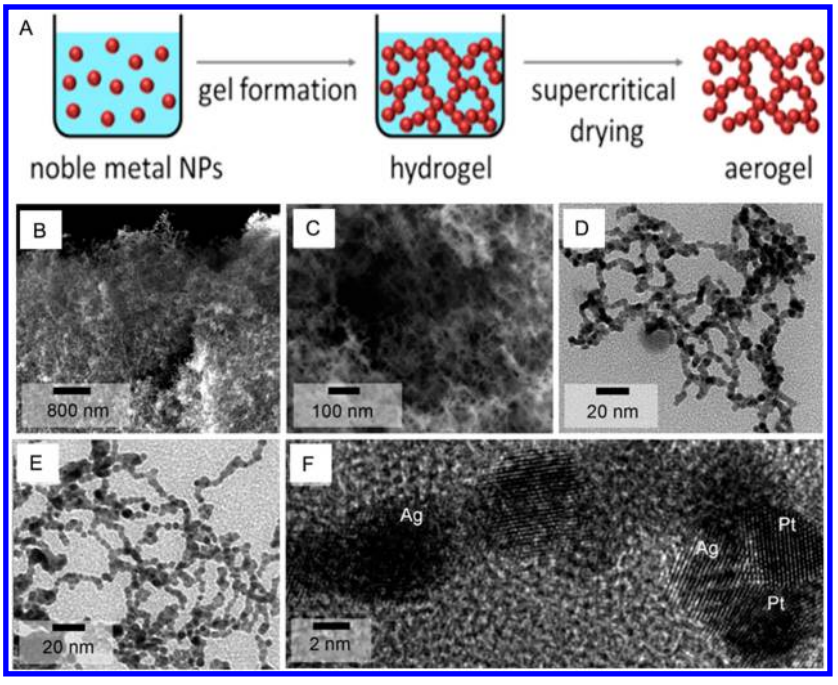

Figure 14. (A) Schematic demonstration of fabrication of aerogels from individual metal NPs. Reprinted with permission from ref 164. Copyright 2014 American Chemical Society. (B, C) SEM images of Pt/Ag aerogels and (D, E) TEM images of a Pt/Ag hydrogel (D) and aerogel (E). (F) HRTEM image of the Pt/Ag nanochains, showing individual Ag and Pt nanodots (diameters of ca. 3–6 nm). The lattice distances for the NPs indicated were $d(111)$Ag = 0.236 nm and $d(111)$Pt = 0.222 nm. Reprinted with permission from ref 161. Copyright 2009 Wiley-VCH.

DOI: 10.1021/acs.chemrev.5b00255
Chem. Rev. XXXX, XXX, XXX–XXX

creation of these aerogel was attributed to the direct cross-linking of the individual nanoshells without any intermediate aggregates, which is very consistent with the previous reports mentioned above. With regard to the mechanism of gel formation, the colloid solution becomes unstable and tends to aggregate due to the reduced electrostatic repulsions when the salt ions reach a critical concentration. Meanwhile, the citrate groups weakly bound on the surface of colloidal sols can be partially removed through vigorous shaking, which is favorable for the aggregation of the NPs by van der Waals forces. More recently, Wen et al. reported the controlled creation of Pd aerogels with large surface area and high porosity through Ca^{2+}-induced assembly of citrate-capped Pd NPs (Figure 15).[167] The

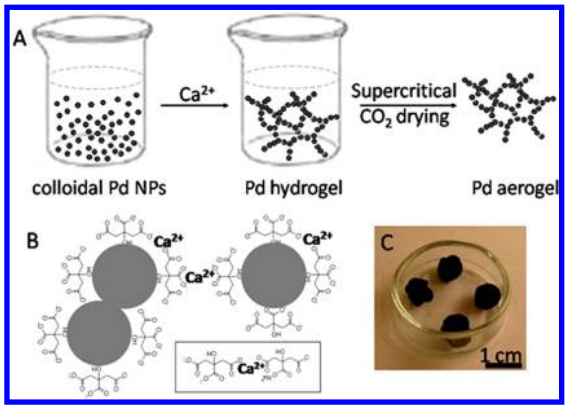

Figure 15. (A) Schematic illustration of synthetic procedure of the Pd aerogel. (B) Possible mechanism for the Ca^{2+}-induced assembly of citrate-stabilized Pd NPs. (C) Digital photograph of the resulting Pd aerogels. Reprinted with permission from ref 167. Copyright 2014 American Chemical Society.

gelation time can be easily adjusted by tuning the concentrations of Ca^{2+}. The connection of Pd NPs via Ca^{2+} and the instability of the surface citrate groups on the surface of Pd sols are beneficial to the generation of Pd hydrogels. However, the effects of other cations on the gel formation were not provided in these two works, and cation-induced metallic aerogels should be investigated further.

These previously mentioned metallic aerogels are based on the self-assembly of prepared colloidal sols with further concentration. The high concentrations of the colloidal sols play key roles in the synthesis of the corresponding hydrogels/aerogels. The resulting aerogels have a lot in common with respect to their morphologies. Namely, direct fusion of the pristine metal NPs is involved, where the atom diffusion between the adjacent NPs is expected to form network-like aerogels. Several factors, such as the temperature, functional groups on the surfaces of colloidal NPs, salt effects, and complexing effects, were assumed to play key roles in the fusion of NPs and, subsequently, the evolution of the corresponding hydrogel. Moreover, the metal interdiffusion rates are directly determined by the inherent properties of the noble metals. For example, only AuAg aerogel with well alloyed nanostructures can be obtained within the bimetallic aerogel systems.[168] Understanding the interactions of the pristine building blocks especially atom diffusion between connected NPs, is critical to the advancement of this emerging research topic.

In addition to the self-assembly method, other attractive alternatives were developed to construct a variety of metallic aerogels. Eychmüller et al. for the first time illustrated a simple method for constructing Pd aerogel through the reduction of K_2PdCl_4 with $NaBH_4$ at room temperature in the presence of different cyclodextrins.[169,170] They found that Pd hydrogel formation involves four main stages, i.e., the formation of Pd NPs, short Pd nanowires, Pd nanowire networks, and eventually the Pd hydrogel. The Pd aerogels exhibited remarkably enhanced electrocatalytic activities toward ethanol oxidation in alkaline media. Significantly, this $NaBH_4$ reduction method was extended to the controlled preparation of bimetallic PtPd and monometallic Pt and Pd aerogels without any additional capping agents at room temperatures.[171] The PtPd aerogels composed of 3D network-like nanostructures show large surface areas, high porosities, and excellent electrocatalytic activity toward ORR. As a matter of fact, the formation of the aerogel involving the in situ reduction method also originated from the self-assembly of NPs produced through metal interdiffusion. However, the synthetic process is significantly simplified because the concentration step can be avoided. It is anticipated that this novel method will not only pave a new route to a host of noble metal-based aerogels but also broaden the electrochemical applications of PNMNs.

3.1.3. Kinetically Controlled Reduction Derived Network-Like Nanostructures. Like metal aerogels, explosive studies on PNMNs have sparked new interests toward other 3D network-like nanomaterials and nanostructures. Many techniques have been developed to obtain these 3D network-like PNMNs, such as solution-based methods, electrochemical reduction, etc. Sodium borohydride reduction is a traditional method for synthesizing metal NPs from their precursors by virtue of diversified capping agents. Recent advances revealed that $NaBH_4$ reduction was considered the most facile yet efficient method for the construction of 3D network-like PNMNs. Eswaramoorthy and co-workers reported for the first time a strikingly simple, kinetically controlled $NaBH_4$ reduction process without any capping agent to obtain different noble metal-based nanosponges with high surface area.[172] By carefully tailoring the concentration of the metal precursors and $NaBH_4$, the bare metal nuclei formed during the reduction process was fused and initiated to instantaneously form 3D network-like PNMNs. Dong et al.[173,174] and other groups[175] further extended this concept to bimetallic/trimetallic alloy nanosponges and investigated them as advanced electrocatalysts in ethanol/methanol electro-oxidation (Figure 16A,B). Furthermore, nonprecious metals, such as Ni and Co, can also be easily introduced into this network-like bimetallic nanomaterial.[176−178] As shown in Figure 16C,D, the as-synthesized porous PdNi nanostructures possess 3D network-like architectures with ultralow bulk densities.[176] Unlike the agglomerated structures, the present PdNi showed the fused irregular NPs with the diameter between 2 and 10 nm. Taking advantage of the porous nanostructures, the bare surface as well as the synergistic effects between their compositions, the resulting PdNi showed significantly enhanced electrochemical performances for methanol oxidation in an alkaline solution. This kinetically controlled synthetic process using $NaBH_4$ reduction has some distinctive advantages: the creation of 3D architectures through rapid fusion of initial bare metal nuclei and subsequent assembly into the porous nanostructures can be completed within 5 min at room temperature. More importantly, the electrochemical performance can be improved through the formation of bimetallic/trimetallic nanostructures with tunable compositions. However, the rapid reaction allows for little control especially over the noble/nonprecious metal

DOI: 10.1021/acs.chemrev.5b00255
Chem. Rev. XXXX, XXX, XXX−XXX

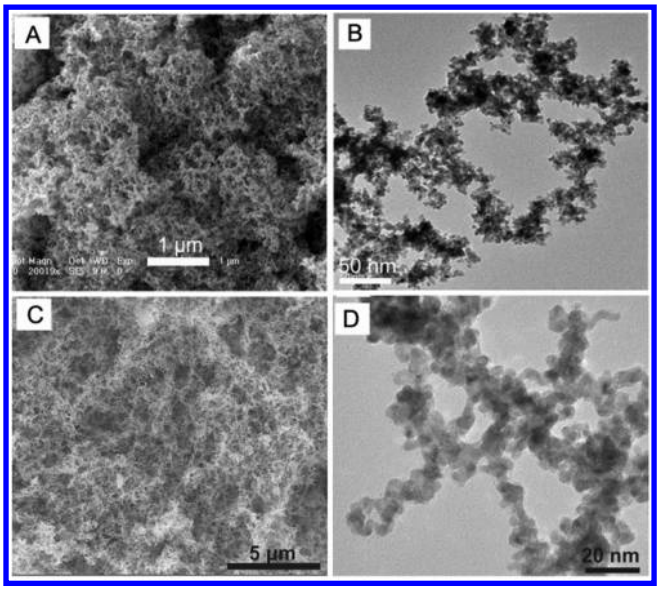

Figure 16. SEM (A) and TEM (B) images of PdPt bimetallic nanosponges. Reprinted with permission from ref 173. Copyright 2013 Wiley-VCH. SEM (C) and TEM (D) images of PdNi porous nanostructures. Reprinted with permission from ref 176. Copyright 2015 Wiley-VCH.

systems. Take PdNi for example, the final product was composed of a Pd enriched core and Ni-enriched shell because of the difference in reduction potentials.[176] Further control over the compositions of the surfaces of these systems is estimated to furnish more opportunities for tuning and optimizing their properties and enabling their improved performances. Recently, Meng et al. also use this kinetically controlled synthesis for the construction of many different metal nanosponges with high surface areas without using a template or a surfactant.[179] The synthesis involves the fast reduction of metal precursors followed by a slow network assembly in ethanol−glycerol mixed solvents, realizing the formation of a series of metal networks with controllable compositions, porosities, ligaments, and grain sizes.

3.1.4. Template Method Derived Network-Like Nanostructures. In contrast to the kinetically controlled reduction process, a host of 3D network-like nanomaterials can also be produced via reduction with the help of capping agents. For example, a soft surfactant template formed by cetyltrimethylammonium bromide (CTAB) in a two-phase water−chloroform system has been successfully implemented for preparing Pt (Figure 17)[180] and some Pt-based[181] alloy nanowire networks. After that, Zhang et al. successfully synthesized Pt_3Ni alloy networks by coreduction of metal precursors with $NaBH_4$ in an ethylene glycol modified CTAB/water/chloroform system at room temperature.[182] The confined growth mechanism was proposed to account for the fabrication of Pt_3Ni networks: the nucleation and growth are closely confined within a soft template composed of a network of swollen inverse worm-like micelles. The results also indicated that ethylene glycol poses a significant effect on both the network-like nanostructure and filament size. 3D Pd−P nanoparticle networks have also been successfully synthesized by their group using Brij 58 as a soft template.[183] It should be noted that the instability of the soft templates and the weak interactions between the soft templates and the metal precursors ensures the transcription from the soft templates to the metal

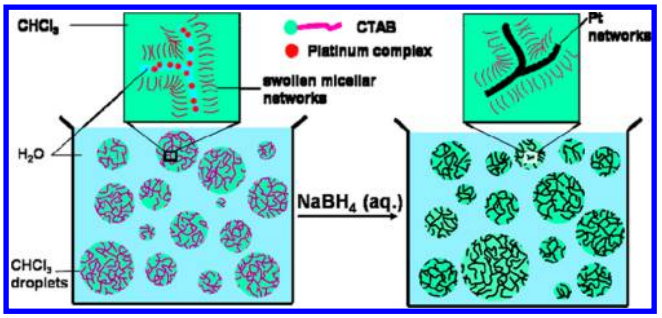

Figure 17. Schematic illustration of the potential mechanism for the synthesis of Pt nanowire networks using a soft template with the wormlike micellar network formed inside droplets of chloroform. Reprinted with permission from ref 180. Copyright 2007 American Chemical Society.

nanostructures is difficult. To this end, Zheng et al. fabricated zwitterionic wormlike micelles with precursor counterions for the first time and used them as the soft templates for creating Au and Au-based alloy nanowire networks.[184]

The synthesis of metallic networks using sacrificial templates has also been demonstrated. Recently, Lu et al. used cyanogel, a jelly like inorganic polymer, to prepare different 3D PNMNs, including Pt−Pd alloy,[185] Pt−Pd−Co trimetallic alloy,[186] Pd−Co−P ternary alloy networks,[187] and PdNi@Pt core−shell[188] network nanostructures by the aid of its double-metal property and specific 3D backbone. These multimetallic network nanostructures exhibited high electrocatalytic activities and have significant potential for use in fuel cells. Research into the synthesis of these related materials also frequently use poly(ethylenimine) hydrogel,[189] starch gels,[190,191] and bicontinuous interfacially jammed emulsion gel[192] as soft sacrificial templates; several significant breakthroughs have occurred within the past few years. Other interesting methods, such as the chemical reduction of solid assemblies of nonzero-valent nanostructures[193] and combustion synthesis[194] are also proposed for the preparation of different PNMNs on large scales with high yields.

A new green and promising template, i.e., gas bubble dynamic template, was proposed for the formation of porous nanostructures with a uniform pore size. Liu et al. demonstrated the pioneering works on electrodepositing a variety of 3D foam films of non-noble metals, such as Cu, Sn, and CuSn alloys in acidic media.[195,196] This method involves a metal electrodeposition process and an accompanying hydrogen evolution. During this process, H^+ are reduced and the resulting H_2 molecules conglomerate into bubbles that act as a dynamic template and at the same time the metal particles deposit between the hydrogen bubbles and form the 3D porous structure directly on electrode surface.[195] Compared with other methods, this process is simplified due to the elimination of the troublesome procedures used for the removal of traditional templates and the resulting 3D PNMNs can be used directly for myriad applications. A significant number of 3D PNMNs were prepared using the H_2 bubble templates directly and indirectly. The direct electrodeposition of 3D noble metallic foams, such as Au,[197] Ag,[198] Pt,[199] Pd,[200] and bimetallic nanostructures,[201,202] can occur more quickly using precursor ions of noble metals in solution, while the indirect method involves the formation of 3D PNMNs via galvanic replacement reaction.[203−205] It is worth noting that the filament sizes within the metal foam are usually larger than 10 nm and not favorable

DOI: 10.1021/acs.chemrev.5b00255
Chem. Rev. XXXX, XXX, XXX−XXX

for their applications. In addition to this dynamic template, porous nanostructures on the electrode can also be realized through underpotential deposition,[206] electrochemical dissolution and reduction,[207,208] etc.[209] In these electrochemical approaches mentioned above, appropriate control of the key deposition parameters on the morphology of the metal foam, including the deposition potential, deposition time, and electrolyte, allows for the precise design of nanostructures composed of the deposited products with advanced electrochemical performance. In addition, other methods, such as dealloying, can be integrated to further modify the morphology and composition, enabling more functionalities and advanced applications.

3.1.5. Oriented Attachment Derived Network-Like Nanostructures. In addition to template-directed growth, an oriented attachment-based strategy is frequently adopted to fabricate network-like nanoarchitectures. Oriented attachment involves the attachment of existing nanocrystals along a given crystal orientation and then generation of nanowire networks. Liu et al. utilized Triton X-114 as a structure-director and weak binding stabilizer to produce ultrathin Au, Pd, and Pt nanowires network by KBH_4.[210,211] The formation of the final product was attributed to the fact that TX-114 preferentially adsorbed on a specific facet, rendering NPs capable of attaching to each other via the less covered facets to form NWs. This method was also extended to PdCu[212] and AuCu[213] network-like nanostructures. Yang et al. described the fabrication of PtAg alloy nanowire-like nanostructure by the assistance of oleylamine (OAm) and oleic acid (OA) through oriented attachment.[214] They found the formation of worm-like nanowires occurs largely at a composition around $Pt_{50}Ag_{50}$. As shown in Figure 18, there was little change in the width of nanowires throughout the whole process, illustrating that these PtAg nanowires transformed from pristine NPs formed at initial stage through oriented attachment. Experiment and simulation results indicated the evolution of alloy nanowires was largely initiated by the interaction between the binding energy of stabilizers on alloy surfaces and atom diffusion at the interface upon nanoparticle collision. Taking advantage of interactions between surface ligands and metals, a series of Pt,[215,216] Pd,[217,218] and Au-based[219] worm-like nanowires were produced by a hydrothermal method. It can be rationally envisioned that multiple sophisticated metallic nanowire networks may be constructed when more versatile surfactant are accurately utilized in this solution-based synthesis.

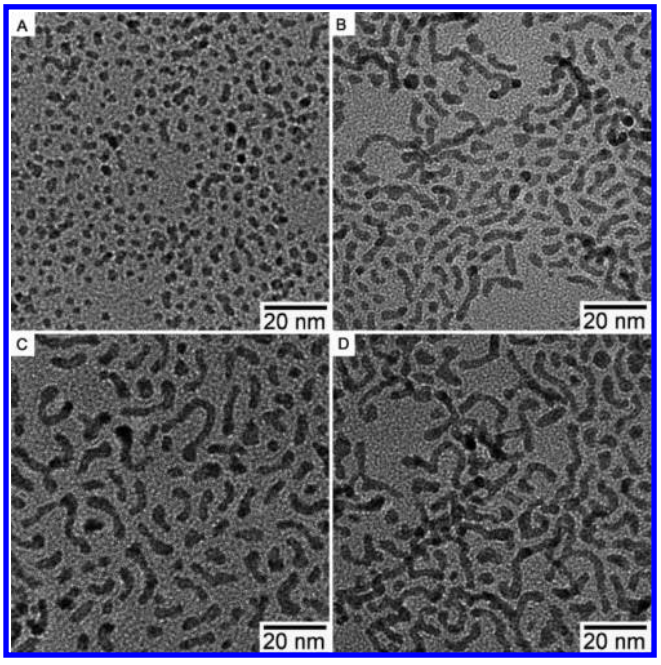

Figure 18. TEM images of $Pt_{53}Ag_{47}$ alloy nanostructures at different reaction stages: (A) 2, (B) 10, (C) 30, and (D) 180 min. Reprinted with permission from ref 214. Copyright 2010 American Chemical Society.

3.1.6. Self-Assembly Derived Nanosponges. Self-assembly is a facile route for the formation of sponge-like nanostructures from single metal NPs.[220] The capping agents anchored on the surface are favorable for the stability of the colloidal Au NPs in solution due to the presence of electrostatic repulsion, which is provided by the electric double layer surrounding the nanoparticle. The force of the electric double layer is greatly depended on the ionic strength of the solution and the Au NPs aggregation could be observed with the color changing from red to blue when excessive salt is intentionally introduced into the Au NPs.[221] It is revealed that the introduction of halide ions will replace the capping agent on the surface of Au NPs and result in the coalescence and fusion of the Au NPs to construct sponge-like nanostructures.[222,223] Additionally, sponge-like Au nanostructures were formed by precisely controlling the solution pH in aqueous media[224] or by the addition of $NaBH_4$.[225] However, development of a simple way to finely tailor the ligaments and pores size of the Au nanosponges still remains a great challenge. Zhang et al. systematically investigated the influence of various halide ions (F^-, Cl^-, Br^-, and I^-) on the resulting Au NPs.[223] As shown in Figure 19, Br^- and I^- ions were strongly linked to Au NPs surface and the different affinities of halide ions toward the Au NPs play a critical role in tuning the evolution process of the sponge-like Au nanostructures. The citrate ions linked on the surface of Au NPs were replaced by the halide ions to different extents. This displacement directly affects the fusion and aggregation behaviors of the Au NPs and finally the evolution of various nanosponges. Moreover, Au nanosponges prepared via hydrothermally[226] or thermally[227] activated self-assembly of Au NPs were also reported previously.

3.2. Hollow Nanostructures

Hollow metallic nanostructures have aroused great attention due to their exceptional properties and wide applications.[228,229] These unique nanostructures have a unique combination of two surfaces (internal and external), cavities and pores in the wall surfaces, and tunable morphologies and compositions. These properties are particularly advantageous for electrocatalysis. Recently, template methods, including galvanic replacement, the Kirkendall effect, surface-protected etching and other efficient approaches, have been demonstrated to prepare a series of hollow metallic micro/nanostructures with some unique characteristics, such as finely tailored sizes and shapes, porous walls, hollow interiors, as well as tunable compositions.

3.2.1. Galvanic Replacement. Among these strategies that have been reported to fabricate such unique hollow nanostructures, galvanic replacement reactions offer a particularly effective, versatile, and robust approach for the generation of hollow nanostructures by replacing original metal or metal oxide sacrificial templates. These replacement reactions are driven by the redox potential difference of the two metal species. After the first report on the fabrication of Au

DOI: 10.1021/acs.chemrev.5b00255
Chem. Rev. XXXX, XXX, XXX−XXX

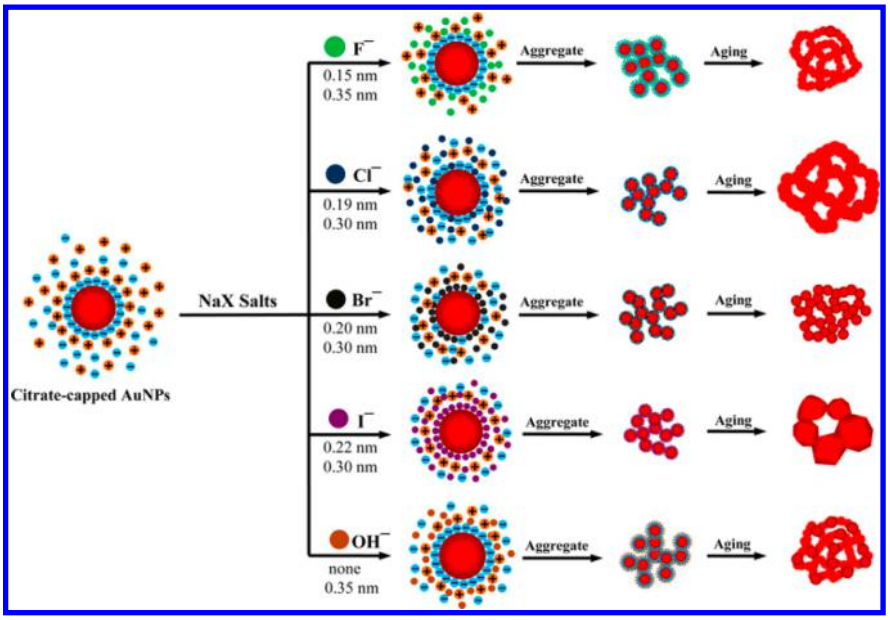

Figure 19. Effects of halide ions on the Au NPs and formation of sponge-like Au nanostructures. Reprinted with permission from ref 223. Copyright 2014 American Chemical Society.

hollow nanostructures from Ag NPs,[230] several research groups successfully extended the method to create other complex, multifunctional porous nanostructures and thus explore their novel applications over the past decade.[231−234] For example, using morphology controlled Ag nanostructures as sacrificial templates, a wide range of complex hollow nanostructures, such as spherical nanoshells,[235] core−shell NPs,[236] nanodots,[237] nanocages,[238] nanotubes,[239] nanoframes,[240] and nanodendrites[241] composed of Au, Pd, Pt, and multimetallic compositions, have been prepared via galvanic replacement reactions. Specifically, Xia and colleagues systematically uncovered the detailed mechanism of the galvanic replacement reaction between Ag NP and $HAuCl_4$ in aqueous solution.[242,243] As shown in Figure 20, the whole process of replacement reaction included two distinctive stages.[231] At the initial stage, replacement reaction started at specific sites with relatively high surface energies and then seamless hollow nanostructures with smooth Au−Ag alloy walls were evolved through an integration of galvanic replacement with alloying. Ag atoms also simultaneously migrate into the Au shell to form a seamless, hollow nanostructure with Au−Ag alloy wall. The latter stage refers to the dealloying process that selectively dissolves the Ag atoms from the resulting alloyed wall, leads to morphological reconstruction, and eventually, induces the evolution of porous nanoboxes or even fragments of nanoboxes. This mechanism for galvanic replacement is applicable irrespective of the morphology and composition of the sacrificial templates as long as the presence of appropriate reduction potentials difference between the two metals involved.

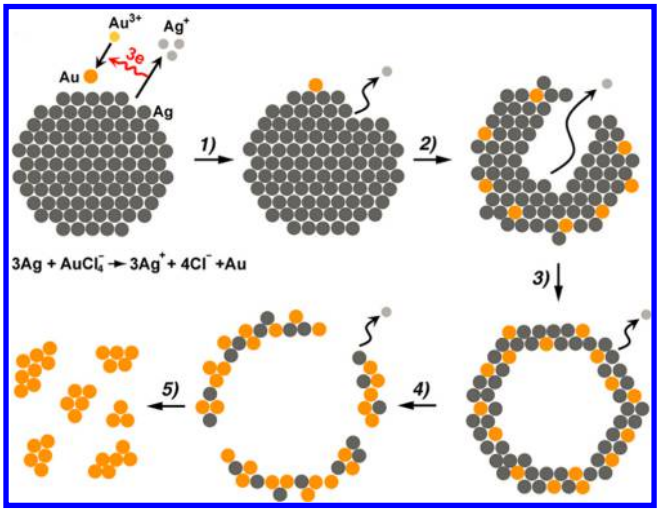

Figure 20. Schematic illustration of the morphological and structural evolutions at different stages of the galvanic replacement reaction between Ag NP and $HAuCl_4$ in an aqueous solution. Reprinted with permission from ref 231. Copyright 2013 Wiley-VCH.

Several key parameters, such as metal precursors, reaction temperature, and the additional reagents, have an influence on accurately controlling the final products with profuse morphologies and compositions and creating more functional properties for their applications. The alloying process at the initial step of galvanic replacement is critical to maintain the template morphology. However, the choice of metal precursors was claimed to have a significant influence on the resulting nanostructures. For instance, Xia et al. found that reaction of Ag nanocubes with Na_2PdCl_4 induced the formation of smooth, single-crystal nanoboxes comprised of a Pd−Ag alloy, while poly crystalline nanoboxes with bumpy surfaces comprised of Pt NPs were obtained when Na_2PtCl_4 was introduced.[244] The morphological differences observed were attributed to the fact that, different from Au and Pd, Pt are not inclined to form a conformal Pt−Ag alloy because of the difficultly in solid−solid interdiffusion over the entire Ag surface. They also investigated the effects of Au precursors with different chemical valences (e.g., $AuCl_2^-$ and $AuCl_4^-$) on the galvanic replacement reactions with cubic Ag nanostructures (Figure 21).[245] In comparison to Au^{3+}, Au−Ag alloy nanoshells with thicker walls were formed during the first stage, further intriguing the occurrence of the incomplete dealloying of Ag from Au at the later stage of replacement when using Au^+. These distinct differences observed for these two cases were ascribed to the

DOI: 10.1021/acs.chemrev.5b00255
Chem. Rev. XXXX, XXX, XXX−XXX

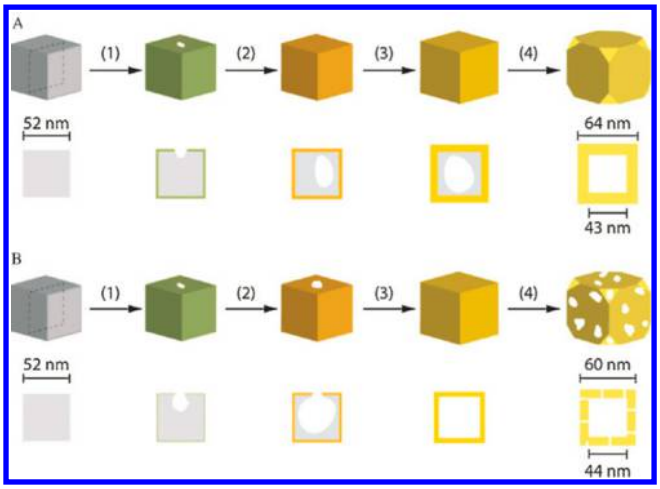

Figure 21. Schematic illustrating of the effect of different precursors, i.e., (A) $AuCl_2^-$ and (B) $AuCl_4^-$, on the morphological and structural evolution during the galvanic replacement reaction using Ag nanocubes as sacrificial template in an aqueous solution. The cross-sectional view corresponds to the plane along the dashed lines. Reprinted with permission from ref 245. Copyright 2008 Wiley-VCH.

differences in reaction stoichiometry, originating from the Au precursors with different valence states. In another report, Yu et al. confirmed that the valence of the chosen metal precursors plays a key role in selectively synthesizing Pt nanotubes, Pt nanowires, and Pd nanowires using ultrathin Te nanowires as sacrificial templates.[246] When H_2PtCl_6 was added, Pt nanotubes derived from Te can be facilely obtained. In contrast, due to the stoichiometric relationship, Pt and Pd nanowires were obtained instead of nanotubes under similar reaction in the presence of Pt^{2+} and Pd^{2+}, respectively. Variations in external factors can inevitably influence the actual values of the reduction potentials of the metal precursors, which may alter and even reverse the direction of a replacement reaction. Millstone et al. demonstrated that OH^--substituted $[PtCl_6]^{2-}$ showed a high reduction potential and can react with Au nanoprism to produce mixed metal nanoframes.[247] I^- ions induced highly stable Ag@Au core–shell nanoplates[248] and hollow rhodium nanotubes[249] can be realized because the reduction potentials of the metal precursors can be effectively tuned. With regard to the reaction temperature, the evolution of smooth shells rather than rough shells was achieved using Ag as template at the high temperatures.[242,250] This is because the AgCl solubility at different temperatures has an obvious effect on the precipitates as well as interdiffusion rates between metal precursors and Ag template.

It has been generally accepted that the surface free energies of the low-index facets of an fcc noble metal crystal decrease in the order γ (110) > γ (100) > γ (111). There is no facet selectivity in the process of galvanic replacement when the templates are covered by the same facet. In contrast, the dissolution of atoms should initiate from facets with higher surface free energies, while the deposition of the other metal atoms should proceed on the facets with lower surface free energies regardless of the size and shape of the facets. The effects of the facet directing agents are more profound in the construction of diverse nanomaterials with desired facets.[249] The intentional introduction of these capping agents changes the surface free energies of the specific facets and, thus, selectively produces novel hollow nanostructures. The prominent example is that Ag cuboctahedrons, enclosed by six (100) and eight (111) facets, were adopted as sacrificial templates to synthesize well-defined nanocages.[251,252] Due to the involvement of poly(vinylpyrrolidone) (PVP), the removal of Ag atoms initiated from the (111) facets, while the deposition of Au atoms proceeded on the (100) facets stabilized by PVP. In addition, the morphological and structural evolution of the galvanic replacement reaction between $PtCl_6^{2-}$ and a Pd nanocube whose (100) facets were adsorbed with Br^- was systematically studied.[253] Pd atoms on the (100) facets of the nanocube were preferentially oxidized and removed, leading to the evolution of Pd–Pt concave nanocubes and eventually octapods.

Apart from tuning the surface free energies of facets as mentioned above, surfactants were also used to adjust the reduction kinetics of metal precursors, enabling the initial formation of active metals and subsequent using them as the template to synthesize hollow nanostructures through one-step

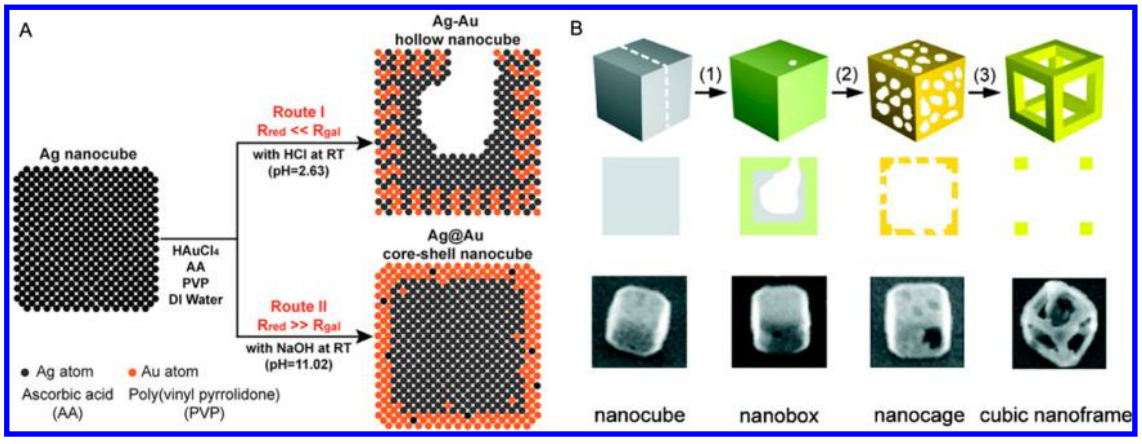

Figure 22. (A) Schematic illustration of the two possible routes and products for syntheses that involve Ag nanocubes and $HAuCl_4$ in the presence of a weak (route I) and strong (route II) reducing agent based on AA at different pH values. The structure of the product is determined by the AA reduction rate (R_{red}) relative to the galvanic reaction rate (R_{gal}). Reprinted with permission from ref 262. Copyright 2014 American Chemical Society. (B) Schematic illustration of a nanocage formation composed of a Au/Ag alloy and then a cubic nanoframe composed of pure Au by selectively removing the Ag atoms from a Au/Ag alloy nanobox with an aqueous etchant based on $Fe(NO_3)_3$ or NH_4OH. Reprinted with permission from ref 238. Copyright 2007 American Chemical Society.

DOI: 10.1021/acs.chemrev.5b00255
Chem. Rev. XXXX, XXX, XXX–XXX

method. Upon addition of specific surfactants, it is possible to fabricate metallic hollow nanostructures when all the reactants are added to the container at the same time.[254] Of these hollow nanomaterials constructed through a one-pot approach, Pt−Cu alloy with hollow nanostructures have been widely investigated. Novel cubic $PtCu_3$ nanocages were prepared through dissolution of $H_2PtCl_6{\cdot}6H_2O$, $Cu(acac)_2$, and CTAB in OAm, with subsequent solvothermal process.[255,256] Due to the introduction of CTAB, the reduction order of Pt and Cu species were reversed and therefore Cu nanocrystals are initially evolved although the standard reduction potential for Cu^{2+}/Cu (0.34 V) is more negative than that of the Pt^{2+}/Pt pair (1.18 V). Then, the in situ preformed Cu nanocrystals can react with Pt species through galvanic replacement reaction, finally leading to the evolution of $PtCu_3$ hollow nanocages. Similar mechanism was also postulated in the construction of Pt−Cu hollow nanocrystals[257] and highly open rhombic dodecahedral PtCu nanoframes.[258] Moreover, through glycine-mediated sequential reduction kinetics, Wang et al. presented a simple method to fabricate Pt−Cu nanostructures with controlled morphologies through one-step hydrothermal approach.[259,260] It is found that glycine added was important to alter the reduction kinetics of metal precursors, which enable the first reduction of Cu^{2+} ahead of H_2PtCl_6 and galvanic replacement reaction between Cu and H_2PtCl_6. Using glycine as surface controller and coreductant, three kinds of Pt−Cu alloy nanocrystals, i.e., dendrite, yolk-cage and box, could be successfully realized using PVP as reducing agent and stabilizer through simply modulating the glycine concentration.[260] In other report, combing with shape controllers (NaI), surface controller (ethanolamine) and stabilizing agent (PVP), the synthesis of octahedral Pt−Cu nanoframes in the presence of glycine were facilely realized.[259] It is anticipated that this galvanic replacement reaction based on the in situ formed active metals can also applicable to synthesize other bimetallic/multimetallic hollow nanostructures with the assistance of appropriate surfactants and/or other reagents.

In some cases, additional reagents, such as reducing/oxidizing agents, were added to prevent the replacement reaction process or further control the resulting nanostructures with structural complexity.[261,262] Qin et al. proposed a robust route to create Ag@Au core−shell nanocubes by directly depositing Au atoms on the surfaces of Ag nanocubes as conformal, ultrathin shells.[262] As shown in Figure 22A, due to the introduction of the reducing agent AA to this system, $AuCl_4^-$ will be re1duced to generate Au atoms through two parallel reactions involving Ag and AA, respectively. The reduction by Ag is a galvanic reaction (with a rate of R_{gal}) that will induce the evolution of a hollow structure whereas the reduction by AA (with a rate of R_{red}) will lead to the evolution of a conformal Au shell on the Ag nanocube. As a result, the final products can be well regulated by altering the pH value of the reaction system and, thus, optimizing the reduction power of AA. Significantly, Ag@Au core−shell nanocubes exhibited surface plasmonic properties essentially identical to those of the original Ag nanocubes, while the SERS activity showed a 5.4-fold enhancement due to an improvement in the chemical enhancement. Similarly, controlled syntheses of PdPt alloy hollow nanostructures, including nanocages with porous walls, dendritic hollow structures and Pd@Pt core−shell dendritic nanocubes, were also reported by Han's group.[263] Fine inhibition of galvanic replacement via the addition of a fast parallel reduction by AA and hydrazine also allowed for the preparation of mesoporous, hollow Pt nanoarchitectures with controlled shell thicknesses[264] and Pd−Ni−Pt core-sandwich-shell NPs,[265] respectively. Other strong reducing agents, such as hydroxylamine paired with NaOH, were also used to effectively suppress the replacement reaction between a Ag template and metal precursor and finally induced the formation of Ag@Au core−shell nanoprisms.[266] As mentioned above, the dealloying process in the later step of the galvanic replacement corresponds to the selective removal of template atoms from the alloyed wall. Xia et al. found that $Fe(NO_3)_3$ could be used as a wet etchant to separate the dealloying of the Ag from the deposition of the Au, making the dealloying process and the morphology of the product better controlled (Figure 22B).[238] The well-defined Au−Ag nanocages could be facilely tuned by simply controlling the amount of $Fe(NO_3)_3$ added. Using this different dissolution mechanism, the same strategies using the different etchants, such as H_2O_2 or NH_4OH were also reported for the synthesis of novel metallic hollow structures.[267−269] In another report, Lu et al. developed a controlled galvanic replacement reaction for the synthesis of Pt/Ag bimetallic nanostructures characterized by controlled number of void spaces.[270] The essence of this reaction lie in the fact that use of HCl caused rapid AgCl precipitation on the surface of Ag nanocubes, which could utilize as a removable secondary template to further deposit Pt. Furthermore, the quantity of void spaces can also be rationally controlled by changing the amount of HCl added or by introducing PVP to the reaction system. Together, the utilization of these additional reagents allows us to extend galvanic replacement to the fabrication of more complex metallic nanostructures with optimized properties.

Coupling with other chemical/physical processes, galvanic replacement provides an alternative for synthesizing hybrid PNMNs characterized by complex configurations in terms of geometries and compositions. In early reports, Sun et al. prepared hollow metal nanostructures (nanoshells and nanotubes) using sequential galvanic replacement.[271,272] At the same time, hollow bimetallic shell−shell nanocages were also prepared by Mahmoud's group using this method.[273,274] Recently, Park et al. developed a synthetic strategy for preparing Pt@Au nanorings.[275] This synthetic approach comprised of successive reactions involving site-selective growth of Pt on the rims of Au nanoplates through galvanic replacement, the subsequent etching of the Au nanoplates, and finally, followed by regrowth of Au on the Pt rim. Not only can Au^{3+} ions acted as metal precursors but also an etchant during the process, aiding in the formation of the resulting product. Sun et al. synthesized interfaced asymmetric dimers composed of more complex compositions and geometries by integrating the controlled design of interfaced dimers with galvanic replacement reactions (Figure 23).[276] It is believed that the strong coupling effect resulting from the direct contact in the interfaced dimers greatly contribute to their unique properties and potential applications. The smallest metallic nanobowls were also obtained by applying the concept of a protecting group (magnetic NPs) to colloidal synthesis, which could be spontaneously detached from the reactants during the reaction and could easily be removed using a magnet.[277]

Furthermore, some other nonprecious metal NPs, including Ni,[278−280] Co,[281,282] Cu,[283,284] and even the more active Mg[285] and Zn,[286] were also employed as sacrificial templates for constructing various hollow nanostructures. Among them, Pt monolayer electrocatalysts were synthesized using galvanic

DOI: 10.1021/acs.chemrev.5b00255
Chem. Rev. XXXX, XXX, XXX−XXX

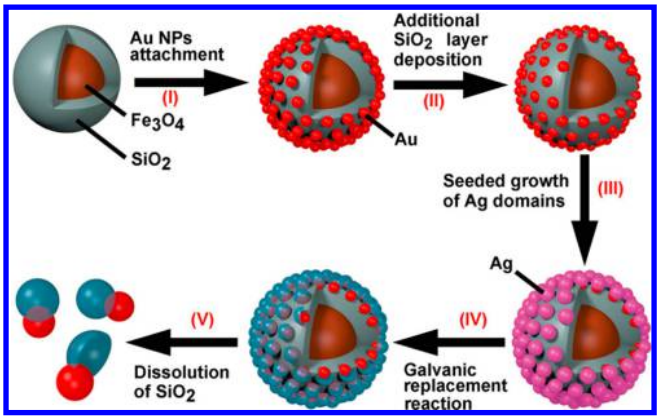

Figure 23. Schematic illustration of the synthesis of interfaced dimers made of Au NPs and bimetallic nanoshells: (I) seeding of Au NPs on the surface of a superparamagnetic Fe_3O_4@SiO_2 core−shell colloid; (II) selective deposition of a second SiO_2 layer on the original SiO_2 shell; (III) epitaxial overgrowth of Ag domains on the exposed surfaces of the Au seeds; (IV) galvanic replacement reaction between the Ag domains with appropriate noble metal precursors; (V) release of the interfaced Au NP-bimetallic nanoshell dimers from the colloid by removing the SiO_2 layer. Reprinted with permission from ref 276. Copyright 2014 Wiley-VCH.

replacement of an underpotentially deposited Cu monolayer on other metal or alloy cores.[287−289] These unique nanocatalysts characterized by Pt monolayer nanostructures exhibited high Pt mass activities and have significant potential for use as promise in ORR electrocatalysts. Compared to the above widely reported templates, non-noble metal templates have many obvious advantages. First, the use of these nonprecious metals significantly decreases the cost of the metal-based hollow nanostructures in comparison to Ag and Pd sacrificial templates. Furthermore, the generation of undesirable component (e.g., AgCl) is avoidable and further simplifies the experiment process. Moreover, some unexpected results could be obtained due to the unique properties of the templates. For example, chain-like CoPt, ring-like CoPt hollow NPs[290] and AuPt bimetallic hollow tube-like nanostructures[291] can be synthesized through a facile yet efficient process at a relatively low temperature. Due to the good dispersion, small diameter, high aspect ratio and valence, 1D Te nanowires provided many opportunities for the construction of various 1D noble metal-based nanomaterials, such as monometallic nanowires/nanotubes,[246] bimetallic core−shell nanostructures[292−294] and bimetallic alloys.[295,296] Some oxides also hold great promise for being used as both templates and reductants to create porous hollow noble metal-based nanostructures. Fang et al. synthesized polyhedral Au hollow mesostructures using Cu_2O as the templates, which possessed a highly roughened surface topography and exhibit a remarkably high SERS activity.[297] Xu et al. further investigated this reaction system and explored interfacial nanodroplets as structural guides to fabricate hierarchical porous Au particles using octahedral Cu_2O (Figure 24).[298] Interfacial nanodroplets derived from surfactant-free emulsions were discretely distributed on the surfaces of template particle, which were employed as soft templates to direct the evolution of Au porous nanostructures. The spontaneous deposition of Pt on the surface of Mn_3O_4 NPs through a galvanic replacement process between Mn_3O_4 and $[PtCl_6]^{2-}$ was also demonstrated by Kim's group.[299] This new approach provided a general strategy for loading metal nanocatalysts on metal oxide surface and fabricating functional hybrid composites, further enhancing their electrocatalytic performances.

3.2.2. Kirkendall Effect. The Kirkendall effect is defined as a nonequilibrium mutual diffusion process through the interface of coupled materials.[300,301] The creation of voids, i.e., Kirkendall voids, at the interface is the major consequences of the Kirkendall effect because of the differences in the diffusion rates of the different metal atoms. The Kirkendall effect has received significant attention and has wide applications in the generation and design of hollow nanostructures.[302−305] Considering the universality of the diffusion process, the Kirkendall effect might make significant contributions to the formation of some noble metal-based hollow nanostructures. It is believed that the galvanic replacement reaction occurs accompanying with the Kirkendall effect, both of which played significant roles for evolving hollow interiors between the sacrificial templates and metal precursors.[306−308] Specifically, combining the galvanic replacement with the Kirkendall effect, Puntes and co-workers reported a novel strategy to create complex hollow nanostructures at room temperature.[302] In this procedure, multimetallic hollow NPs with various morphologies and compositions were obtained using Ag nanocrystals as templates. Recently, Yang's group

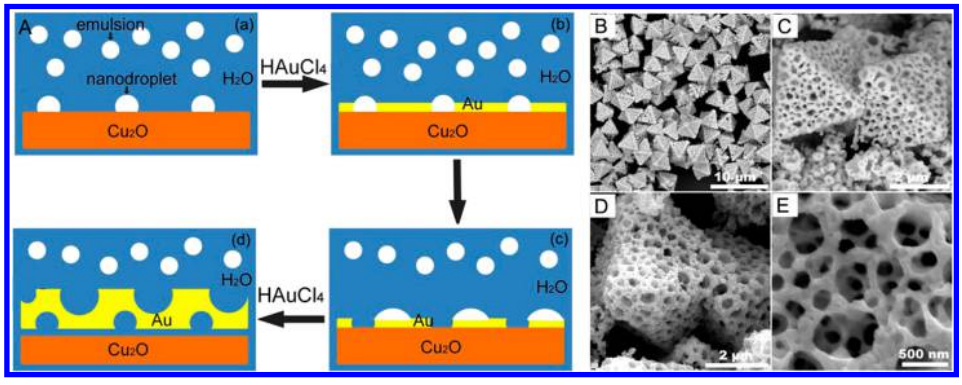

Figure 24. (A) Scheme of synthesis of 3D porous Au nanostructures. (a) Formation of interfacial nanodroplets on the surface of Cu_2O particle, (b) formation of first porous Au layer via galvanic reaction, (c) formation of new interfacial nanodroplets at the as-formed Au porous layer surface via continuous adsorption of emulsions, (d) further formation of second porous Au layer on the top of the first Au layer. This process continued until the formation of 3D porous structure. (B−E) SEM images of porous Au nanostructures. Reprinted with permission from ref 298. Copyright 2014 Nature Publishing Group.

DOI: 10.1021/acs.chemrev.5b00255
Chem. Rev. XXXX, XXX, XXX−XXX

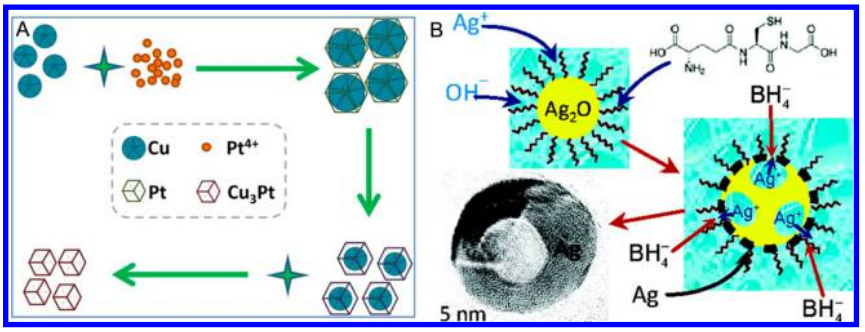

Figure 25. (A) Schematic illustration for the structural evolution from Cu@Pt core−shell NPs to alloy Cu_3Pt nanoframes in toluene at ambient conditions. Reprinted with permission from ref 309. Copyright 2014 Nature Publishing Group. (B) Schematic illustration of synthesis of single crystal hollow Ag NPs in a fast reaction-diffusion process. Reprinted with permission from ref 311. Copyright 2011 American Chemical Society.

synthesized polyhedral Cu_3Pt alloy nanoframes through a unique structural evolution.[309] In detail, polyhedral Cu@Pt core−shell NPs were first synthesized via the anisotropic deposition of Pt on multiply twinned Cu seed NPs (Figure 25A). Thanks to the Kirkendall effect between the Cu core and Pt shell, Cu_3Pt alloy nanoframes can be subsequently obtained, which are more effective for ORR.

Qi et al. presented the controlled construction of hollow Ag microstructures employing Ag_3PO_4 as the sacrifice template and AA, hydrazine and $NaBH_4$ as the reducing agents.[310] The resulting Ag structures were closely associated with the inward diffusion rate of the reducing agent versus the outward diffusion rate of the Ag^+ ions. In detail, single-walled and double-walled rhombododecahedra can be prepared using AA and hydrazine as the reducing agents, respectively. This finding provided favorable support for the Kirkendall effect and could be extended to the other materials via accurately controlled core material solubility and ion diffusion rates. Recently, Markovich and co-workers synthesized hollow Ag nanostructures using the fast reaction-diffusion process.[311] As shown in Figure 25B, solid Ag_2O NPs can also be evolved to hollow Ag nanospheres because of the Kirkendall effect. This facile method may contribute to the fabrication of a large variety of hollow metal nanostructures with varying compositions and shapes, which have significant potential in niche applications.

3.2.3. Etching Template. Etching is another important approach for preparing hollow nanostructures. Several types of hollow nanomaterials synthesized via selective etching processes have been demonstrated. For example, Wang et al. developed a simple approach to create Pt−Pd bimetallic nanocages with a porous dendritic shell. This unique nanostructure can be facilely obtained by selective chemical etching of Pd from dendritic Pd@Pt core−shell NPs.[312] Functional porphyrin nanowires, namely Zinc meso-tetra(4-pyridyl)porphyrin (ZnTPyP), were first synthesized through a modified confined self-assembly protocol.[313] As shown in Figure 26A, photocatalytic deposition of Pt shell networks can be achieved on the surface of the obtained template. After acid dissolution of ZnTPyP, well-defined Pt nanotubes with interconnected nanoporous shell were produced. Note that hollow Pt octahedrons can also be facilely achieved by using octahedral porphyrin templates. The corrosion combined with template approach was also reported for the preparation of different types of nanoporous framework. Stellated Pt NPs with hollow nanostructure,[314] hollow Pt nanospheres,[315] and porous Pt−Ni−P composite nanotube arrays[316] were also synthesized via chemical etching of Ag templates, SiO_2 nanorod arrays and ZnO nanorod arrays, respectively. In contrast to post-treatment

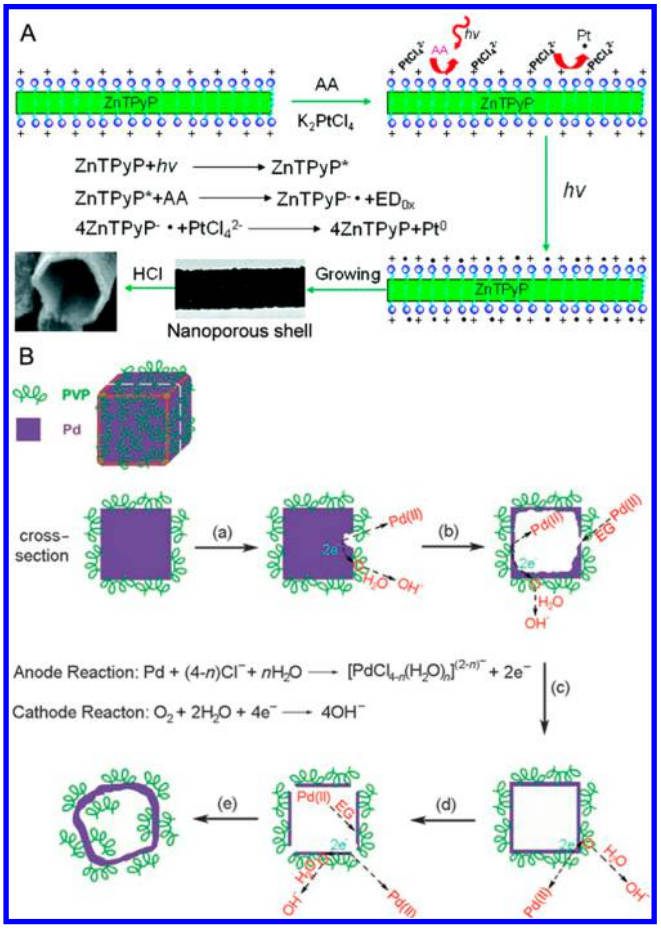

Figure 26. (A) Templated photocatalytic synthesis of hollow Pt nanostructures. Reprinted with permission from ref 313. Copyright 2011 American Chemical Society. (B) Schematic illustration of all the major morphological transformation involved in the construction of Pd nanoboxes and nanocages by corrosive etching. Reprinted with permission from ref 318. Copyright 2005 Wiley-VCH.

with strong acid/base, Chio et al. reported that ZnO nanowires can offer heterogeneous nucleation sites and facilitate the reduction of metal precursors and metal atoms deposition on the surface of ZnO nanowires by lowering the activation energy for nucleation.[317] Simultaneously, as the reaction proceeds, the pH value of the reaction system progressively decreases and leads to the removal of the ZnO nanowires. In another report, Xiong et al. presented a unique morphological evolution of single-crystal Pd nanocubes during corrosive etching and

DOI: 10.1021/acs.chemrev.5b00255
Chem. Rev. XXXX, XXX, XXX−XXX

successfully synthesized nanoboxes and nanocages by controlling the reaction time through a one-pot synthetic strategy in the absence of exotic templates.[318] As shown in Figure 26B, O_2, Cl^-, and H_2O are all critical for the initiation of pitting on the surfaces of Pd nanocubes. Typical process, including pitting at a specific site, formation of the hollow nanostructures and the following completely enclosed Pd nanobox, Pd nanocages due to the selective dissolution, and structural reconstruction were successively involved to generate target product. In addition, a large amount of capping agents adsorbed on the surface of each Pd nanocube and the existing thin Pd oxide also ensure the formation the hollow nanostructures. Correspondingly, the SPR peaks of Pd nanostructures exhibited a wide range from 410 to 520 nm because of the formation of the hollow nanostructures. This type of oxidative etching mechanism was also presented to account for the one-pot synthesis of Pd_2Sn hollow nanostructures.[319]

3.2.4. Soft Template. Soft templates, including microemulsion approach and surfactant micelles, have been widely used for synthesizing hollow nanostructures.[320,321] In the case of microemulsion approach, an emulsion can be effectively evolved when two immiscible liquids are mixed together through mechanical agitation. Liquid droplets of one phase can be dispersed in the other continuous phase. The evolution of the hollow nanostructures is ascribed to the fact that the shell materials exclusively deposit around the interface between the emulsion droplets and the continuous phase.[322,323] Microemulsions were applied for the first time to prepare hollow Au nanospheres. The resulting hollow nanospheres have a wall thickness of 2−6 nm and an inner diameter of 20−40 nm.[324] With regard to the surfactant micelles, amphiphilic molecules can self-assemble into micelles or vesicles when their concentrations are over CMC. They display different kinds of morphologies in the nanometer scale and are excellent templates for the construction of hollow nanostructures.[325,326] A wide variety of micelles or vesicles have been employed as soft templates for fabricating various hollow nanostructures.[327−329] For the noble metal nanostructures, Li and Zhang found that tetrabutylammonium bromide (Bu_4NBr) can rapidly assembly into vesicles in water in the presence of metal precursors such as $PdCl_2$, $KAuCl_4$, $AgNO_3$, K_2PtCl_4, or the mixtures of these compounds.[329] The obtained vesicles can serve as efficient templates and carriers of metal precursors for the rapid synthesis of hollow alloy nanospheres when mixed with $NaBH_4$.

Additionally, hollow Ag nanostructures were successfully fabricated using double-hydrophilic block copolymer−surfactant complex micelles as templates, i.e., the mixed poly(ethylene oxide)-*block*-poly(methacrylic acid)-sodium dodecyl sulfate (PEO-*b*-PMAA-SDS) system.[330] However, this hollow nanostructures prepared by the above method were significantly limited because of the rough surfaces and nonuniformity in shell thickness. Furthermore, micelles containing ABA- and AB-type block copolymers become unstable when the precursor is adsorbed onto/into the coronas, resulting in the deformation of the micelles and subsequent aggregation. To address this issue, spherical core−shell-corona architecture of ABC-type asymmetric block copolymer is exploited as a novel soft template for synthesizing hollow nanostructures.[331,332] The prominent example is that Russell's group demonstrated the creation of Pt/Au concentric nanospheres using ABC triblock copolymer polystyrene-*block*-poly(2-vinylpyridine)-*block*-poly(ethylene oxide) (PS-*b*-P2VP-*b*-PEO).[333] As shown in Figure 27, when aqueous H_2PtCl_6 solution was introduced into a trifluorotoluene (TFT) solution of PS-*b*-P2VP-*b*-PEO, the

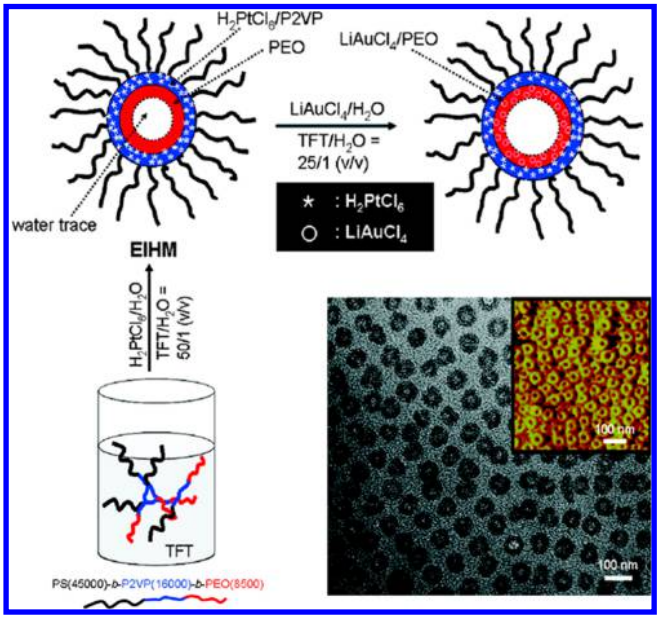

Figure 27. Schematic presentation for the synthesis of an emulsion-induced hollow micelle and the TEM image of the obtained product. Aqueous H_2PtCl_6 and $LiAuCl_4$ solutions were dispersed into the TFT solution of PS-*b*-P2VP-*b*-PEO, one after the other. First, H_2PtCl_6 (*) coordinates with the pyridine group of the P2VP, not the PEO, and then $LiAuCl_4$ (○) is exclusively coordinated with the PEO block. Reprinted with permission from ref 333. Copyright 2010 American Chemical Society.

hollow micelles were produced, comprising a water nanodroplet stabilized by PEO, H_2PtCl_6/P2VP, and PS, sequentially. In this procedure, the introduction of water plays a critical role in separating PEO from P2VP in the microphase. The insoluble Pt/PVP is well situated in between PEO and PS blocks, which is soluble in water and TFT, respectively. The $LiAuCl_4$ metallic precursor was subsequently added to enable the formation of the ($LiAuCl_4$/PEO) complex. Finally, O_2 plasma treatment was adopted to simultaneously remove the polymer and reduce the both metal precursors, realizing the fabrication of the Pt/Au concentric hollow nanospheres with the average diameter of 60 nm. Similarly, Sasidharan et al. developed a facile yet efficient protocol for the synthesis of hollow Ag nanospheres of size less than 30 nm using this type of triblock copolymer without any reducing agents.[334] Typically, the polymer was dissolved to obtain micelles. The polyethylene glycol domains of the template micelles act as both a stabilizer of the micelle architecture and as the reducing agent, similar to poly(vinyl alcohol), which simultaneously reduces metal ions and acts as the capping agent.

Besides these block copolymer-induced spherical templates, the synthesis of metallic hollow nanospheres based on liposomes was also reported by Shelnutt's group.[335] Hydrophobic Sn^{IV} octaethylporphyrin (SnOEP) was first incorporated into the unilamellar liposomes. Then, photocatalytic reduction of Pt precursors produced a number of Pt seeds, which finally evolved into the dendritic Pt nanosheets. These dendritic nanosheets joined together within bilayer to form Pt nanocages with 2 nm shell thickness and diameters up to 200

DOI: 10.1021/acs.chemrev.5b00255
Chem. Rev. XXXX, XXX, XXX−XXX

nm. Dendritic nanosheets as well as hollow interiors offer the resulting product more porosity and wide applications.

Apart from these nanosphere templates, lipid tubes have also received significant attention for the construction of hollow nanostructures. Self-assembled lipid molecules in liquid media can yield open-ended, tubular structures, making them excellent soft templates for synthesizing various nanostructures.[336,337] They have some obvious advantages as follows. Hydrophilic microenvironments of internal and external membrane surfaces provide the excellent places for chemical reactions and the hollow tubule structures can be well-inherited after the removal of the templates. The fine-tunability of lipid nanotubes, such as diameter, length and further functionalization, enable the diversity of the 1D hollow nanostructures. Besides, the formation of lipid nanotubes is rapid and favorable for the synthesis of final products. Although several significant achievements were made to fabricate 1D nanotubes, the synthesis of noble metal hollow nanostructures based on lipid tubules is little reported.[338,339] Very recently, Han's group successfully illustrated the creation of Pd nanotubes using lipid tubules as soft templates.[340] As shown in Figure 28, 1,2-

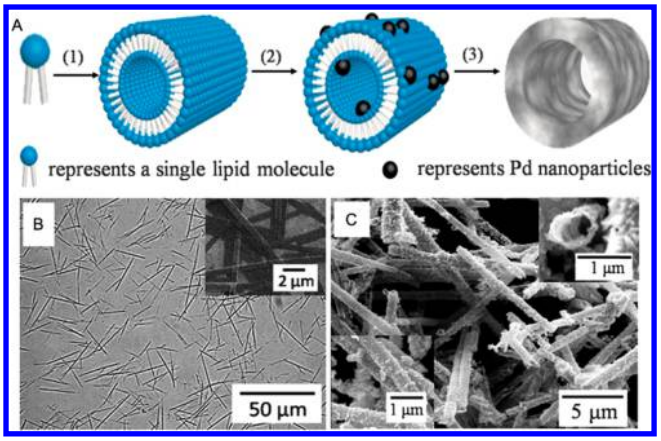

Figure 28. (A) Schematic illustration of the synthesis process of Pd nanotubes. (B) Optical micrograph of lipid tubules formed by 10 wt % DOTAP-doped $DC_{8,9}PC$. Inset: the SEM image. (C) SEM image of Pd nanotubes. Reprinted with permission from ref 340. Copyright 2015 Wiley-VCH.

dioleoyl-3-trimethylammoniumpropane (DOTAP)-doped 1,2-bis(10,12-tricosadiynoyl)-*sn*-glycero-3-phosphocholine ($DC_{8,9}PC$) tubules were first prepared, which endowed the positive charges to adsorb Pd precursors. The resulting DOTAP-doped tubules exhibited significant stability in wide pH range at optimized synthetic conditions. Using AA as reducing agent, the Pd nanotubes can be facilely produced after removal of the template within short time. It is worthwhile to note that the wall thickness of the Pd nanotubes could be efficiently tailored through the amount of metal precursors added. The obtained 1D Pd nanotubes showed high electrocatalytic activity and stability toward ethanol oxidation because of the unique hollow nanotubular structures. This facile protocol opens the new avenue to synthesize 1D hollow nanostructure with structural and compositional complexity, holding great promise for its further applications in electrochemistry.

3.2.5. Other Methods of Interest. Interestingly, Yang et al. synthesized PdCu alloyed nanocubes with hollow nanostructures using an innovative one-pot template-free approach.[341] Only solid PdCu alloyed NPs with small sizes were formed during the early stages. Then, the evolution of the PdCu alloyed nanocubes with hollow nanostructures was observed due to the self-assembly of initial formed PdCu alloyed NPs through oriented attachment mechanism. Additionally, Han et al. demonstrated a facile one-pot hydrothermal approach to synthesize well-defined Pt hollow nanostructures without any presynthesized template and structure-directing surfactant or polymer.[342] This self-templating route for the hollow nanostructures involves the in situ formation of polymeric coordination complexes followed by Pt deposition and a thermally activated hollowing process.

3.3. Highly Branched Nanocrystals

During the past decade, rational creation of colloidal noble metal NPs in solution has received a tremendous amount of attention due to control of the structure at nanoscale. Of these different types of nanocrystals, highly branched nanocrystals formed from noble metals are emerging as a new class of interesting nanostructured material and are highly attractive for many applications.[343] Combined with their large specific surface areas, low densities, rich edges, and corner atoms, these unique nanostructures with branched morphologies, such as multipod and nanodendrite, show unexpected catalytic properties and the synergistic effects from compositions and other favorable factors. The sizes and shapes of these branched nanocrystals are significantly dependent on the specific nucleation and growth processes in solution. Generally, two typical mechanisms were proposed to describe the evolution of the highly branched nanocrystals. One was overgrowth in which some small particles were initially formed as seeds and then rapidly grew into dendrites, and the other one was aggregation-based growth in which a large number of NPs aggregated in a diffusion-controlled manner.[344,345] Here, the formation of branched nanostructures based on these different mechanisms is selectively demonstrated (Table 1).

3.3.1. Overgrowth. Overgrowth has received considerable attention to precisely tune the morphology and composition of nanocrystals. In this process, the preformed nanocrystals act as seeds for further growth of the corresponding metal nanostructures. This synthetic concept has also enabled the synthesis of a variety of monodispersed NPs with highly branched morphologies and tunable compositions. Thus, intense research has been devoted to these dendritic NPs.[364] For example, Shelnutt et al. demonstrated unique 2D and 3D Pt nanodendrites through seeding and autocatalytic growth via the reduction of Pt precursors with the help of surfactants.[365] That is, spherical metal nanodentrites were obtained in micellar surfactant solutions, while dendritic Pt sheets in the form of thin circular disks or solid foam-like nanostructures were synthesized with liposomes as the template. As such, using the H_2-mediated reduction approach, Lacroix's group designed Pt nanostructures with complex morphologies, including cubic dendrites and 5-fold stars, by a fairly simple reaction of H_2PtCl_6 in OAm at different temperatures.[366] Huang et al. successfully synthesized highly porous Pd nanostructures with perpendicular pore channels using hexadecylpyridinium chloride as the structure-directing agent, AA as the reductant, and H_2O as the solvent (Figure 29).[367] As for the formation mechanism, a slow, continuous nucleation and fast autocatalytic growth, i.e. seeding/autocatalytic growth mechanism, was generally accepted to account for the growth of metallic NPs, especially Pt nanodendrites.[365,368,369] Typically, Pt nanoparticle growth

DOI: 10.1021/acs.chemrev.5b00255
Chem. Rev. XXXX, XXX, XXX−XXX

Table 1. Highly Branched Noble Metal-Based Nanocrystals

branched nanostructure	precursors	reductant, surfactant and additive	synthetic condition	ref
Pt nanodendrites	K_2PtCl_4	formic acid and Pluronic F127	ultrasonic synthesis	346
Pt nanodendrites	H_2PtCl_6	AA and NaOH	aqueous solution at 60 °C	347
Pt nanoflowers	H_2PtCl_6	HCOOH	aqueous solution at room temperature	348
Pd nanodendrites	$PdCl_2$	OA and OAm	solvothermal process	349
Pd dendrites	$PdCl_2{\cdot}(CH_3CN)_2$	toluene, OAm, OA and H_2	solution phase synthesis at room temperature	350
hierarchical Ag mesoparticles	$AgNO_3$	AA	aqueous solutionat room temperature	351
Ag dendrites	$AgNO_3$	hydroxylamine and PVP	aqueous solution at room temperature	352
star-shaped Au NPs	$HAuCl_4$	AA, CTAB, $AgNO_3$ and Au seeds	aqueous solution at room temperature	353
branched Au NPs	$HAuCl_4$	hydroxyphenol	aqueous solution at room temperature	354
PtPd alloy nanodendrites	K_2PtCl_4 and Na_2PdCl_4	AA and Pluronic F127	aqueous solution at room temperature	355
Pd and Au@Pd nanodendrites	Na_2PdCl_4 and $HAuCl_4$	AA and ODA[a]	solvothermal method	356
CoPt nanopolypods	$Pt(acac)_2$ and $Co(CH_3CO)_2$	OAm	thermolytic reduction at high temperature	357
Pt-on-Au nanodendrites	$HAuCl_4$ and K_2PtCl_4	AA and F127	aqueous solution at room temperature	358
PdAu nanodendrites	Na_2PdCl_4 and $HAuCl_4$	hydroquinone and PVP	aqueous solution at 50 °C	359
PtFe and PtRuFe nanodendrites	$Pt(acac)_2$, $Ru(acac)_3$ and $Fe(acac)_2$	DMF,[b] KI and PVP	one-pot solvothermal method	360
PtNi nanodendrites	$Pt(acac)_2$ and $Ni(acac)_2$	ODE,[c] OAm, OA and DDAB[d]	one-pot solvothermal method	361
hierarchical PtCu superstructures	H_2PtCl_6 and $CuCl_2$	PVP and NaI	hydrothermal conditions	362
1D Au/Pt and Au/Pt_3Ni nanodendrites	$Pt(acac)_2$ and $Ni(acac)_2$	OAm and Au nanowires	solvothermal method	363

[a]ODA: octadecylamine. [b]DMF: dimethylformamide. [c]ODE: octadecene. [d]DDAB: didodecyldimethylammonium bromide.

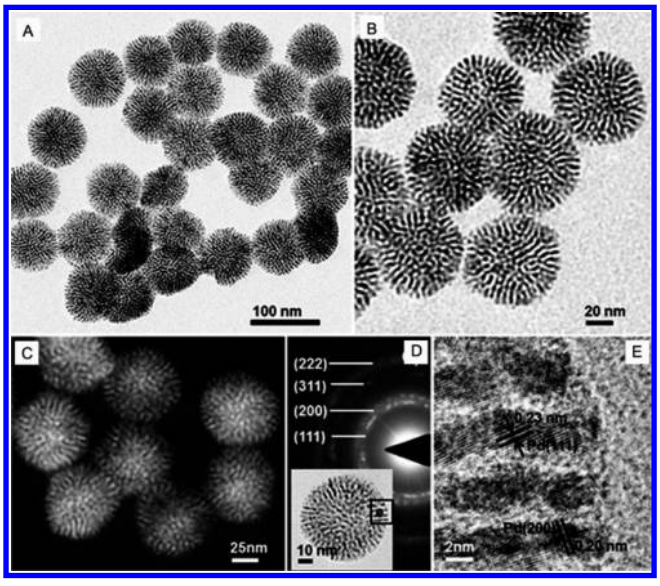

Figure 29. (A, B) Representative TEM and (C) HAADF-STEM images of as-prepared porous Pd nanostructures. (D) SAED pattern of an individual porous Pd nanostructure. Inset shows the corresponding TEM image with a box around the portion shown in (E). (E) HRTEM image of the branches of a porous Pd nanostructure. Reprinted with permission from ref 367. Copyright 2013 Wiley-VCH.

centers (seeds) were produced through the slow chemical reduction of Pt precursors by the reductant. Once the seeds reached a certain size (approximately 500 atoms), the reduction rate of Pt precursors was greatly accelerated via an autocatalytic reduction process. Single-crystal Pt dendrites on seed surface was formed via a highly anisotropic mode, further leading to the highly branched nanocrystals.

In the other cases, preformed nanocrystals were intentionally introduced and acted as growth seeds for the construction of novel nanodendrites. The advantage of seed-mediated growth is that various physical/chemical parameters, such as the precursors, the shapes of the seed and reductants and surfactants, could be selected or tuned to direct the heterogeneous growth on the surface of seed particles in a wet-chemistry preparation.[370−372] El-Sayed et al. synthesized multiarmed nanostar single crystals using tetrahedral Pt nanocrystals as seeds.[373] Yan et al. first synthesized Pd seed solutions and used them to form porous single-crystalline Pd NPs through rapid homoepitaxial growth. The initially formed Pd NPs with many small crevices then underwent oxidation etching because of the presence of Cl^-/O_2 pair in the solution, which occurred preferentially at the highly active sites in the crevices and then resulted in the porous structure. The resulting porous Pd NPs exhibited enhanced catalytically activity for the Suzuki coupling.[345] In addition to these previously mentioned monometallic nanostructures, bimetallic/trimetallic nanostructures can also be easily synthesized. Typical example is that Xia et al.[374] and Yang et al.[375] independently prepared bimetallic Pd−Pt nanodendrites. In the former report, Pd−Pt bimetallic nanodendrites were synthesized with uniform Pd nanocrystal seeds using K_2PtCl_4 and AA as Pt precursor and reducing agents, respectively (Figure 30).[374] The as-prepared Pd−Pt nanodendrites composed of a large number of Pt nanobranches on a Pd core surface exhibited excellent 3D dendritic morphologies, and the lattice fringes coherently extended from the Pd core to the Pt branches indicated that the Pt nanobranches were grown epitaxially on the surface of Pd seed because of the close lattice match between these two metals.

Engineering the structural diversity of heterogeneous metallic nanocrystals plays an important role for increasing the versatility of metallic nanostructures and widening their application range. It is noted that the aforementioned branched nanostructures are characterized by asymmetric branching patterns. The seed-mediated methods also turned out to be an effective approach to fabricate symmetrically branched metal nanostructures, where the symmetry of the seeds guides the growth of the final nanocrystals with high symmetry.[376−379] Skrabalak's group made significant contributions to the creation

DOI: 10.1021/acs.chemrev.5b00255
Chem. Rev. XXXX, XXX, XXX−XXX

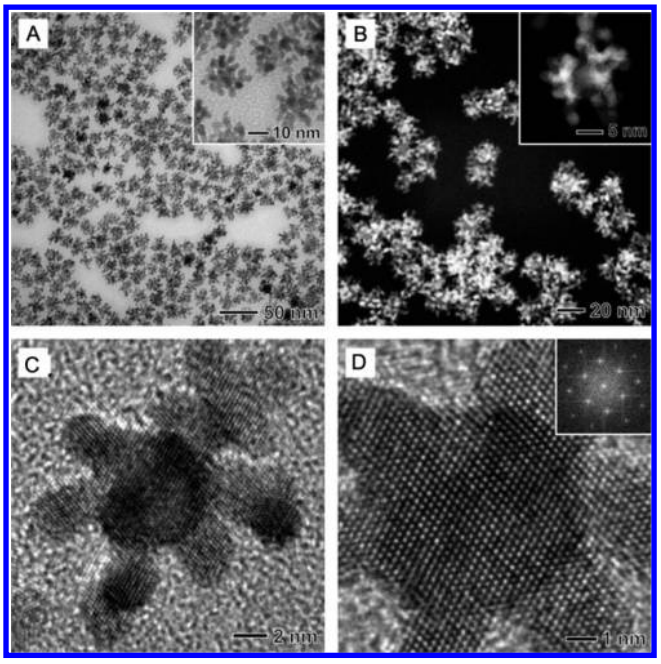

Figure 30. (A) TEM, (B) HAADF-TEM, and (C,D) HRTEM images of Pd−Pt bimetallic nanodendrites synthesized by reducing K_2PtCl_4 with AA in the presence of truncated octahedral Pd seeds in an aqueous solution. Reprinted with permission from ref 374. Copyright 2009 American Association for the Advancement of Science.

of branched Au/Pd nanocrystals with different symmetries, which were realized by seed-mediated coreduction where the seed structures determine the number and symmetry patterns of the branches.[377] Two key parameters, i.e., the number of seed vertices and the growth directions of the branches, are proved to be important for the final symmetrically branched nanostructures. In the meantime, they studied the coreduction of Au and Pd precursors with a variety of shape-controlled Au seeds and outlined the general guidelines to stellated nanocrystals.[378] Based on these important findings, metallic dendrimer hierarchical nanostructures with high symmetries have also been produced by sequential seed-directed overgrowth (Figure 31).[379] The number of branches is facilely tuned by controlling the seed shape. Iterative chain growth with concentric branching can be successfully realized by repeating the seed-mediated coreduction process. In another report, combining the galvanic replacement reaction, Lee et al. realized the selective deposition of satellite nanocrystals on specific site of the central seeds with the help of the geometry-dependent heterogeneous electron distribution.[380]

Despite the successful demonstrations of these branched noble metal nanostructures above, it remains a grand challenge for simultaneous control over the reduction and nucleation process of different metal precursors via one-step methods, constructing multimetallic dendritic structures with alloy and core−shell morphologies. Similar overgrowth processes have been reported to create metal nanodendrites and most of them are associated with the in situ formation of seeds. Wang et al. ingeniously proposed a rapid, convenient, and efficient approach to create dendritic NPs on large scale. This process can be directly achieved by reduction of Pt precursor with AA with the assistance of Pluronic F127 block copolymer.[381] More importantly, this simple method can also be applicable to the Pt-on-Pd bimetallic nanodendrites (Figure 32A)[382] and trimetallic Au@Pd@Pt core−shell NPs using different block copolymers (Figure 32B).[383] The block copolymer molecules involved in these reaction systems not only act as protecting agents but also as important structure-directing agents. The proposed strategy rationally separates the depositions of Au, Pd, and Pt temporally, enabling spontaneous evolution of multimetallic colloidal nanodendrites. Furthermore, they also found that such interesting Au@Pd@Pt NPs can be facilely achieved using PVP instead of Pluronic F127.[384] Moreover, some nonprecious metals were also introduced to construct novel branched nanostructures and, thus, enhance their catalytic performances. More recently, an effective solvothermal method for the direct preparation of 3D Pt[385] and Pt−Co[386] (Figure 32C) nanowire assemblies were reported by Lou and co-workers, both of which exhibited excellent electrocatalytic performances in fuel cell applications. Furthermore, a class of bimetallic dendrites, Pt−Cu hierarchical trigonal bipyramid nanoframes[387] (Figure 32D) and triangular pyramid caps,[388] were synthesized and successfully used as advanced nanocatalysts for formic acid and methanol oxidation, respectively.

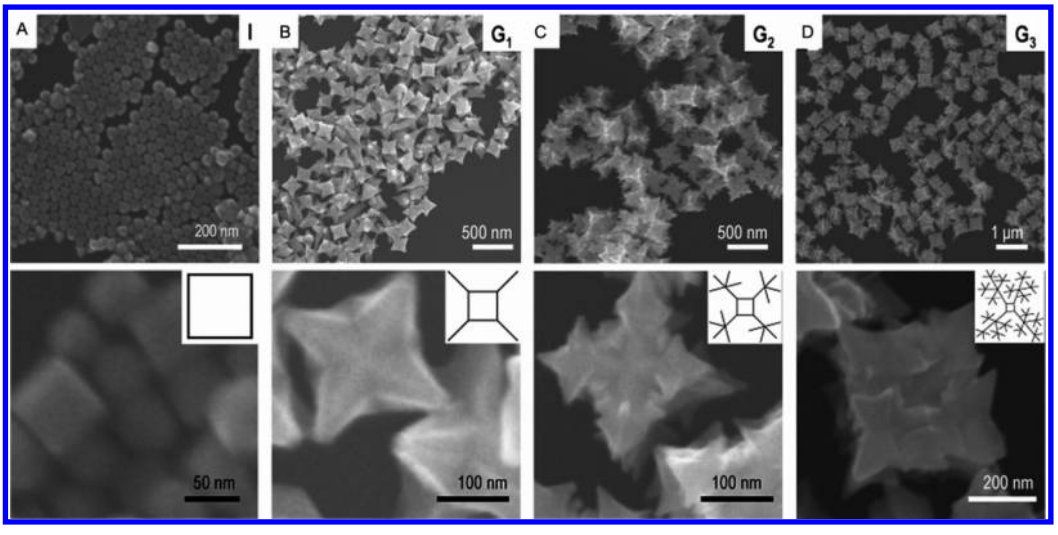

Figure 31. Low- (top) and high-magnification (bottom) SEM images and corresponding 2D stick models of (A) initiator seeds, (B) G1, (C) G2, and (D) G3 nanocrystals. Reprinted with permission from ref 379. Copyright 2014 Wiley-VCH.

DOI: 10.1021/acs.chemrev.5b00255
Chem. Rev. XXXX, XXX, XXX−XXX

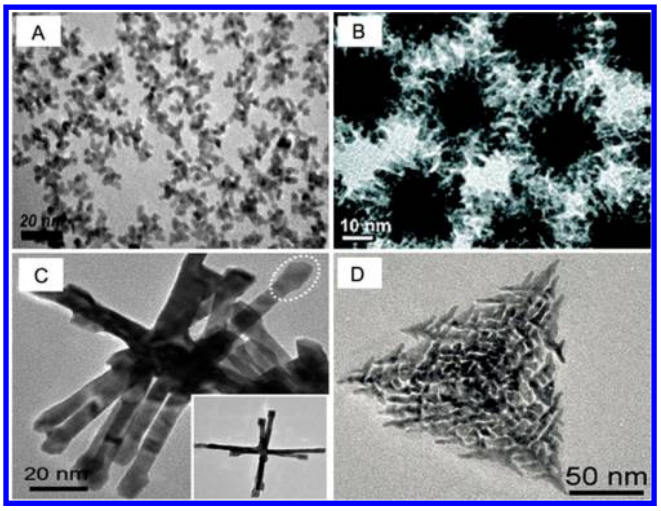

Figure 32. (A) TEM image of the Pt-on-Pd bimetallic nanodendrites. Reprinted with permission from ref 382. Copyright 2011 American Chemical Society. (B) TEM image of dendritic Au@Pd@Pt NPs. Reprinted with permission from ref 383. Copyright 2010 American Chemical Society. (C) TEM image of Pt−Co nanowire assemblies. Reprinted with permission from ref 386. Copyright 2015 Wiley-VCH. (D) TEM image of PtCu hierarchical trigonal bipyramid nanoframes. Reprinted with permission from ref 387. Copyright 2014 Wiley-VCH.

These two nanostructures possessed the same morphology due to the introduction of Cu^{2+} and I^- ions. On the one hand, the key factor for the formation of these novel nanostructures was attributed to the I^- ions, which tune the reduction kinetics of the two precursors. On the other hand, rich structural defects induced by Cu doping played a critical role in synthesizing hierarchical nanostructures. Additionally, highly branched, bimetallic Pt−Ni alloy nanocrystals synthesized using a one-pot solvothermal method were also reported previously.[361]

3.3.2. Aggregation-Based Growth. In addition to the classical overgrowth model, aggregation-based growth has been developed involving a mesoscopic transformation process.[389−391] The aggregation-based growth process refers to the mechanism known as oriented attachment rather than simply random aggregation, where the colloidal NPs align along a specific crystallographic direction to minimize the interfacial energy.[392] The synthesis of metal networks previously mentioned was usually attributed to this grow mechanism. For example, for truncated octahedral PtRu alloy NPs, on the one hand the (111) facets possessed a larger area than the (100) facets. On the other hand, (100) facets have also stronger adsorption ability in comparison to (111) facets. Therefore, the truncated octahedral NPs are likely to attach to each other via the (111) facets, eventually achieving dendritic nanostructures.[389]

It is established that heterogeneous nucleation in the solution are usually involved in a seed-mediated synthesis. As mentioned above, in most cases, a mechanism based on seeding/autocatalytic growth has been demonstrated to account for creating various dendritic nanostructures. The effect of the nucleation and growth rates on the evolution of highly branched NPs was further exploited by Xia's group. Interestingly, they found that this type of bimetallic PdPt dendritic nanostructure using AA as a reductant indeed resulted from the self-aggregation of small Pt NPs initially formed rather than overgrowth.[344] It is demonstrated that both homogeneous and heterogeneous nucleation of Pt are simultaneously involved during the early stages of reduction process and the Pt branches further grew through oriented attachment of small preformed Pt NPs. These results will be greatly beneficial to the understanding of the synthesis of metallic dendritic nanostructures. However, the evolution of branched nanostructures through aggregation is unusually uncertain in that the complicate synthetic conditions make it difficult to accurately control the evolution of the metallic nanodendrites. To this end, through systematic variations of a two-component system consisting of a Pd precursor and OAm, Skrabalak et al. came to a conclusion that the fabrication of metal nanodendrites via aggregation-based growth is closely related with the weak interactions between ligand and both Pd^{2+} and the formed Pd NPs.[393] As shown in Figure 33, different lattice orientations featured by polycrystalline branched NPs are observed, resulting from the misorientation at the nanoparticle interfaces through aggregation-based growth. Additionally, the influence

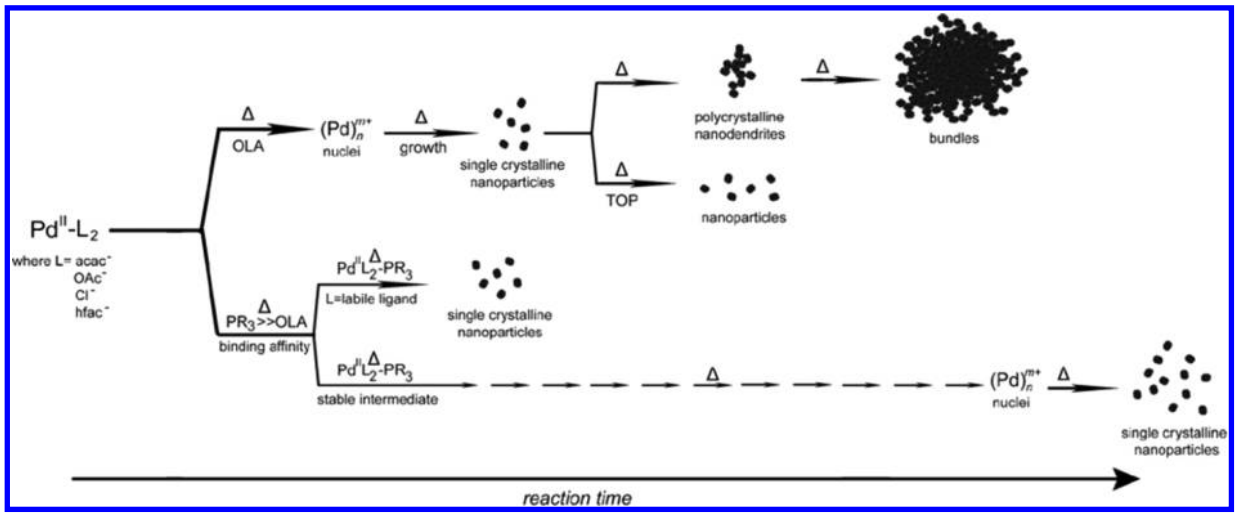

Figure 33. Schematic demonstration of the influence of selective ligand on the overall nucleation and growth processes for the evolution of NPs and nanodendrites. Weakly bound ligands, $acac^-$, OAc^-, Cl^-, and $hfac^-$, facilitated the formation of dendrites in the presence of OAm. The addition of TOP or PPh_3 creates a stable $Pd^{II}L_2-PR_3$ intermediate and thus prolongs the nucleation process. Reprinted with permission from ref 393. Copyright 2012 Wiley-VCH.

DOI: 10.1021/acs.chemrev.5b00255
Chem. Rev. XXXX, XXX, XXX−XXX

of the ligand on the overall nucleation and growth processes for synthesizing NPs and corresponding dendritic nanostructures were outlined. In detail, strong ligands with strong affinities toward Pd^{2+} and Pd^{0} can both delay nucleation and inhibit nanoparticle aggregation, while labile ligands promote the aggregation-based assembly of NPs into nanodendrites.

4. ELECTROCHEMICAL APPLICATIONS OF POROUS NOBLE METAL NANOSTRUCTURES

4.1. Fuel Cells

Fuel cells are considered as the most important energy conversion technology currently in production, because they can directly convert chemical fuels to electricity with high efficiency and they are clean. Generally, among the noble metals, Pt-based materials are still the most promising electrocatalysts for fuel cell applications, which catalyze hydrogen or small molecules oxidation at the anode and ORR at the cathode.[394,395] As a key component in fuel cell devices, developing the novel electrocatalysts with high activity and reliable durability remains a grand challenge and highly desirable, which directly determine the performance of the whole fuel cell and accelerate their commercialization in large scale. However, some critical problem on the design and fabrication of electrocatalysts has raised significant concerns. For example, Pt NPs-based traditional catalysts are readily subject to dissolution, coalescence, detachment and intermediate poisoning during long-term operations, which decrease both the electrochemically active surface area (ECSA) and the catalytic efficiency.[396−398] To move toward a genuinely practical technology that can be mass-produced cost-effectively, further improvements are urgently needed. Developing low-cost, highly active, and stable electrocatalysts is considered one of the high-priority research directions for high performance fuel cells. PNMNs can be directly employed as advanced self-supported nanocatalysts for both cathodic and anodic electrochemical reactions in fuel cells, which can eliminate the use of a carbon support and circumvents the disadvantages of the traditional carbon-supported catalysts. Unlike traditional nanoparticle-based nanocatalysts, PNMNs possess both a remarkably conductive network and a highly accessible open nanoporosity, which is particularly favorable for electrocatalysis. Moreover, synergistic effects resulting from favorable structures and compositions further enhance their electrocatalytic activities. Here, some recent advances in developing high performance PNMN electrocatalysts for fuel cell applications are highlighted.

4.1.1. Methanol Oxidation at Anode. Fuel cell development utilizing small molecules, such as methanol, ethanol, and formic acid as fuels, have been considered favorable options in terms of fuel usage and feed strategies due to some unquestionable advantages over analogous devices fed with hydrogen. Both direct alcohol fuel cells (DAFCs) and direct formic acid fuel cells (DFAFCs) have the potential for miniaturization. The design of new catalysts that have high activities with fast kinetics and tolerable deactivation is grandly desirable. Therefore, significant research efforts are being dedicated to the design and fabrication of more efficient anode electrocatalysts for fuel cells.[399,400] Specifically, a variety of PNMNs have been widely investigated for DAFCs/DFAFCs due to their unique physical and chemical properties as well as striking activity−structure relationship.

To date, Pt is considered a promising candidate electrocatalyst for the methanol oxidation reaction (MOR). However, challenging issues, such as methanol crossover and poor methanol electro-oxidation kinetics are the main obstacles to the commercialization of DMFCs technology.[401,402] Considering the structural advantage mentioned above, PNMNs are the promising electrocatalysts for the MOR. Shape-controlled Pt nanomaterials with abundant edges and corner atoms were developed for MOR in acidic media, which can indeed enhance the electrocatalytic activity due to the valency of the unsaturated atoms. Han et al. reported novel self-supported spiny-porous Pt nanotubes using galvanic replacement reaction in the presence of CTAB.[403] As expected, the ECSA significantly increased in comparison to porous Pt nanotubes. Consequently, this unique dendritic nanostructure increased mass activity by 4.3 and 1.53-fold as compared to porous Pt nanotubes and commercial Pt/C, respectively, which not only increased the Pt utilization efficiency but also decreased their cost. Rauber et al. used electrodeposition to prepare highly ordered large-area network-like nanostructures and employed them as more active and stable electrocatalysts for MOR.[404] The resulting 3D porous architecture characterized by continuously integrating nanowire endowed them with superior transport properties as well as large accessibility of reactants to the catalytic active sites, which greatly contribute to the enhanced electrochemical performances. In addition, porous Pt nanotubes with wall thickness of 5 nm[405] and 3D ordered macro-/mesoporous Pt[406] not only showed excellent peak specific activity in MOR but also demonstrated an improved intermediate tolerance.

Moreover, the electrocatalytic performances of Pt-based electrodes usually suffer severe degradation because of the evolution of strongly adsorbed intermediates (e.g., CO), which leads to the decreased catalytic activity. Rational design of Pt-M-based bimetallic nanostructures is one of the best policies to improve their electrocatalytic performance, benefiting from the so-called bifunctional and electronic structure alteration mechanisms. For the MOR, M is mainly in charge of the water dehydration to produce the M−OH transition state, while Pt catalyzes methanol to produce Pt-CO_{ads} on the basis of the bifunctional mechanism. Furthermore, the introduction of a 3d transition metal, such as Co or Ni, changes the electronic structure of Pt and therefore enhances the electrocatalytic activity and durability while increasing the Pt utilization. As a result, Pt-based bimetallic/multimetallic PNMNs with different structural features provided many opportunities for the construction of advanced MOR electrocatalysts. Xiao et al. created hierarchically porous Au−Pt nanostructures with heterogeneous interfaces by decorating porous Pt shells on the surfaces of 3D Au with rigid skeletons.[149] The as-prepared heterogeneous Au−Pt nanostructure exhibited excellent catalytic activity toward MOR. Meanwhile, the efficiency of Pt usage and mass transfer as well as its tolerance toward the absorbed intermediate species can be significantly enhanced. In addition to the noble metal, non-noble metals have also been incorporated into Pt system to fabricate promising bimetallic electrocatalysts. The typical example is that Pt−Ni−P hybrid nanotube arrays (NTAs) with porous nanostructure were successfully synthesized via template-assisted electrodeposition (Figure 34).[316] The introduction of P can effectually increase the ECSA of the Pt−Ni−P NTAs and thus remarkably enhance their electrochemical activity for methanol electro-oxidation. Moreover, with the aid of the unique tubular nanostructure

DOI: 10.1021/acs.chemrev.5b00255
Chem. Rev. XXXX, XXX, XXX−XXX

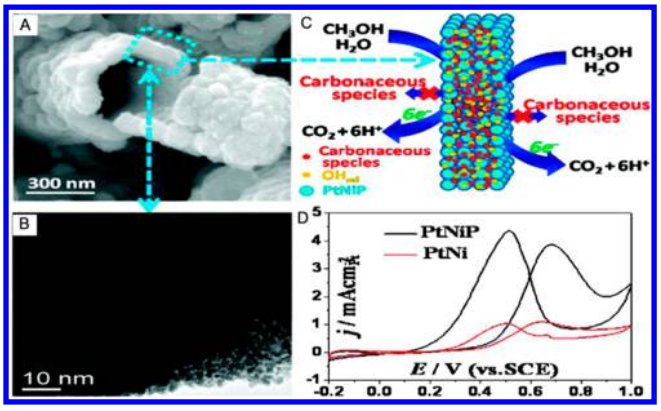

Figure 34. Typical (A) SEM and (B) TEM image of a broken Pt−Ni−P nanotube. (C) Scheme for the almost complete oxidation of carbonaceous species generated during MOR in the porous walls of Pt−Ni−P NTAs. (D) Cyclic voltammograms (CVs) of Pt−Ni−P and Pt−Ni NTAs in 0.5 M CH_3OH + 0.5 M H_2SO_4 at 50 mV/s. Reprinted with permission from ref 316. Copyright 2012 American Chemical Society.

featured by porous walls as well as synergistic electronic effects, the as-prepared Pt−Ni−P NTAs showed a lower degree of poisoning of surface sites by carbonaceous species, leading to high stability of the electrocatalysts. Zhu et al. also reported kinetically controlled synthesis of bimetallic PdNi network-like nanostructures at room temperature.[176] By this method, we can easily control the addition quantity of metal precursors to direct the final product with different mole ratio between Pd and Ni. Due to the integrated networks, bare surface and synergistic electronic effect, the resulting PdNi showed remarkably enhanced activity and durability for MOR in alkaline media. Other reports on different self-supporting bimetallic PNMNs, such as PtCu alloy nanodendrites,[407] Pt_3Ni alloy networks,[351] nanotubular mesoporous Pt/Cu,[151] porous Pt−Co alloy nanowires,[145] Ni@Pt core−shell nanotube with porous nanostructures,[408] and porous Pt−Ni nanoparticle tubes[409] were also synthesized and exhibited satisfactory electrocatalytic activity toward MOR, resulting in significant potential for use in fuel cells.

4.1.2. Ethanol Oxidation at Anode. Ethanol is available worldwide because it comes with a supply chain that is already in place and can be acquired in large scale through a fermentation process from renewable resources. Moreover, nontoxicity and ecological harmlessness also make the direct ethanol fuel cells (DEFCs) more appealing. Recent advances indicated that DEFCs have attracted increasing interest as power sources because ethanol possesses a higher specific energy density than methanol and conventional batteries.[395,410] To further improve the electrochemical performance of DEFCs, it is of great significance to design more active anode electrocatalysts for ethanol oxidation reaction (EOR) than Pt alone.[411] Specifically, Pd-based nanomaterials have emerged as a class of promising electrocatalysts for EOR in alkaline environment. Significantly, unlike Pt-based catalysts the main advantage for Pd-based electrocatalysts lies in their high electrocatalytic activities toward a large number of molecules in alkaline conditions.[412−415] Besides, the significantly improved reaction kinetics and a lower degree of corrosion to the electrodes are also conducive to the development of the DEFCs.

Liu et al. synthesized Pd aerogels through a facile method and revealed that the resulting products possessed high activities toward the EOR.[169] Compared with commercial Pd/C, the as-prepared Pd aerogels (e.g., $Pd_{\alpha\text{-CD}}$, $Pd_{\beta\text{-CD}}$, and $Pd_{\gamma\text{-CD}}$) showed high ECSA values. The current densities for the $Pd_{\alpha\text{-CD}}$, $Pd_{\beta\text{-CD}}$, and $Pd_{\gamma\text{-CD}}$ aerogels are 2.2, 2.3, and 1.2

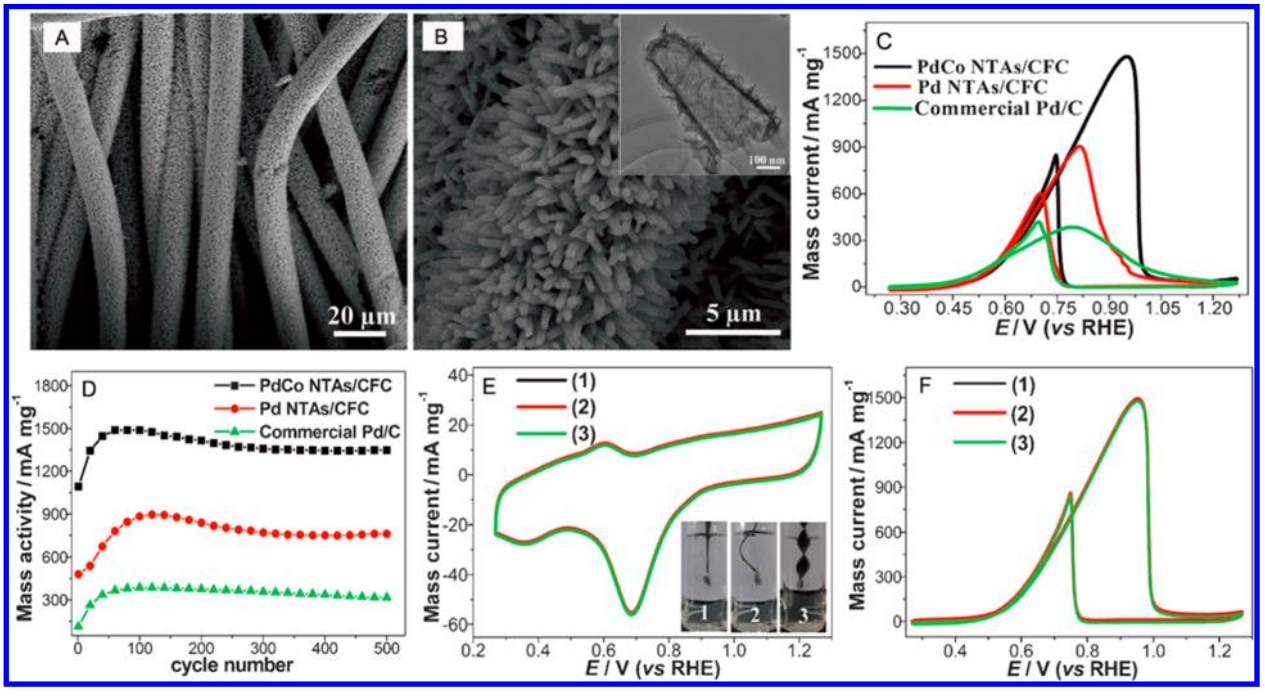

Figure 35. (A, B) SEM images of PdCo NTAs/CFC. Inset: the TEM image of PdCo nanotube. (C) CVs of PdCo NTAs/CFC, Pd NTAs/CFC, and commercial Pd/C in 1.0 M KOH + 1.0 M C_2H_5OH at 50 mV s^{-1}. (D) The cycling stability of peak current densities of the three catalysts above with increasing cycles. CVs of PdCo NTAs/CFC in 1.0 M KOH solution (E) and 1.0 M KOH + 1.0 M C_2H_5OH (F) at 50 mV s^{-1} at different distorted states: (1) normal, (2) bending, and (3) twisting. Reprinted with permission from ref 416. Copyright 2015 Wiley-VCH.

DOI: 10.1021/acs.chemrev.5b00255
Chem. Rev. XXXX, XXX, XXX−XXX

times higher than that of Pd/C. The electrocatalytic activities of the Pd aerogels also outperformed the related nanomaterials reported previously. The strikingly enhanced electrochemical performance of the Pd aerogels benefitted from the highly self-supporting ultrafine network structure of the aerogel. Additionally, the reactant could be substantially accumulated by virtue of the host−guest interaction between the cyclodextrins. Significantly, agglomeration of the nanocatalysts was largely circumvented, resulting in the high electrochemical performance toward the EOR. Compared with monometallic Pd nanostructures, bimetallic PNMNs provide a class of effective candidate catalysts to enhance the functionalities of materials. For example, Li et al. first fabricated ZnO nanorod arrays (NRAs) on the surface of carbon fiber cloth (CFC) to produce ZnO NRAs/CFC. Using ZnO NRAs as template, PdCo alloy layer were further electrodeposited on the surface of ZnO NRAs. Then, the excellent flexibility PdCo NTAs/CFC was synthesized after dissolving ZnO (Figure 35A,B).[416] The resulting binder-free PdCo NTAs/CFC not only showed higher electrocatalytic activity but also significantly improved stability in comparison to monometallic Pd NTAs/CFC and commercial Pd/C (Figure 35C,D). Significantly, this novel nanostructures also exhibited excellent flexibility and the electrochemical performance toward EOR can be well maintained irrespective of the various distorted states (e.g., normal, bending, and twisting states) (Figure 35E,F). Hong et al. found that the flower-shaped PdAg bimetallic nanocrystals with homogeneous alloy nanostructure catalysts exhibited superior electrocatalytic activity and stability toward the EOR under alkaline conditions.[417] It is believed that synergy between Pd and Ag is in favor of the absorption of OH^- and the desorption of the intermediate products evolved during the EOR. The incorporation of Ag into Pd causes a tensile strain in the structure of the Pd surface and shifts the d-band center of Pd up, facilitating the adsorption of OH_{ads} onto the surface of the catalyst and, consequently, enhancing the EOR process. Moreover, high surface areas and large pore volumes of these PNMNs greatly maximize the exposure of active sites, accelerate the transport and diffusion of ethanol because of the existence of abundant mesopores and micropores. A similar enhanced mechanism for EOR was also found in numerous PNMNs, including PdPt nanosponges,[173] hollow Au@Pd core−shell NPs,[236] etc.

4.1.3. Formic Acid Oxidation at Anode. Recently, DFAFCs have received significant attention and have been considered as reliable candidates for portable power applications. As a strong liquid electrolyte, the real attraction of using formic acid as fuel originates from the distinct advantages over methanol in the fuel cell, such as nontoxicity and safety, limited crossover. Furthermore, the DFAFC has a higher theoretical open-circuit potential than either hydrogen or DMFCs.[418] The most commonly accepted mechanism is the so-called "parallel or dual pathway mechanism". Direct oxidation (pathway I) involves a dehydrogenation reaction to directly produce final product CO_2, while the other reaction pathway (pathway II) forms strongly adsorbed intermediate, i.e., CO, by dehydration.[419,420] It is worth noting that formic acid oxidation on pure Pt surfaces primarily occurs through pathway II, which results in poisoning of Pt due to the accumulated CO_{ads} on the surface of Pt and thus remarkably degrades Pt electrocatalytic performance.[421,422] A significant amount of effort has been dedicated to promote the electrocatalytic kinetics of formic acid oxidation on Pt-based catalysts by introducing surface modifiers or developing promising Pd-based electrocatalysts for DFAFCs.

Novel Pt−Cu hierarchical trigonal bipyramid nanoframes with different Pt/Cu ratios were fabricated, which possessed improved electrocatalytic activity for the formic acid oxidation. The optimized nanoframes achieved 5.5-fold improvement in specific activity and 2.1-fold improvement in mass activity relative to commercial Pt/C catalysts.[387] These hierarchical structures with multiple branches provided sufficiently accessible active sites at the surfaces, excellent conductivity, and synergetic effects between Pt and Cu and, therefore, lead to the enhanced catalytic activities. With regard to Pd catalysts, Yang et al. reported hollow Pd NPs by eliminating the Ag component from Ag@Ag−Pd core−shell structures.[423] These hollow structured Pd NPs with decreased sizes exhibited superior catalytic activity and stability toward formic acid because of the high surface areas available for the catalytic reaction. Nanoporous PdCu alloys characterized by uniform ligament size were fabricated using the dealloying method.[140] Compared with nanoporous Pd, nanoporous PdCu exhibited remarkably improved electrocatalytic activity and structural stability for formic acid oxidation. The surface specific activities of the nanoporous metals decreased in the order $Pd_{50}Cu_{50}$, $Pd_{75}Cu_{25}$, $Pd_{30}Cu_{70}$ and Pd. The effect of the alloy ratio on the electrocatalytic behavior was also investigated. The direct pathway was predominant in this electrochemical process when the Cu content was lower than 50 at%, while the formic acid oxidation through the CO poisoning pathway increases when the Cu content reaches 70 at%. Moreover, $Pd_{50}Cu_{50}$ has better resistance to CO poisoning and enhanced structure stability compared with other alloy samples. In another report, Chen and co-workers also investigated the influence of the incorporated metal on the electrocatalytic activity and the durability of the nanoporous Pd-based bimetallic catalysts. They concluded that for the nanoporous Pd, PdCd, and PdPb catalysts, oxidation proceeds through the direct mechanism, whereas the indirect mechanism, along with major CO poisoning, was observed in the PdIr and PdPt catalysts.[424] Combining the porous nanostructures with the alloy effect, other novel PNMNs, such as 3D Pd−P nanoparticle networks,[183] hollow PdCu alloyed nanocubes,[341] and PtPb alloy nanoflowers,[425] were also investigated as promising electrocatalysts for formic acid oxidation.

4.1.4. Oxygen Reduction Reaction at Cathode. One major technical challenge in polymer electrolyte membrane fuel cell (PEMFC) technology is the development of more active and reliable cathode catalysts, which catalyze the ORR, i.e., $O_2 + 4H^+ + 4e^- \rightarrow 2H_2O$. Currently, fine Pt NPs (3 nm) dispersed on carbon supports (Pt/C) are widely utilized as the state-of-the-art ORR electrocatalyst. However, advanced ORR electrocatalysts with satisfactory mass activity are urgently needed and their even more serious problem, namely poor durability, should be also carefully addressed, both of which severely affected their ORR performance and hindered the development of the PEMFC. Fuel-cell vehicles in the test fleets monitored by the United States DOE have used 0.4 mg_{Pt} cm^{-2} or more on the cathode, and in these vehicles the catalyst/MEA stability has still been short of the 5000-h durability target. How to reduce costs by reducing cathode loadings to <0.1 mg_{Pt} cm^{-2} with high mass activity (0.44 A mg_{Pt}^{-1}) and durability is the subject of U.S. Department of Energy's 2017 target.[426] The degradation of Pt/C catalysts resulting from the Pt NP aggregation, dissolution, and detachment will occur because

DOI: 10.1021/acs.chemrev.5b00255
Chem. Rev. XXXX, XXX, XXX−XXX

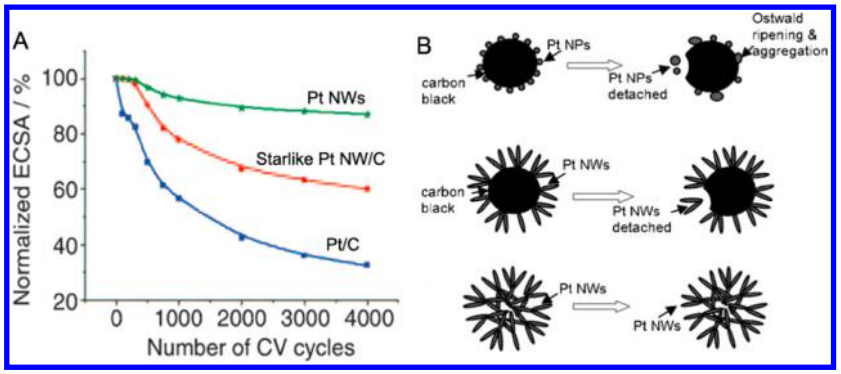

Figure 36. (A) Loss of ECSA of Pt/C, starlike Pt NW/C, and unsupported Pt NWs as a function of cycling numbers in O_2-purged 0.5 M H_2SO_4 solution at room temperature. (B) Schematic illustration of morphology changes that occur in Pt during accelerated electrochemical cycling for these three catalysts. Reprinted with permission from ref 438. Copyright 2011 Wiley-VCH.

of the carbon corrosion and the weak interaction between carbon support and catalyst NPs, which inevitably lead to the decrease of ECSA and ORR performance during long-term operation.[67] Although great progress has been made on ORR catalysts in recent decades, the further development of PEMFC is severely restrained by high-priced Pt in the cathode catalysts and the slow kinetics of the ORR. To overcome these issues, low or non-Pt and metal-free electrocatalysts with low cost, high electrocatalytic activity, and durability have been extensively studied for exploitation as advanced ORR catalysts in recent years.[427−430] Among them, further design and fabrication of appealing low Pt catalysts with great improvement in their activity and stability have been achieved through the synthesis of bimetallic/multimetallic Pt alloys,[431,432] core−shell structures,[433,434] and novel supporting nanomaterials.[435,436] It is well-known that Pt utilization efficiency of these traditional catalysts is usually low because of their low surface areas. It is expected that accurate design of Pt-based PNMNs with high surface area and high pore volume and employ them as high performance ORR electrocatalysts are very promising in fuel cell applications.

PNMNs exhibit inherently high surface areas and can provide numerous advantages in comparison to the traditional nanostructures. PNMNs characterized by 3D continuous and integrated material are efficiently presintered, thus significantly minimizing the loss of ECSA because of agglomeration. At the same time, the elimination of the carbon support would enable a thinner electrode catalyst layer and improved mass transport and Pt utilization within the catalyst layer due to the direct contact between the catalyst layer and the gas diffusion layer. There have been great progress in the fabrication of self-supporting monometallic Pt catalysts with porous nanostructures, most of which exhibited superior activities and durabilities toward the ORR. For instance, Yan and co-workers demonstrated that Pt nanotubes with thin walls (4−7 nm) and long lengths (5−20 mm) can provide both high durability and high ORR activity.[405] Sun et al. reported network-like Pt nanostructures characterized by high specific surface areas and a large overall size, which exhibited much higher durability and 2.9 times the mass activity of the commercial Pt black for ORR.[437] Zhang et al. synthesized single-crystalline, porous Pt dendritic nanotubes using galvanic replacement at room temperature.[241] The resulting Pt nanostructures showed 4.4-fold catalytic activity enhancement and 6.1-fold durability enhancement over commercial Pt/C catalysts. To address the relationship between the ORR electrocatalytic performance and catalyst structure, Sun et al. for the first time employed carbon-supported, multiarmed, starlike Pt nanowires (starlike PtNW/C) as new electrocatalysts to address their activity and durability issues.[438] Based on the electrochemical results, they found that the durability can be further improved when self-supported Pt nanowires served as the ORR catalyst, where the support effect of carbon was eliminated. The accelerated durability tests (Figure 36A) indicated that the ECSA of the unsupported Pt NWs decreased by approximately 13% after 4000 cycles, which was 5.2 and 3.1-fold improvement over commercial Pt/C and carbon-supported PtNW catalysts, respectively. As shown in Figure 36B, the Ostwald ripening, Pt aggregation and carbon support corrosion, can be remarkably mitigated or avoided by introducing the 1D, starlike network Pt morphology. Combining with the unique 1D nanostructure in electrocatalysis, including preferential exposure of low energy crystal facets and improved electron transport characteristics, several self-supporting Pt catalysts with network-like nanostructures also exhibited high activities and stabilities for the ORR.[6,439] Moreover, high surface area mesostructured Pt thin films also exhibited higher specific activities for the ORR.[67] In the meantime, this mesoporous structure with fewer undercoordinated Pt sites contributed to their excellent durability. These self-supported, porous, Pt nanostructures open up an appealing approach to design highly active and durable electrocatalysts, which is crucial for the applications of PEMFCs.

One effective technique for the enhancement of the electrocatalytic performance of the ORR is to partially replace Pt with the other metal and, thus, construct Pt-based alloy nanostructures. Due to the improved atomic and electronic structures of Pt, bimetallic nanostructures involving the other element inherit and modify the properties of the Pt constituent, enabling their superb electrochemical performances in comparison to monometallic Pt counterparts. Theory calculations further demonstrate that alloyed M efficiently downshifts the d-band center of the Pt nanocatalysts, mitigating the adsorption of oxygenated blocking species (such as OH^-) and increasing the number of active sites accessible to oxygen as well.[440−442] Accordingly, significant advances have been achieved to rationally design high performance bimetallic Pt-based electrocatalysts for ORR with a wide range of compositions.[443−446] The highly conductive networks and accessible open nanoporosity contribute to the enhanced ORR performance together with other optimized structural and compositional parameters. Alloyed PdPt aerogels were demonstrated to show

DOI: 10.1021/acs.chemrev.5b00255
Chem. Rev. XXXX, XXX, XXX−XXX

excellent electrocatalytic activity and durability for the ORR (Figure 37A,B).[171] The Pt_xPd_y aerogels composed of 3D

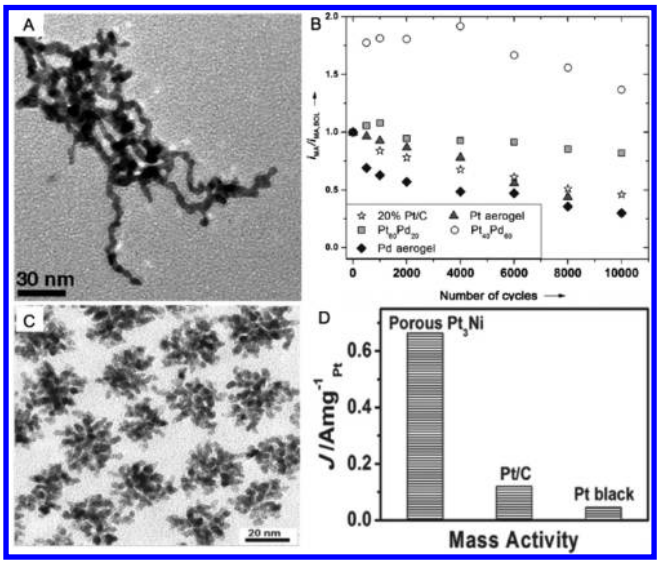

Figure 37. (A) TEM image of the $Pt_{50}Pd_{50}$ aerogel. (B) Relative ORR mass activity of Pt_xPd_y catalysts of different compositions as a function of the number of potential cycles (0.5−1.0 V). Reprinted with permission from ref 171. Copyright 2013 Wiley-VCH. (C) Representative TEM image of as-prepared porous Pt_3Ni nanocrystals. (D) Mass activity at 0.9 V versus RHE for the resulting Pt_3Ni nanocrystals, commercial Pt/C, and Pt black, which are given as kinetic current densities normalized to the loading amount of Pt. Reprinted with permission from ref 446. Copyright 2013 Wiley-VCH.

nanowire-like structures showed very high surface areas and large porosities. The $Pt_{80}Pd_{20}$ aerogel with an optimized composition increased the mass activity by 5-fold as compared to commercial Pt/C catalyst. Significantly, they also showed excellent durability during the test. Huang's group presented an effective wet-chemical method for the preparation of Pt_3Ni nanocrystals with highly porous features. The resulting Pt_3Ni nanocrystals are typically characterized by highly porous nanostructures as well as thin branch diameters of 2.8 nm (Figure 37C).[446] Specifically, the resulting porous Pt_3Ni nanocrystals exhibited satisfactory electrocatalytic activity and stability in comparison to the commercial Pt/C and Pt black catalysts toward the ORR (Figure 37D). Interestingly, Liu et al. successfully prepared quaternary PtCuCoNi nanotubes using a one-step direct electrodeposition approach with a porous membrane as the template.[447] Despite the ultralow Pt content within the final $Pt_5Cu_{76}Co_{11}Ni_8$ nanotubes, the product followed a four-electron pathway and exhibited a markedly enhanced electrocatalytic activity toward the ORR relative to state-of-the-art Pt black and Pt/C catalysts. Benefiting from the advantages of the porous alloyed nanostructures, a series of nanocatalysts, including PtPd porous nanorods,[448] PtPd alloy nanoflowers,[449] and mesoporous PdCo sponge-like nanostructure,[134] were also designed for use as promising ORR electrocatalysts. It is clear that both structural and compositional effects are involved in these porous bi- and multimetallic nanostructures for their ORR catalysis enhancement, providing a new avenue for the design of low-cost and highly efficient electrocatalysts.

Another type of electrocatalysts studied for the ORR is Pt-based core−shell NPs/nanostructures. By fine controlling core−shell composition, size, and shape, and thus taking advantage of the structure-induced strain and electronic effects, it is expected that the electrocatalytic activity and durability of the Pt shell for the ORR can be significantly enhanced.[450] Several types of Pt-based core−shell PNMNs were developed as promising ORR catalysts. Dendritic nanocrystals are the first type of these core−shell structures, where the Pt or Pt alloy is deposited on the core via overgrowth methods. For example, the Pd−Pt nanodendrites composed of a large amount of Pt nanobranches on a Pd core showed relatively high surface areas and particularly active facets for the ORR.[374] In detail, the final product showed 2.5 and 5 times more active mass activities toward the ORR than the commercial Pt/C and Pt black counterparts, respectively. The heterostructures of Pt-on-$Pd_{0.85}Bi_{0.15}$ nanowires with a large amount of Pt nanobranches on the surface of $Pd_{0.85}Bi_{0.15}$ were synthesized through a convenient, one-pot, wet-chemical, and templateless method with the help of OAm and NH_4Br.[451] The as-prepared heterostructures were demonstrated to be more active and stable for the ORR than the commercial Pt/C catalyst.

Other core−shell-like nanostructures can be obtained by dealloying, which is usually performed to selectively remove the active metal and enrich the noble metal on the outermost surface.[138,452−454] The compression in the shell modifies the d-band structure of the Pt atoms, weakens the adsorption energies of the reactive intermediates, and results in an increase in the ORR performance.[132,455] By sequentially removing the active components in a Pt/Ni/Al ternary alloy, Ding et al. obtained unique PtNi porous nanostructures, which showed a monolayer Pt shell on the surface of Pt/Ni alloy ligaments with typical dimensions of approximately 3 nm.[142] The as-prepared catalysts exhibited significantly enhanced electrocatalytic activity and durability for the ORR compared with Pt/C catalyst due to the presence of surface strain and the alloying effect of Ni in this Pt-enriched surface alloy structure. In addition, the unique nanoporous structures characterized by interconnected skeletons and bicontinuous hollow channels are also favorable for the accelerated electron transfer and mass transport during ORR process, promoting their electrochemical performance toward the ORR. Shui et al. produced a nonuniform composition of $PtFe_5$ alloy nanowires by electrospinning and then obtained Pt−Fe alloy nanowires with porous nanostructures using the chemical dealloying method.[456] It was observed that that a nonuniform composition in the precursor alloy nanowires plays a vital role in formation of nanoporous structures. Electrochemical experiments indicated that these self-supporting networks not only showed 2.3 times the specific activity that of conventional Pt/C catalysts but also have better durabilities. In another report, Strasser et al. presented a simple atmosphere-controlled acid leaching approach to tailor the evolution of porosity within PtNi bimetallic NPs and then investigated the influence of porosity on their intrinsic electrocatalytic activity and stability toward the ORR (Figure 38A).[457] They found that the formation of porosity in NPs larger than ca. 10 nm is intrinsically associated with a remarkable removal of Ni and, hence, a rapid drop in the intrinsic specific activity toward the ORR. In contrast, an O_2-free acid leaching route can efficiently suppress the evolution of porosity, leading to Ni-enriched solid alloy core−Pt shell architecture even at large particle sizes. As shown in Figure 38B−E, the solid porous core−shell NPs formed by O_2-free acid leaching showed the higher activity and stability toward the ORR compared with porous NPs. Due to the absence of

DOI: 10.1021/acs.chemrev.5b00255
Chem. Rev. XXXX, XXX, XXX−XXX

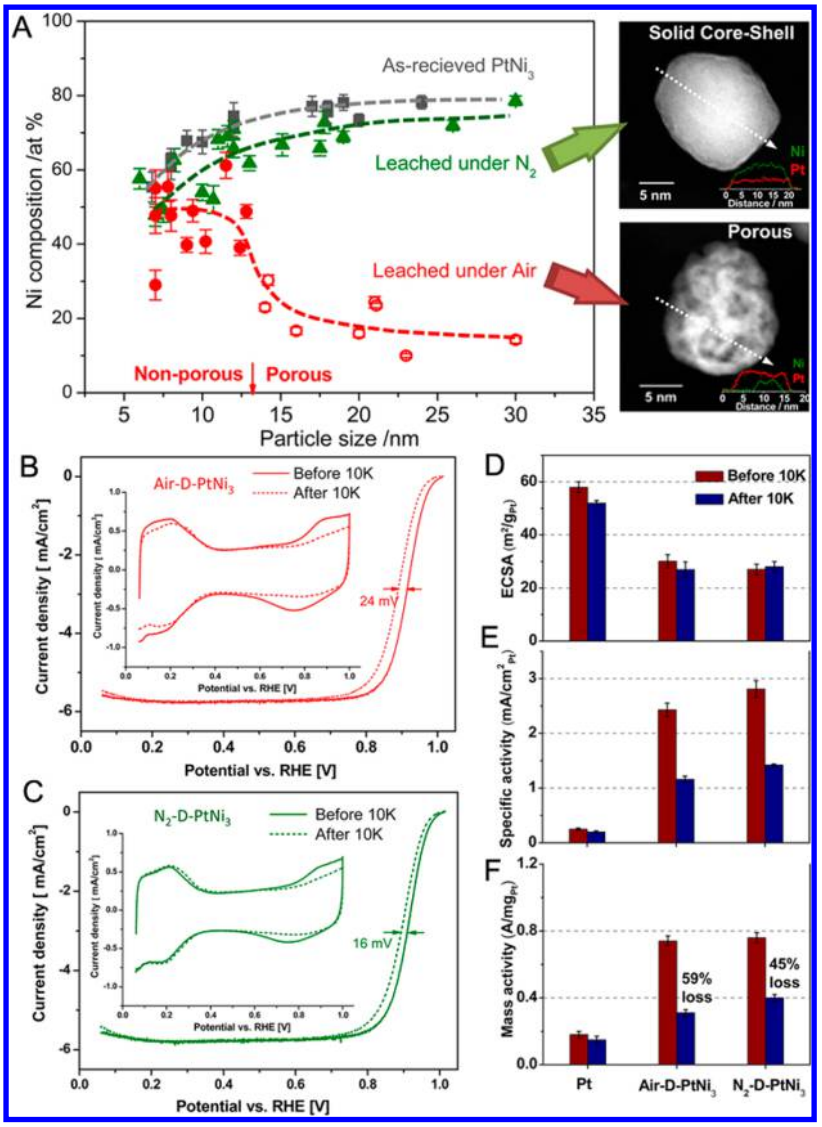

Figure 38. (A) Correlations between particle size, composition, and porosity in the three catalysts. (B, C) ORR voltammograms of air−D−$PtNi_3$ and N_2−D−$PtNi_3$ catalyst in O_2-saturated 0.1 M $HClO_4$ at 5 mV/s before (solid) and after (dash) stability test. The inset shows the CVs in N_2-saturated 0.1 M $HClO_4$ before and after 10 K cycles. (D−F) Comparisons of ECSA, specific activity, and mass activity before and after stability test, respectively. Reprinted with permission from ref 457. Copyright 2013 American Chemical Society.

nanopores, the controlled synthesize catalyst NPs below 10 nm is greatly recommended to further enhance their ORR performance. This research not only uncovered the degradation of bimetallic nanocatalysts but also provided an invaluable design guidance to prepare more active and stable electrocatalysts toward the ORR.

In addition, Yang and co-workers reported the Pt_3Ni nanoframes with Pt-skin shell nanostructures, which exhibited the extremely enhanced ORR activity and duability.[458] Several critical aspects, such as high surface-to-volume ratio, 3D surface molecular accessibility and low but optimal the usage of noble metals, are significantly addressed to rational design of high performance ORR nanocatalysts. As shown in Figure 39A, $PtNi_3$ polyhedra with uniform rhombic dodecahedron morphology and size was first synthesized, which further evolved into 3D Pt_3Ni nanoframes spontaneously without morphology change. Finally, the 3D opened Pt-skin structures were obtained via heat treatment. The favorable factors for ORR including 3D opened Pt-skin structure and high surface-to-volume ratio were well involved for these resulting Pt_3Ni nanoframes. These synergistic effects between these structural and compositional attributes maximized the Pt utilization efficiency and facilitate O_2 accessibility in the entire catalytic surfaces exposed. Furthermore, the electronic interaction between 2 monolayers of Pt-skin and subsurface PtNi was also verified to the improved ORR performance. As expected, in comparison to state-of-the-art Pt/C and solid PtNi/C catalysts, Pt_3Ni nanoframes showed substantially higher electroactivity with a lower slope of 46 mV dec^{-1} (Figure 39B,C). It is worth noting that the Pt_3Ni nanoframe catalysts showed 16 times the specific activity and 22 times the mass activity of the conventional Pt/C catalysts (Figure 39C,D). Moreover, the ORR electrocatalytic durability was also significantly improved. They also found that ORR performance can be further enhanced when protic ionic liquids were introduced to the Pt_3Ni nanoframe. The enhanced ORR performance is due to the high oxygen solubility in ionic liquids, which increased the O_2 concentration at the catalyst surface.[459]

DOI: 10.1021/acs.chemrev.5b00255
Chem. Rev. XXXX, XXX, XXX−XXX

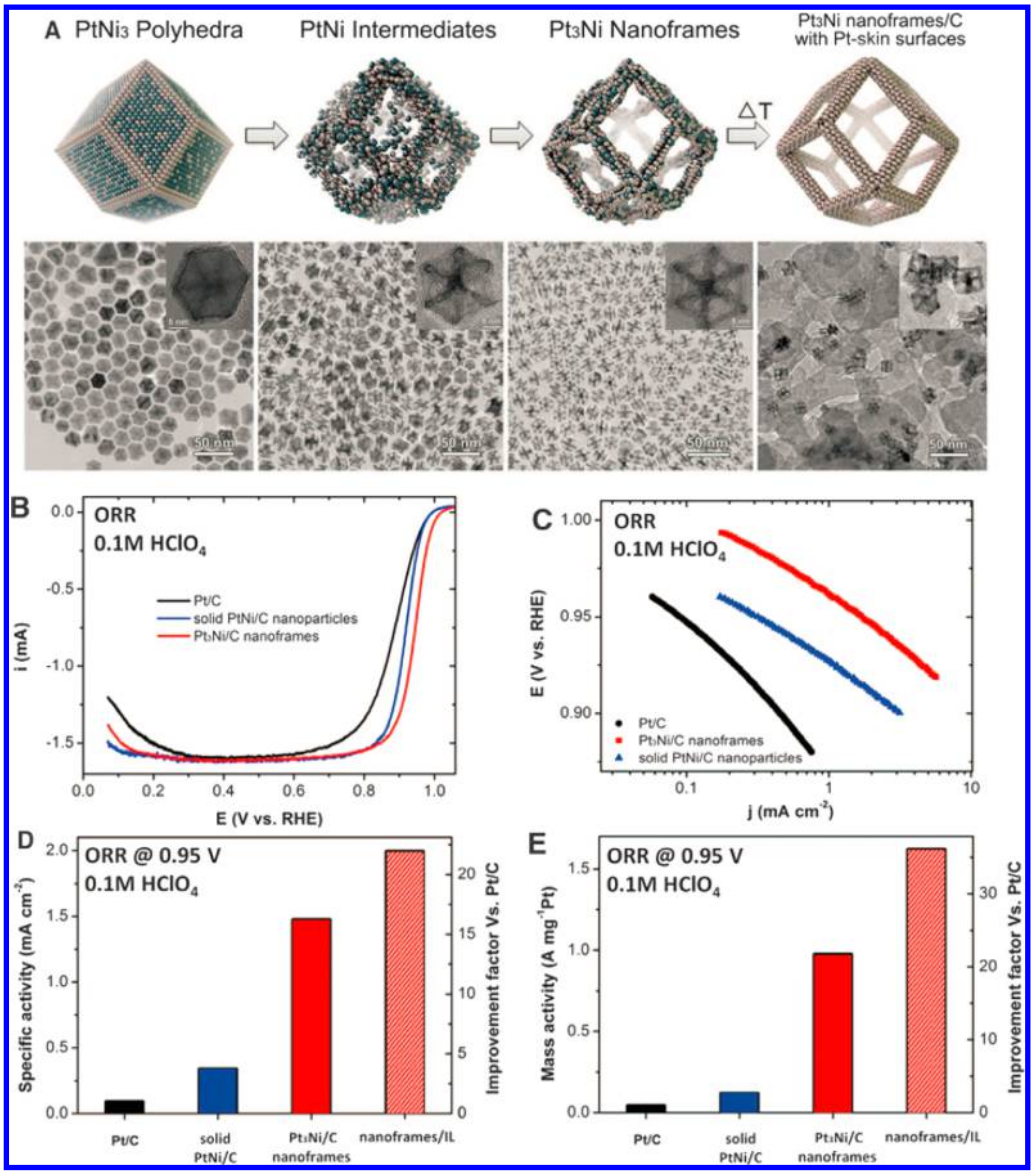

Figure 39. (A) Schematic illustrations and corresponding TEM images of the samples obtained at different stages during the evolution process from polyhedra to nanoframes. (B) ORR polarization curves and (C) the corresponding Tafel plots. Specific activities (E) and mass activities (F) measured at 0.95 V, and improvement factors versus Pt/C catalysts. Reprinted with permission from ref 458. Copyright 2014 American Association for the Advancement of Science.

4.2. Electrochemical Sensors and Biosensors

Considerable attention has been aroused in recent decades for the integration of recognition elements with electronic elements to fabricate fascinating electrochemical sensors and biosensors.[460−462] As a key part of electrochemical sensing systems, electrode materials play a pivotal role in constructing high-performance electrochemical sensing platforms to sensitively determine targets via various analytical approaches. The introduction of nanomaterials into electrochemical sensing interfaces allows for the incorporation of novel functions and, thus, leads to high sensitivities.[463,464] Specifically, PNMNs featured by the large surface area and high pore volume can yield a synergistic effect among catalytic activity, conductivity and biocompatibility. In addition, PNMNs are well interconnected and do not require any supports; therefore, corrosion can be avoided to a large extent. These PNMN-enhanced electrochemical sensing platforms can effectively accelerate signal transduction, resulting in higher sensitivity and lower detection limits. A wide variety of PNMNs have been explored in electrochemical sensors and biosensors, including small molecule sensors, enzyme-based biosensors, DNA sensors, immunosensors and cytosensors.

4.2.1. Small Molecule Sensors. Electrochemical detection of small molecules is very important in varieties of fields. PNMNs have been employed as advanced electrode materials to fabricate sensors for sensitively detecting different analytes due to their large active area and high molecule accessibility. The enhanced electrochemical signals and the lower overvoltages were usually achieved with PNMNs modified electrodes compared with bare electrodes. Enzyme-free electrochemical sensors have been widely used for determination of numerous small molecules including, hydrogen peroxide, glucose, metal ions, etc. Ghanem investigated the electrochemical sensing of catechol and hydroquinone at nanostructured mesoporous Pt film, which was electrochemically deposited from LLCs plating mixtures.[465] Compared with bare

DOI: 10.1021/acs.chemrev.5b00255
Chem. Rev. XXXX, XXX, XXX−XXX

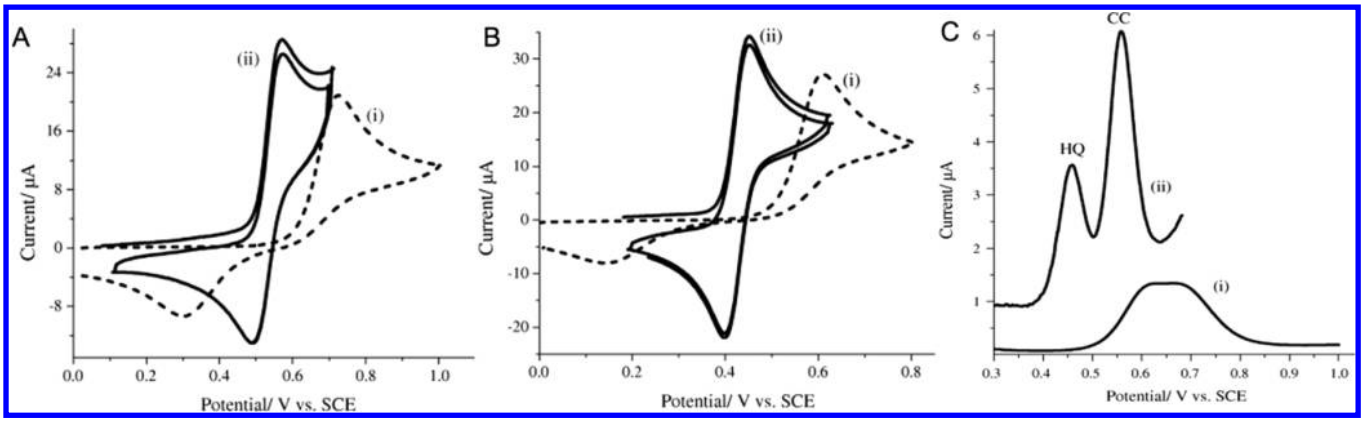

Figure 40. CVs obtained at (i) polycrystalline and (ii) nanostructured mesoporous Pt electrode (two cycle) in 1.0 M $HClO_4$ containing 5 mM catechol (A) and 5 mM hydroquinone (B) at a scan of rate 50 mV s^{-1}. (C) Differential pulse voltammetry curves observed at (i) polycrystalline and (ii) mesoporous Pt electrode in a mixture solution of 0.5 mM catechol and 0.5 mM hydroquinone in 1.0 M $HClO_4$. Reprinted with permission from ref 465. Copyright 2007 Elsevier.

electrode, the obtained mesoporous Pt electrode exhibited better electrocatalytic activity and reversibility for the oxidation of catechol and hydroquinone. As shown in Figure 40A–C, the peak-to-peak separation (ΔE) decreased from 430 to 75 mV for catechol and from 485 to 55 mV for hydroquinone at bare and mesoporous Pt electrodes, respectively. The enhanced peak currents for both targets were also found at the mesoporous Pt electrode. This implies mesoporous nanostructures exhibited faster electron rate kinetics and, thus, better electrochemical performances compared with bare electrode. At the same time, a highly selective and simultaneous detection of hydroquinone and catechol was achieved at mesoporous Pt electrode. Combining the quasi-hemispherical diffusion with large electroactive area of electrode, Denuault et al. constructed mesoporous Pt microelectrodes to sensitively detect H_2O_2 over a wide range of concentrations.[466] Moreover, well-defined nanoporous PtNi alloy nanowires[467] and 3D NPG film[468] were fabricated by dealloying method, both of which showed a remarkably enhanced electrocatalytic activity toward H_2O_2 sensing properties. In addition, Chung et al. constructed 3D Au nanodendrites through electrodeposition of Au using a gas bubble dynamic template method.[469] The resulting porous Au nanostructures possessed ultrahigh surface areas and were used as advanced electrode materials to detect As (III) at ultralow concentration.

The nonenzymatic sensing of glucose based on the direct electrochemical oxidation of glucose is a rapid and cost-effective approach.[470,471] Noble metals are considered to be the most promising candidate electrocatalysts in nonenzymatic sensors for the detection of glucose. Shao and co-workers prepared bimetallic PtCu nanochains through a simple wet chemical approach.[472] The compositions of the PtCu nanochains can be conveniently controlled using a facile dealloying process. The novel nonenzymatic sensors based on PtCu nanomaterials were built, which are very sensitive and specific for glucose sensing because of the network-like porous nanostructure and synergistic electronic effect between the alloyed compositions. The constructed sensor not only achieved a high sensitivity of 135 μA mM^{-1} cm^{-2} but also performed good accuracy for the detection of glucose in serum samples. Similarly, mesoporous Pt–Au alloy films were constructed via electrodeposition in the presence of surfactant, which demonstrated superb electrocatalytic activity, stability, and reproducibility for glucose oxidation due to the favorable factors resulting from the mesoporous structures and Pt–Au alloyed surfaces.[88] Using optimized $Pt_{51}Au_{49}$ alloy films, the detection range of glucose is 6.0–11 mM with a sensitivity of 352 mA cm^{-2} mM^{-1} and a detection limit of 6.0 mM. The sensitive determination of glucose can also be realized on the electrodes using other PNMNs, such as Au nanocages,[473] nanoporous Pt,[474] dendritic Pt nanostructures,[475] and bimetallic PtPd nanoflakes.[476]

4.2.2. Enzyme-Based Biosensors. The coupling of enzymes with electrochemical sensors enables the convenient detection of target molecules due to the combination of the high specificity of enzymes with the sensitivity of electrochemical transducers.[477,478] A good deal of nanomaterials with different sizes, shapes, and compositions have been prepared and employed as advanced electrode materials to immobilize enzymes and therefore fabricate electrochemical enzyme-based biosensors. Taking advantage of the large surface area and high pore volume, PNMNs can efficiently increase the enzyme loading and protect the enzyme from the surrounding environment. Of them, NPG has received significant interest for constructing electrochemical enzyme-based biosensing platform thanks to its unique physical and chemical properties associated with 3D porous nanostructure. Using a combination of the Langmuir–Blodgett technique and electrochemical deposition, highly ordered macroporous Au was synthesized with the controllable pore size, spatial arrangement of the pores, and number of pore layers.[479] Using Ca^{2+} ions as electrostatic bridges between (4-carboxy-2,5,7-trinitro-9-fluorenylidene) malononitrile (TNF) and NAD^+, the entire inner surface of the porous Au was modified with monolayer redox mediator (Figure 41). The electrocatalytic current for glucose oxidation with glucose dehydrogenase (GDH) on the porous Au electrodes can be significant enhanced by more than 1 order of magnitude in comparison to that on a nonporous counterpart. Pariente et al. also constructed porous Au with rough surfaces using an electrochemical approach and subsequently developed lactate oxidase-based biosensors.[480] This sensor, using hydroxymethylferrocene as a redox mediator in solution, could sensitively detected lactate up to 1.2 mM with a sensitivity of 1.49 μA mM^{-1}. In addition, Chen et al.[481] and Huang et al.[482] used dealloyed Au nanostructures as electrode materials to develop glucose oxidase-modified electrochemical biosensors, both of which exhibit effective enzyme immobilization and showed good analytical performance for biosensing glucose due to the clean, reproducible and uniformly

DOI: 10.1021/acs.chemrev.5b00255
Chem. Rev. XXXX, XXX, XXX–XXX

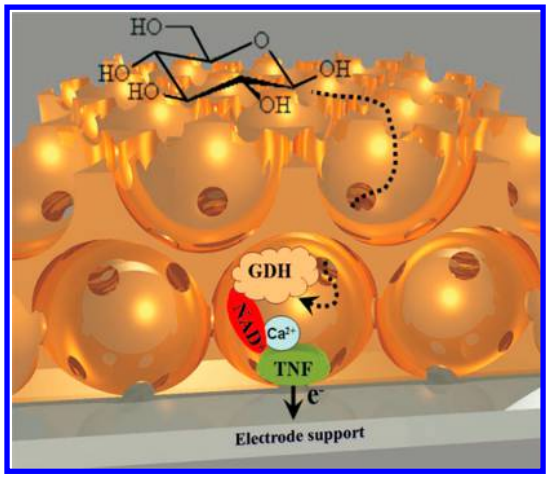

Figure 41. Schematic illustration of an electrode with $1^1/_2$ layers of hollow spheres modified with a mediator monolayer (TNF), Ca^{2+}, and NAD^+, and its reaction in a solution containing the enzyme GDH and the substrate glucose. Reprinted with permission from ref 479. Copyright 2006 Wiley-VCH.

distributed microstructures of the Au nanostructures. In addition to these Au-based porous nanostructures, porous PtAg and PtCu alloyed nanofoams with hollow ligaments were also reported to construct glucose oxidase-modified electrochemical biosensors.[483] The hierarchical nanoporous structures provided a good microenvironment for enzymes and enabled sensitive determination of glucose over a wide linear range (0.6−20 mM). Therefore, it is also expected that these PNMNs would have potential applications in enzyme-based biosensors.

4.2.3. DNA Sensors. Due to the intrinsic advantages mentioned above, NPG electrodes were also constructed as advanced electrochemical sensing platforms for DNA sensors.[209,484] For example, Lin's group fabricated an electrochemical DNA biosensor based on NPG electrodes for the determination of promyelocytic leukemia/retinoic acid receptor α (PML/RARα) fusion genes in acute promyelocytic leukemia using methylene blue (MB) as an electroactive indicator.[209] Typically, the NPG electrode was prepared using repetitive square-wave oxidation reduction cycles and the active surface area of the resulting NPG electrode was 9.9-fold of a bare flat counterpart. The peak current of MB decreased when the probe was hybridized with target DNA. The resulting electrochemical DNA biosensor showed the specificity toward complementary strand and achieved a large determination range from 60 pM to 220 pM with a detection limit of 6.7 pM. Some distinct advantages of NPG electrode, such as superior conductivity, high surface area and biocompatibility, contributed significantly to the relatively high selectivity and sensitivity of the constructed DNA biosensor. Mehrgardi et al. also used the NPG electrode to amplify the detection signal of DNA biosensor. Ferrocene carboxylic acid as an electroactive reporter was covalently attached on the top of probe DNA, which was hybridized with target DNA. Capitalizing on the elimination of direct electro-oxidation signal of reporter on the surface of electrode and the remarkable enhancement of electrochemical signal based on NPG electrode, the sensitively detection of single base mismatches and complementary target DNA was achieved.[484]

4.2.4. Immunosensors and Cytosensors. PNMNs were also widely used in other electrochemical biosensors. Specifically, Zhu et al. also constructed 3D ordered macroporous Au film and used them as advanced electrode material to develop a novel label-free immunosensor for the determination of C-reactive protein (CRP) using electrochemical impedance spectroscopy (EIS).[485] First, the resulting ordered macroporous Au nanostructures possessed large surface area, which was up to 14.4 times higher than that of bare flat counterpart. At the same time, the 3D ordered macroporous Au film consisting of interconnected Au NPs not only endows them with a good biocompatible microenvironment for the immobilization of proteins but also increases the conductivity and stability. With the help of the specific binding of CRP antigen and CRP antibody, the impedance values increased linearly with CRP concentration. The present strategy could achieve a linear range from 0.1 to 20 ng mL^{-1} for the detection of CRP. Recently, Zhu et al. designed a sandwich electrochemical cytosensor enhanced by robust nonenzymatic hybrid nanoelectrocatalysts (Figure 42).[486]

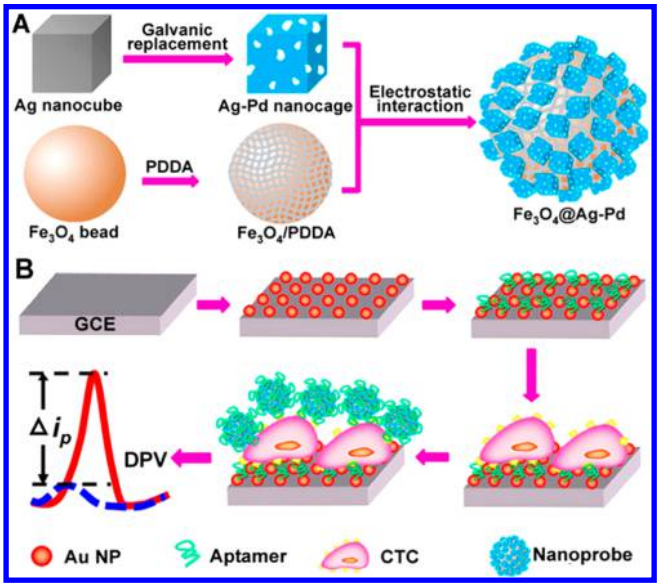

Figure 42. Representation of the fabrication of Fe_3O_4@Ag−Pd hybrid NPs (A) and the cytosensor assembly process (B). Reprinted from ref 486. Copyright 2014 American Chemical Society.

Compared with Fe_3O_4 beads, the catalytic electrochemical signals can be further enhanced by attaching Ag−Pd nanocages as efficient signal amplifiers. These hybrids showed significantly higher electrocatalytic activities than the enzymatic peroxidase/H_2O_2 system, achieving low detection limits of ~4 MCF-7 and ~5 T47D cells in a 1 mL sample. These research efforts indicated that these smart PNMNs provide powerful and reliable electrochemical platforms for the detection of various biomolecules, thus providing potential broad applications in bioanalytical chemistry.

5. CONCLUSION

In this review, we extensively covered different types of PNMNs, ranging from ordered to nonordered porous nanostructures. From the perspective of the synthetic approaches, a broad range of PNMNs, such as aerogels, nanofoams, hollow structures, and highly branched nanomaterials, can be rationally designed. Based on the advantages provided by the attractive and unique properties of these PNMNs, their electrochemical applications with an emphasis on fuel cells and electrochemical sensors and biosensors are

DOI: 10.1021/acs.chemrev.5b00255
Chem. Rev. XXXX, XXX, XXX−XXX

highlighted. These fascinating PNMNs provide a wealth of opportunities in multidisciplinary environments for promoting the rapid development of different research fields.

In spite of significant progress made in the synthesis of porous nanostructures, there are still many challenges ahead in the development of novel PNMNs with functional applications. Because the properties of the PNMNs largely depend on the size, shape, composition, and structure of their building blocks, precise control of these factors is necessary to improve their potential applications. To make further progress, a reliable method for synthesizing high-quality PNMNs with defined structures and properties is highly desirable. In particular, few reports have demonstrated the production of well-designed PNMNs with building blocks that are rich in high-index facets. With regard to the composition, extensive investigations have been focused on the controlled synthesis of bimetallic/multimetallic systems and their related applications, showing synergistic effects between the compositions and the enhanced by 3D porous nanostructures. For example, significant contributions have been made to the construction of the ordered PNMNs using hard templates. However, most of the ordered porous nanostructures are based on monometallic systems, while multimetallic nanostructures are rarely demonstrated. For the new emerging noble metal aerogels, the effects of composition, especially for the introduction of non-noble metals and the new synthetic methods, should be considered simultaneously. A better understanding of PNMN growth mechanisms is critical. The salient experimental and theoretical advances should also bring new avenues for probing the formation mechanism of the PNMNs constructed through different synthetic protocols.

With respect to electrochemical applications, PNMNs with hierarchically porous nanostructures hold great promise. The effect of integrated parameters of PNMNs, such as pore size and volume, the structure and composition of ligament, on the performance of the constructed electrochemical devices should be well investigated. Using highly active electrocatalysts for fuel cell and electrochemical sensors and biosensors has attracted increasing attention from the electrochemists community for the fabrication of superior electrochemical devices. In the case of fuel cells, flexibly controlling the pore structure and the surface engineering, including size, shape, composition and high-index facets of the PNMNs should be addressed in order to produce new electrocatalysts with low cost, high activities, and good durabilities. Another interesting aspect is that for electrochemical sensors and biosensors, it is necessary to rationally design and synthesize functional PNMN-based materials for fabricating novel electrochemical sensors with high sensitivity and specificity. Moreover, researchers should also focus on the porous hybrid systems involving carbon and metal oxides. These porous hybrids are expected to provide additional properties and synergistic effects, which are most likely to be exploited in different electrochemical applications involving multifunctional nanomaterials. With the development of new material fabrication approaches and characterization techniques, it is anticipated that major advancement in PNMNs and their enhanced applications in electrochemistry will emerge in the future.

AUTHOR INFORMATION

Corresponding Author

*E-mail: Yuehe.lin@wsu.edu.

Notes

The authors declare no competing financial interest.

Biographies

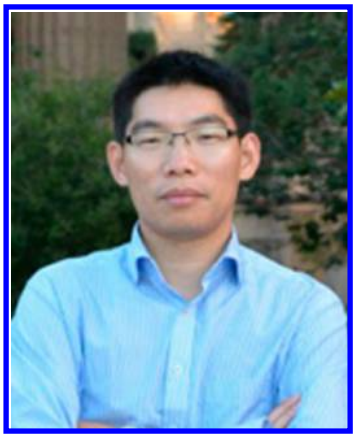

Chengzhou Zhu received his Ph.D. in Analytical Chemistry at the Changchun Institute of Applied Chemistry under the supervision of Prof. Shaojun Dong in January 2013. Since then he did postdoctoral work with Prof. Alexander Eychmüller supported by the Alexander von Humboldt Foundation in Dresden University of Technology. Currently, he is a postdoctoral research associate in the School of Mechanical and Materials Engineering at Washington State University under the supervision of Prof. Yuehe Lin. He has coauthored over 55 peer-reviewed publications. His scientific interests focus on carbon and metal nanomaterials for electrochemical and analytical applications.

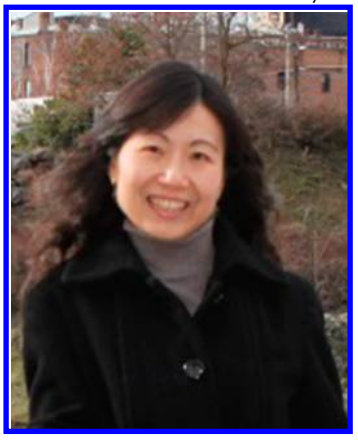

Dan Du received her Ph.D. in Analytical Chemistry from Nanjing University in 2005. She joined Central China Normal University in 2005 and was promoted to Full Professor in 2011. Currently she is a Research Professor at Washington State University. Her research interests include functional nanomaterials for biosensing and drug delivery. Dr. Du has published over 110 papers, with citations of ~3200,and an h-index of 35.

DOI: 10.1021/acs.chemrev.5b00255
Chem. Rev. XXXX, XXX, XXX−XXX

The academic career of Alexander Eychmüller started in Göttingen with studies of physics (Ph.D., MPI for Biophysical Chemistry, A. Weller and K. H. Grellmann) and continued at UCLA (postdoc with M. A. El-Sayed), Berlin (HMI with A. Henglein), and the University of Hamburg (with H. Weller). Since 2005 he has held a chair in Physical Chemistry at TU Dresden. His research interests include the synthesis and characterization of nanosized objects and their photophysical, electrochemical, and structural properties.

Yuehe Lin is a professor at Washington State University and a Laboratory Fellow at Pacific Northwest National Laboratory. His research interests include electrochemistry, bioanalytical chemistry, chemical sensors and biosensors, fuel cells and batteries, material synthesis, and applications. He has over 10 patents and has published about 340 papers, with total citation ~20 000, and an h-index of 75. He is a fellow of the American Association of the Advancement of Science (AAAS), the Royal Society of Chemistry of the U.K., and the American Institute for Medical and Biological Engineering (AIMBE).

ACKNOWLEDGMENTS

This work was supported by a start-up grant from WSU and a Laboratory Directed Research and Development program at Pacific Northwest National Laboratory (PNNL). PNNL is operated by Battelle for US-DOE under Contract DE-AC05-76RL01830. C.Z. and A.E. also acknowledge the Alexander von Humboldt Foundation. D.D. acknowledges the financial support of the National Natural Science Foundation of China (21275062) and the Program for New Century Excellent Talents in University (NCET-12-0871).

ABBREVIATIONS

NPs nanoparticles
PNMNs porous noble metal nanostructures
DG double gyroid
AA ascorbic acid
CMC critical micelle concentration
LLCs lyotropic liquid crystals
EDIT evaporation-mediated direct templating
PAAMs porous anodic alumina membranes
LBL layer-by-layer
HPC hexadecylpyridinium chloride
BCPs block copolymers
PS–PLLA polystyrene-*b*-poly(L-lactide)
3DON Au 3D ordered nanoporous Au
ISO isoprene-*block*-styrene-*block*-ethylene oxide
PI-*b*-PDMAEMA poly(isoprene)-*block*-poly(2-(dimethylamino)ethyl methacrylate)
NPG nanoporous gold
ORR oxygen reduction reaction
AAO anodic aluminum oxide
CTAB cetyltrimethylammonium bromide
OAm oleylamine
OA oleic acid
PVP poly(vinylpyrrolidone)
ZnTPyP Zinc meso-tetra(4-pyridyl)porphyrin
Bu_4NBr tetrabutylammonium bromide
PEO-*b*-PMAA-SDS poly(ethylene oxide)-*block*-poly-(methacrylic acid)-sodium dodecyl sulfate
PS-*b*-P2VP-*b*-PEO polystyrene-*block*-poly(2-vinylpyridine)-*block*-poly(ethylene oxide)
TFT trifluorotoluene
SnOEP Sn^{IV} octaethylporphyrin
DOTAP 1,2-dioleoyl-3-trimethylammoniumpropane
ODA octadecylamine
DMF dimethylformamide
ODE octadecene
DDAB didodecyldimethylammonium bromide
ECSA electrochemically active surface area
DAFCs direct alcohol fuel cells
DFAFCs direct formic acid fuel cells
MOR methanol oxidation reaction
CVs cyclic voltammograms
NTAs nanotube arrays
DEFCs direct ethanol fuel cells
EOR ethanol oxidation reaction
NRAs nanorod arrays
CFC carbon fiber cloth
PEMFC polymer electrolyte membrane fuel cell
TNF (4-carboxy-2,5,7-trinitro-9-fluorenylidene) malononitrile
GDH glucose dehydrogenase
PML/RARα promyelocytic leukemia/retinoic acid receptor α
MB methylene blue
CRP C-reactive protein
EIS electrochemical impedance spectroscopy

REFERENCES

(1) Gong, J.; Li, G.; Tang, Z. Self-assembly of noble metal nanocrystals: Fabrication, optical property, and application. *Nano Today* **2012**, *7*, 564–585.
(2) Heiligtag, F. J.; Niederberger, M. The fascinating world of nanoparticle research. *Mater. Today* **2013**, *16*, 262–271.
(3) Wang, T.; LaMontagne, D.; Lynch, J.; Zhuang, J.; Cao, Y. C. Colloidal superparticles from nanoparticle assembly. *Chem. Soc. Rev.* **2013**, *42*, 2804–2823.

DOI: 10.1021/acs.chemrev.5b00255
Chem. Rev. XXXX, XXX, XXX–XXX

(4) Nykypanchuk, D.; Maye, M. M.; van der Lelie, D.; Gang, O. DNA-guided crystallization of colloidal nanoparticles. *Nature* **2008**, *451*, 549−552.
(5) Walcarius, A. Mesoporous materials and electrochemistry. *Chem. Soc. Rev.* **2013**, *42*, 4098−4140.
(6) Liang, H.-W.; Cao, X.; Zhou, F.; Cui, C.-H.; Zhang, W.-J.; Yu, S.-H. A Free-Standing Pt-Nanowire Membrane as a Highly Stable Electrocatalyst for the Oxygen Reduction Reaction. *Adv. Mater.* **2011**, *23*, 1467−1471.
(7) Tang, F. Q.; Li, L. L.; Chen, D. Mesoporous Silica Nanoparticles: Synthesis, Biocompatibility and Drug Delivery. *Adv. Mater.* **2012**, *24*, 1504−1534.
(8) Lin, H. P.; Mou, C. Y. Structural and morphological control of cationic surfactant-templated mesoporous silica. *Acc. Chem. Res.* **2002**, *35*, 927−935.
(9) Ma, T.-Y.; Liu, L.; Yuan, Z.-Y. Direct synthesis of ordered mesoporous carbons. *Chem. Soc. Rev.* **2013**, *42*, 3977−4003.
(10) Liu, J.; Yang, T.; Wang, D.-W.; Lu, G. Q.; Zhao, D.; Qiao, S. Z. A facile soft-template synthesis of mesoporous polymeric and carbonaceous nanospheres. *Nat. Commun.* **2013**, *4*, 2794.
(11) Xiao, Q.; Sohn, H.; Chen, Z.; Toso, D.; Mechlenburg, M.; Zhou, Z. H.; Poirier, E.; Dailly, A.; Wang, H.; Wu, Z.; et al. Mesoporous Metal and Metal Alloy Particles Synthesized by Aerosol-Assisted Confined Growth of Nanocrystals. *Angew. Chem., Int. Ed.* **2012**, *51*, 10546−10550.
(12) Wang, H.; Jeong, H. Y.; Imura, M.; Wang, L.; Radhakrishnan, L.; Fujita, N.; Castle, T.; Terasaki, O.; Yamauchi, Y. Shape- and Size-Controlled Synthesis in Hard Templates: Sophisticated Chemical Reduction for Mesoporous Monocrystalline Platinum Nanoparticles. *J. Am. Chem. Soc.* **2011**, *133*, 14526−14529.
(13) Ren, Y.; Ma, Z.; Bruce, P. G. Ordered mesoporous metal oxides: synthesis and applications. *Chem. Soc. Rev.* **2012**, *41*, 4909−4927.
(14) Gu, D.; Schuth, F. Synthesis of non-siliceous mesoporous oxides. *Chem. Soc. Rev.* **2014**, *43*, 313−344.
(15) Choi, D.-H.; Ryoo, R. Template synthesis of ordered mesoporous organic polymeric materials using hydrophobic silylated KIT-6 mesoporous silica. *J. Mater. Chem.* **2010**, *20*, 5544−5550.
(16) He, W.; Jiang, C.; Wang, J.; Lu, L. High-Rate Oxygen Electroreduction over Graphitic-N Species Exposed on 3D Hierarchically Porous Nitrogen-Doped Carbons. *Angew. Chem., Int. Ed.* **2014**, *53*, 9503−9507.
(17) Xu, Y.; Zhang, B. Recent advances in porous Pt-based nanostructures: synthesis and electrochemical applications. *Chem. Soc. Rev.* **2014**, *43*, 2439−2450.
(18) Parlett, C. M. A.; Wilson, K.; Lee, A. F. Hierarchical porous materials: catalytic applications. *Chem. Soc. Rev.* **2013**, *42*, 3876−3893.
(19) Zhu, C.; Zhai, J.; Dong, S. Ionic liquid-induced three-dimensional macroassembly of graphene and its applications in electrochemical energy storage. *Nanoscale* **2014**, *6*, 10077−10083.
(20) Han, S.; Wu, D. Q.; Li, S.; Zhang, F.; Feng, X. L. Porous Graphene Materials for Advanced Electrochemical Energy Storage and Conversion Devices. *Adv. Mater.* **2014**, *26*, 849−864.
(21) Valtchev, V.; Tosheva, L. Porous Nanosized Particles: Preparation, Properties, and Applications. *Chem. Rev.* **2013**, *113*, 6734−6760.
(22) Meek, S. T.; Greathouse, J. A.; Allendorf, M. D. Metal-Organic Frameworks: A Rapidly Growing Class of Versatile Nanoporous Materials. *Adv. Mater.* **2011**, *23*, 249−267.
(23) Zhang, S.; Guo, S.; Zhu, H.; Su, D.; Sun, S. Structure-Induced Enhancement in Electrooxidation of Trimetallic FePtAu Nanoparticles. *J. Am. Chem. Soc.* **2012**, *134*, 5060−5063.
(24) Zhang, L.; Guo, S.; Dong, S.; Wang, E. Pd Nanowires as New Biosensing Materials for Magnified Fluorescent Detection of Nucleic Acid. *Anal. Chem.* **2012**, *84*, 3568−3573.
(25) Xu, J.; White, T.; Li, P.; He, C.; Yu, J.; Yuan, W.; Han, Y.-F. Biphasic Pd−Au Alloy Catalyst for Low-Temperature CO Oxidation. *J. Am. Chem. Soc.* **2010**, *132*, 10398−10406.
(26) Shang, L.; Dong, S.; Nienhaus, G. U. Ultra-small fluorescent metal nanoclusters: Synthesis and biological applications. *Nano Today* **2011**, *6*, 401−418.
(27) Jin, Y.; Jia, C.; Huang, S.-W.; O'Donnell, M.; Gao, X. Multifunctional nanoparticles as coupled contrast agents. *Nat. Commun.* **2010**, *1*, 41.
(28) Kim, D.; Resasco, J.; Yu, Y.; Asiri, A. M.; Yang, P. Synergistic geometric and electronic effects for electrochemical reduction of carbon dioxide using gold−copper bimetallic nanoparticles. *Nat. Commun.* **2014**, *5*, 4948.
(29) Shen, Z.; O'Carroll, D. M.; Nanoporous Silver. Thin Films: Multifunctional Platforms for Influencing Chain Morphology and Optical Properties of Conjugated Polymers. *Adv. Funct. Mater.* **2015**, *25*, 3302−3313.
(30) Quan, Z.; Wang, Y.; Fang, J. High-Index Faceted Noble Metal Nanocrystals. *Acc. Chem. Res.* **2012**, *46*, 191−202.
(31) Guo, S.; Wang, E. Noble metal nanomaterials: Controllable synthesis and application in fuel cells and analytical sensors. *Nano Today* **2011**, *6*, 240−264.
(32) Wang, D.; Li, Y. Bimetallic Nanocrystals: Liquid-Phase Synthesis and Catalytic Applications. *Adv. Mater.* **2011**, *23*, 1044−1060.
(33) Zhang, L.; Niu, W.; Xu, G. Synthesis and applications of noble metal nanocrystals with high-energy facets. *Nano Today* **2012**, *7*, 586−605.
(34) Kloke, A.; von Stetten, F.; Zengerle, R.; Kerzenmacher, S. Strategies for the Fabrication of Porous Platinum Electrodes. *Adv. Mater.* **2011**, *23*, 4976−5008.
(35) Guo, D.-J.; Ding, Y. Porous Nanostructured Metals for Electrocatalysis. *Electroanalysis* **2012**, *24*, 2035−2043.
(36) Biener, J.; Nyce, G. W.; Hodge, A. M.; Biener, M. M.; Hamza, A. V.; Maier, S. A. Nanoporous plasmonic metamaterials. *Adv. Mater.* **2008**, *20*, 1211−1217.
(37) Yang, S.; Luo, X. Mesoporous nano/micro noble metal particles: synthesis and applications. *Nanoscale* **2014**, *6*, 4438−4457.
(38) Lu, L.; Eychmüller, A.; Kobayashi, A.; Hirano, Y.; Yoshida, K.; Kikkawa, Y.; Tawa, K.; Ozaki, Y. Designed Fabrication of Ordered Porous Au/Ag Nanostructured Films for Surface-Enhanced Raman Scattering Substrates. *Langmuir* **2006**, *22*, 2605−2609.
(39) Shin, H. J.; Ko, C. H.; Ryoo, R. Synthesis of platinum networks with nanoscopic periodicity using mesoporous silica as template. *J. Mater. Chem.* **2001**, *11*, 260−261.
(40) Jiao, F.; Jumas, J.-C.; Womes, M.; Chadwick, A. V.; Harrison, A.; Bruce, P. G. Synthesis of Ordered Mesoporous Fe_3O_4 and γ-Fe_2O_3 with Crystalline Walls Using Post-Template Reduction/Oxidation. *J. Am. Chem. Soc.* **2006**, *128*, 12905−12909.
(41) Lai, X.; Li, X.; Geng, W.; Tu, J.; Li, J.; Qiu, S. Ordered Mesoporous Copper Oxide with Crystalline Walls. *Angew. Chem., Int. Ed.* **2007**, *46*, 738−741.
(42) Zhou, M.; Wu, H. B.; Bao, J.; Liang, L.; Lou, X. W.; Xie, Y. Ordered Macroporous $BiVO_4$ Architectures with Controllable Dual Porosity for Efficient Solar Water Splitting. *Angew. Chem., Int. Ed.* **2013**, *52*, 8579−8583.
(43) Hoffmann, C.; Thieme, S.; Brückner, J.; Oschatz, M.; Biemelt, T.; Mondin, G.; Althues, H.; Kaskel, S. Nanocasting Hierarchical Carbide-Derived Carbons in Nanostructured Opal Assemblies for High-Performance Cathodes in Lithium−Sulfur Batteries. *ACS Nano* **2014**, *8*, 12130−12140.
(44) Yamauchi, Y. Field-Induced alignment controls of one-dimensional mesochannels in mesoporous materials. *J. Ceram. Soc. Jpn.* **2013**, *121*, 831−840.
(45) Ryoo, R.; Joo, S. H.; Jun, S. Synthesis of Highly Ordered Carbon Molecular Sieves via Template-Mediated Structural Transformation. *J. Phys. Chem. B* **1999**, *103*, 7743−7746.
(46) Stein, A.; Li, F.; Denny, N. R. Morphological Control in Colloidal Crystal Templating of Inverse Opals, Hierarchical Structures, and Shaped Particles. *Chem. Mater.* **2007**, *20*, 649−666.
(47) Velev, O. D.; Kaler, E. W. Structured Porous Materials via Colloidal Crystal Templating: From Inorganic Oxides to Metals. *Adv. Mater.* **2000**, *12*, 531−534.

DOI: 10.1021/acs.chemrev.5b00255
Chem. Rev. XXXX, XXX, XXX−XXX

(48) Lu, L.; Eychmüller, A. Ordered Macroporous Bimetallic Nanostructures: Design, Characterization, and Applications. *Acc. Chem. Res.* **2008**, *41*, 244−253.
(49) Jiang, P. Surface-Templated Nanostructured Films with Two-Dimensional Ordered Arrays of Voids. *Angew. Chem., Int. Ed.* **2004**, *43*, 5625−5628.
(50) Jiang, P.; Cizeron, J.; Bertone, J. F.; Colvin, V. L. Preparation of Macroporous Metal Films from Colloidal Crystals. *J. Am. Chem. Soc.* **1999**, *121*, 7957−7958.
(51) Lu, L.; Randjelovic, I.; Capek, R.; Gaponik, N.; Yang, J.; Zhang, H.; Eychmüller, A. Controlled Fabrication of Gold-Coated 3D Ordered Colloidal Crystal Films and Their Application in Surface-Enhanced Raman Spectroscopy. *Chem. Mater.* **2005**, *17*, 5731−5736.
(52) Lu, L.; Capek, R.; Kornowski, A.; Gaponik, N.; Eychmüller, A. Selective Fabrication of Ordered Bimetallic Nanostructures with Hierarchical Porosity. *Angew. Chem., Int. Ed.* **2005**, *44*, 5997−6001.
(53) Kuroda, Y.; Yamauchi, Y.; Kuroda, K. Integrated structural control of cage-type mesoporous platinum possessing both tunable large mesopores and variable surface structures by block copolymer-assisted Pt deposition in a hard-template. *Chem. Commun.* **2010**, *46*, 1827−1829.
(54) Tessier, P. M.; Velev, O. D.; Kalambur, A. T.; Rabolt, J. F.; Lenhoff, A. M.; Kaler, E. W. Assembly of Gold Nanostructured Films Templated by Colloidal Crystals and Use in Surface-Enhanced Raman Spectroscopy. *J. Am. Chem. Soc.* **2000**, *122*, 9554−9555.
(55) Liu, Z.; Che, R.; Elzatahry, A. A.; Zhao, D. Direct Imaging Au Nanoparticle Migration Inside Mesoporous Silica Channels. *ACS Nano* **2014**, *8*, 10455−10460.
(56) Zhu, J.; Xie, X.; Carabineiro, S. A. C.; Tavares, P. B.; Figueiredo, J. L.; Schomacker, R.; Thomas, A. Facile one-pot synthesis of Pt nanoparticles/SBA-15: an active and stable material for catalytic applications. *Energy Environ. Sci.* **2011**, *4*, 2020−2024.
(57) Han, Y.-J.; Kim, J. M.; Stucky, G. D. Preparation of Noble Metal Nanowires Using Hexagonal Mesoporous Silica SBA-15. *Chem. Mater.* **2000**, *12*, 2068−2069.
(58) Huang, M. H.; Choudrey, A.; Yang, P. Ag nanowire formation within mesoporous silica. *Chem. Commun.* **2000**, 1063−1064.
(59) Takai, A.; Ataee-Esfahani, H.; Doi, Y.; Fuziwara, M.; Yamauchi, Y.; Kuroda, K. Pt nanoworms: creation of a bumpy surface on one-dimensional (1D) Pt nanowires with the assistance of surfactants embedded in mesochannels. *Chem. Commun.* **2011**, *47*, 7701−7703.
(60) Shin, H. J.; Ryoo, R.; Liu, Z.; Terasaki, O. Template synthesis of asymmetrically mesostructured platinum networks. *J. Am. Chem. Soc.* **2001**, *123*, 1246−1247.
(61) Guo, X. J.; Yang, C. M.; Liu, P. H.; Cheng, M. H.; Chao, K. J. Formation and growth of platinum nanostructures in cubic mesoporous silica. *Cryst. Growth Des.* **2005**, *5*, 33−36.
(62) Jiang, J.; Kucernak, A. Synthesis of highly active nanostructured PtRu electrocatalyst with three-dimensional mesoporous silica template. *Electrochem. Commun.* **2009**, *11*, 623−626.
(63) Doi, Y.; Takai, A.; Sakamoto, Y.; Terasaki, O.; Yamauchi, Y.; Kuroda, K. Tailored synthesis of mesoporous platinum replicas using double gyroid mesoporous silica (KIT-6) with different pore diameters via vapor infiltration of a reducing agent. *Chem. Commun.* **2010**, *46*, 6365−6367.
(64) Wang, D.; Zhou, W. L.; McCaughy, B. F.; Hampsey, J. E.; Ji, X.; Jiang, Y. B.; Xu, H.; Tang, J.; Schmehl, R. H.; O'Connor, C.; Brinker, C. J.; Lu, Y. Electrodeposition of Metallic Nanowire Thin Films Using Mesoporous Silica Templates. *Adv. Mater.* **2003**, *15*, 130−133.
(65) Tominaka, S.; Wu, C.-W.; Momma, T.; Kuroda, K.; Osaka, T. Perpendicular mesoporous Pt thin films: electrodeposition from titania nanopillars and their electrochemical properties. *Chem. Commun.* **2008**, 2888−2890.
(66) Wang, D.; Luo, H.; Kou, R.; Gil, M. P.; Xiao, S.; Golub, V. O.; Yang, Z.; Brinker, C. J.; Lu, Y. A General Route to Macroscopic Hierarchical 3D Nanowire Networks. *Angew. Chem., Int. Ed.* **2004**, *116*, 6295−6299.
(67) Kibsgaard, J.; Gorlin, Y.; Chen, Z.; Jaramillo, T. F. Meso-Structured Platinum Thin Films: Active and Stable Electrocatalysts for the Oxygen Reduction Reaction. *J. Am. Chem. Soc.* **2012**, *134*, 7758−7765.
(68) Karthika, P.; Ataee-Esfahani, H.; Wang, H.; Francis, M. A.; Abe, H.; Rajalakshmi, N.; Dhathathreyan, K. S.; Arivuoli, D.; Yamauchi, Y. Synthesis of Mesoporous Pt−Ru Alloy Particles with Uniform Sizes by Sophisticated Hard-Templating Method. *Chem.—Asian J.* **2013**, *8*, 902−907.
(69) Wang, H.; Imura, M.; Nemoto, Y.; Park, S.-E.; Yamauchi, Y. Synthesis of Olive-Shaped Mesoporous Platinum Nanoparticles (MPNs) with a Hard-Templating Method Using Mesoporous Silica (SBA-15). *Chem.—Asian J.* **2012**, *7*, 802−808.
(70) Chen, P.-K.; Lai, N.-C.; Ho, C.-H.; Hu, Y.-W.; Lee, J.-F.; Yang, C.-M. New Synthesis of MCM-48 Nanospheres and Facile Replication to Mesoporous Platinum Nanospheres as Highly Active Electrocatalysts for the Oxygen Reduction Reaction. *Chem. Mater.* **2013**, *25*, 4269−4277.
(71) Yamauchi, Y.; Kuroda, K. Rational Design of Mesoporous Metals and Related Nanomaterials by a Soft-Template Approach. *Chem.—Asian J.* **2008**, *3*, 664−676.
(72) Attard, G. S.; Corker, J. M.; Göltner, C. G.; Henke, S.; Templer, R. H. Liquid-Crystal Templates for Nanostructured Metals. *Angew. Chem., Int. Ed.* **1997**, *36*, 1315−1317.
(73) Attard, G. S.; Bartlett, P. N.; Coleman, N. R. B.; Elliott, J. M.; Owen, J. R.; Wang, J. H. Mesoporous platinum films from lyotropic liquid crystalline phases. *Science* **1997**, *278*, 838−840.
(74) Zhang, X.; Lu, W.; Dai, J.; Bourgeois, L.; Hao, N.; Wang, H.; Zhao, D.; Webley, P. A. Ordered Hierarchical Porous Platinum Membranes with Tailored Mesostructures. *Angew. Chem., Int. Ed.* **2010**, *49*, 10101−10105.
(75) Sugimoto, W.; Makino, S.; Mukai, R.; Tatsumi, Y.; Fukuda, K.; Takasu, Y.; Yamauchi, Y. Synthesis of ordered mesoporous ruthenium by lyotropic liquid crystals and its electrochemical conversion to mesoporous ruthenium oxide with high surface area. *J. Power Sources* **2012**, *204*, 244−248.
(76) Jiang, J.; Kucernak, A. Mesoporous Microspheres Composed of PtRu Alloy. *Chem. Mater.* **2004**, *16*, 1362−1367.
(77) Liang, Y.-C.; Juan, Y.-W.; Lu, K.-T.; Jeng, U. S.; Chen, S.-A.; Chuang, W.-T.; Su, C.-J.; Liu, C.-L.; Pao, C.-W.; Lee, J.-F.; et al. Formation Process of Mesostructured PtRu Nanoparticles Electrodeposited on a Microemulsion Lyotropic Liquid Crystalline Template As Revealed by in Situ XRD, SAXS, and XANES. *J. Phys. Chem. C* **2012**, *116*, 26649−26655.
(78) Jiang, J.; Kucernak, A. Electrocatalytic properties of nanoporous PtRu alloy towards the electrooxidation of formic acid. *J. Electroanal. Chem.* **2009**, *630*, 10−18.
(79) Yamauchi, Y.; Momma, T.; Kitoh, H.; Osaka, T.; Kuroda, K. Fabrication of mesoporous Pt inside micrometer channels via "solvent-evaporation-mediated direct physical casting. *Electrochem. Commun.* **2005**, *7*, 1364−1370.
(80) Takai, A.; Saida, T.; Sugimoto, W.; Wang, L.; Yamauchi, Y.; Kuroda, K. Preparation of Mesoporous Pt−Ru Alloy Fibers with Tunable Compositions via Evaporation-Mediated Direct Templating (EDIT) Method Utilizing Porous Anodic Alumina Membranes. *Chem. Mater.* **2009**, *21*, 3414−3423.
(81) Yamauchi, Y.; Ohsuna, T.; Kuroda, K. Synthesis and Structural Characterization of a Highly Ordered Mesoporous Pt−Ru Alloy via "Evaporation-Mediated Direct Templating. *Chem. Mater.* **2007**, *19*, 1335−1342.
(82) Luo, K.; Walker, C. T.; Edler, K. J. Mesoporous Silver Films from Dilute Mixed-Surfactant Solutions by Using Dip-Coating. *Adv. Mater.* **2007**, *19*, 1506−1509.
(83) Yamauchi, Y.; Sugiyama, A.; Morimoto, R.; Takai, A.; Kuroda, K. Mesoporous Platinum with Giant Mesocages Templated from Lyotropic Liquid Crystals Consisting of Diblock Copolymers. *Angew. Chem., Int. Ed.* **2008**, *47*, 5371−5373.
(84) Yamauchi, Y.; Takai, A.; Nagaura, T.; Inoue, S.; Kuroda, K. Pt Fibers with Stacked Donut-Like Mesospace by Assembling Pt Nanoparticles: Guided Deposition in Physically Confined Self-Assembly of Surfactants. *J. Am. Chem. Soc.* **2008**, *130*, 5426−5427.

DOI: 10.1021/acs.chemrev.5b00255
Chem. Rev. XXXX, XXX, XXX−XXX

(85) Takai, A.; Yamauchi, Y.; Kuroda, K. Fabrication of mesoporous Pt nanotubes utilizing dual templates under a reduced pressure condition. *Chem. Commun.* **2008**, 4171−4173.
(86) Takai, A.; Sakamoto, Y.; Terasaki, O.; Yamauchi, Y.; Kuroda, K. Platinum Nanopeapods: Spatial Control of Mesopore Arrangements by Utilizing a Physically Confined Space. *Chem.—Eur. J.* **2013**, *19*, 11564−11567.
(87) Wang, H.; Wang, L.; Sato, T.; Sakamoto, Y.; Tominaka, S.; Miyasaka, K.; Miyamoto, N.; Nemoto, Y.; Terasaki, O.; Yamauchi, Y. Synthesis of Mesoporous Pt Films with Tunable Pore Sizes from Aqueous Surfactant Solutions. *Chem. Mater.* **2012**, *24*, 1591−1598.
(88) Li, C.; Wang, H.; Yamauchi, Y. Electrochemical Deposition of Mesoporous Pt−Au Alloy Films in Aqueous Surfactant Solutions: Towards a Highly Sensitive Amperometric Glucose Sensor. *Chem.—Eur. J.* **2013**, *19*, 2242−2246.
(89) Wang, H.; Imura, M.; Nemoto, Y.; Wang, L.; Jeong, H. Y.; Yokoshima, T.; Terasaki, O.; Yamauchi, Y. Electrochemical Design of Mesoporous Pt−Ru Alloy Films with Various Compositions toward Superior Electrocatalytic Performance. *Chem.—Eur. J.* **2012**, *18*, 13142−13148.
(90) Wang, H.; Yamauchi, Y. Synthesis of Mesoporous Platinum−Palladium Alloy Films by Electrochemical Plating in Aqueous Surfactant Solutions. *Chem.—Asian J.* **2012**, *7*, 2133−2138.
(91) Li, C.; Dag, Ö.; Dao, T. D.; Nagao, T.; Sakamoto, Y.; Kimura, T.; Terasaki, O.; Yamauchi, Y. Electrochemical synthesis of mesoporous gold films toward mesospace-stimulated optical properties. *Nat. Commun.* **2015**, *6*, 6608.
(92) Li, C.; Yamauchi, Y. Synthesis of Mesoporous Platinum−Copper Films by Electrochemical Micelle Assembly and Their Electrochemical Applications. *Chem.—Eur. J.* **2014**, *20*, 729−733.
(93) Li, C.; Malgras, V.; Aldalbahi, A.; Yamauchi, Y. Dealloying of Mesoporous PtCu Alloy Film for the Synthesis of Mesoporous Pt Films with High Electrocatalytic Activity. *Chem.—Asian J.* **2015**, *10*, 316−320.
(94) Wang, H.; Ishihara, S.; Ariga, K.; Yamauchi, Y. All-Metal Layer-by-Layer Films: Bimetallic Alternate Layers with Accessible Mesopores for Enhanced Electrocatalysis. *J. Am. Chem. Soc.* **2012**, *134*, 10819−10821.
(95) Li, C.; Sato, T.; Yamauchi, Y. Electrochemical Synthesis of One-Dimensional Mesoporous Pt Nanorods Using the Assembly of Surfactant Micelles in Confined Space. *Angew. Chem., Int. Ed.* **2013**, *52*, 8050−8053.
(96) Li, C.; Imura, M.; Yamauchi, Y. Displacement Plating of a Mesoporous Pt Skin onto Co Nanochains in a Low-Concentration Surfactant Solution. *Chem.—Eur. J.* **2014**, *20*, 3277−3282.
(97) Li, C.; Imura, M.; Yamauchi, Y. A universal approach to the preparation of colloidal mesoporous platinum nanoparticles with controlled particle sizes in a wide range from 20 to 200 nm. *Phys. Chem. Chem. Phys.* **2014**, *16*, 8787−8790.
(98) Ataee-Esfahani, H.; Liu, J.; Hu, M.; Miyamoto, N.; Tominaka, S.; Wu, K. C. W.; Yamauchi, Y. Mesoporous Metallic Cells: Design of Uniformly Sized Hollow Mesoporous Pt−Ru Particles with Tunable Shell Thicknesses. *Small* **2013**, *9*, 1047−1051.
(99) Li, C.; Sato, T.; Yamauchi, Y. Size-controlled synthesis of mesoporous palladium nanoparticles as highly active and stable electrocatalysts. *Chem. Commun.* **2014**, *50*, 11753−11756.
(100) Bates, F. S.; Fredrickson, G. H. Block Copolymer Thermodynamics: Theory and Experiment. *Annu. Rev. Phys. Chem.* **1990**, *41*, 525−557.
(101) Orilall, M. C.; Wiesner, U. Block copolymer based composition and morphology control in nanostructured hybrid materials for energy conversion and storage: solar cells, batteries, and fuel cells. *Chem. Soc. Rev.* **2011**, *40*, 520−535.
(102) Hsueh, H.-Y.; Huang, Y.-C.; Ho, R.-M.; Lai, C.-H.; Makida, T.; Hasegawa, H. Nanoporous Gyroid Nickel from Block Copolymer Templates via Electroless Plating. *Adv. Mater.* **2011**, *23*, 3041−3046.
(103) Crossland, E. J. W.; Kamperman, M.; Nedelcu, M.; Ducati, C.; Wiesner, U.; Smilgies, D. M.; Toombes, G. E. S.; Hillmyer, M. A.; Ludwigs, S.; Steiner, U.; et al. A Bicontinuous Double Gyroid Hybrid Solar Cell. *Nano Lett.* **2009**, *9*, 2807−2812.
(104) Tseng, W.-H.; Chen, C.-K.; Chiang, Y.-W.; Ho, R.-M.; Akasaka, S.; Hasegawa, H. Helical Nanocomposites from Chiral Block Copolymer Templates. *J. Am. Chem. Soc.* **2009**, *131*, 1356−1357.
(105) Hsueh, H.-Y.; Chen, H.-Y.; She, M.-S.; Chen, C.-K.; Ho, R.-M.; Gwo, S.; Hasegawa, H.; Thomas, E. L. Inorganic Gyroid with Exceptionally Low Refractive Index from Block Copolymer Templating. *Nano Lett.* **2010**, *10*, 4994−5000.
(106) Vukovic, I.; Punzhin, S.; Vukovic, Z.; Onck, P.; De Hosson, J. T. M.; ten Brinke, G.; Loos, K. Supramolecular Route to Well-Ordered Metal Nanofoams. *ACS Nano* **2011**, *5*, 6339−6348.
(107) Vukovic, I.; Brinke, G. t.; Loos, K. Block copolymer template-directed synthesis of well-ordered metallic nanostructures. *Polymer* **2013**, *54*, 2591−2605.
(108) Crossland, E. J. W.; Ludwigs, S.; Hillmyer, M. A.; Steiner, U. Control of gyroid forming block copolymer templates: effects of an electric field and surface topography. *Soft Matter* **2010**, *6*, 670−676.
(109) Scherer, M. R. J.; Cunha, P. M. S.; Steiner, U. Labyrinth-Induced Faceted Electrochemical Growth. *Adv. Mater.* **2014**, *26*, 2403−2407.
(110) Hsueh, H.-Y.; Chen, H.-Y.; Hung, Y.-C.; Ling, Y.-C.; Gwo, S.; Ho, R.-M. Well-Defined Multibranched Gold with Surface Plasmon Resonance in Near-Infrared Region from Seeding Growth Approach Using Gyroid Block Copolymer Template. *Adv. Mater.* **2013**, *25*, 1780−1786.
(111) Vignolini, S.; Yufa, N. A.; Cunha, P. S.; Guldin, S.; Rushkin, I.; Stefik, M.; Hur, K.; Wiesner, U.; Baumberg, J. J.; Steiner, U. A 3D Optical Metamaterial Made by Self-Assembly. *Adv. Mater.* **2012**, *24*, OP23−OP27.
(112) Cowman, C. D.; Padgett, E.; Tan, K. W.; Hovden, R.; Gu, Y.; Andrejevic, N.; Muller, D.; Coates, G. W.; Wiesner, U. Multicomponent Nanomaterials with Complex Networked Architectures from Orthogonal Degradation and Binary Metal Backfilling in ABC Triblock Terpolymers. *J. Am. Chem. Soc.* **2015**, *137*, 6026−6033.
(113) Hoheisel, T. N.; Hur, K.; Wiesner, U. B. Block copolymer-nanoparticle hybrid self-assembly. *Prog. Polym. Sci.* **2015**, *40*, 3−32.
(114) Rauda, I. E.; Buonsanti, R.; Saldarriaga-Lopez, L. C.; Benjauthrit, K.; Schelhas, L. T.; Stefik, M.; Augustyn, V.; Ko, J.; Dunn, B.; Wiesner, U.; Milliron, D. J.; et al. General Method for the Synthesis of Hierarchical Nanocrystal-Based Mesoporous Materials. *ACS Nano* **2012**, *6*, 6386−6399.
(115) Warren, S. C.; Wiesner, U. Self-assembled ordered mesoporous metals. *Pure Appl. Chem.* **2009**, *81*, 73−84.
(116) Li, Z.; Sai, H.; Warren, S. C.; Kamperman, M.; Arora, H.; Gruner, S. M.; Wiesner, U. Metal Nanoparticle−Block Copolymer Composite Assembly and Disassembly. *Chem. Mater.* **2009**, *21*, 5578−5584.
(117) Warren, S. C.; Messina, L. C.; Slaughter, L. S.; Kamperman, M.; Zhou, Q.; Gruner, S. M.; DiSalvo, F. J.; Wiesner, U. Ordered Mesoporous Materials from Metal Nanoparticle−Block Copolymer Self-Assembly. *Science* **2008**, *320*, 1748−1752.
(118) Arora, H.; Li, Z.; Sai, H.; Kamperman, M.; Warren, S. C.; Wiesner, U. Block Copolymer Directed Nanoporous Metal Thin Films. *Macromol. Rapid Commun.* **2010**, *31*, 1960−1964.
(119) Li, Z.; Hur, K.; Sai, H.; Higuchi, T.; Takahara, A.; Jinnai, H.; Gruner, S. M.; Wiesner, U. Linking experiment and theory for three-dimensional networked binary metal nanoparticle−triblock terpolymer superstructures. *Nat. Commun.* **2014**, *5*, 3247.
(120) Tappan, B. C.; Steiner, S. A.; Luther, E. P. Nanoporous Metal Foams. *Angew. Chem., Int. Ed.* **2010**, *49*, 4544−4565.
(121) Erlebacher, J.; Aziz, M. J.; Karma, A.; Dimitrov, N.; Sieradzki, K. Evolution of nanoporosity in dealloying. *Nature* **2001**, *410*, 450−453.
(122) Raney, M. Method of producing Finely Divided Nickel. U.S. Patent 1,628,190, 1927; *Chem. Abstr.* 1927, *21*, 2116.
(123) Wittstock, A.; et al. Nanoporous Au: An Unsupported Pure Gold Catalyst? *J. Phys. Chem. C* **2009**, *113*, 5593−5600.

DOI: 10.1021/acs.chemrev.5b00255
Chem. Rev. XXXX, XXX, XXX−XXX

(124) Ding, Y.; Kim, Y. J.; Erlebacher, J. Nanoporous Gold Leaf: "Ancient Technology"/Advanced Material. *Adv. Mater.* **2004**, *16*, 1897−1900.
(125) Ding, Y.; Erlebacher, J. Nanoporous Metals with Controlled Multimodal Pore Size Distribution. *J. Am. Chem. Soc.* **2003**, *125*, 7772−7773.
(126) Qi, Z.; Weissmueller, J. Hierarchical Nested-Network Nanostructure by Dealloying. *ACS Nano* **2013**, *7*, 5948−5954.
(127) Qi, Z.; Vainio, U.; Kornowski, A.; Ritter, M.; Weller, H.; Jin, H.; Weissmüller, J. Porous Gold with a Nested-Network Architecture and Ultrafine Structure. *Adv. Funct. Mater.* **2015**, *25*, 2530−2536.
(128) Zhang, J.; Liu, P.; Ma, H.; Ding, Y. Nanostructured porous gold for methanol electro-oxidation. *J. Phys. Chem. C* **2007**, *111*, 10382−10388.
(129) Wang, X.; Wang, W.; Qi, Z.; Zhao, C.; Ji, H.; Zhang, Z. Electrochemical catalytic activities of nanoporous palladium rods for methanol electro-oxidation. *J. Power Sources* **2010**, *195*, 6740−6747.
(130) Zhang, Z.; Wang, Y.; Qi, Z.; Zhang, W.; Qin, J.; Frenzel, J. Generalized Fabrication of Nanoporous Metals (Au, Pd, Pt, Ag, and Cu) through Chemical Dealloying. *J. Phys. Chem. C* **2009**, *113*, 12629−12636.
(131) Koh, S.; Strasser, P. Electrocatalysis on Bimetallic Surfaces: Modifying Catalytic Reactivity for Oxygen Reduction by Voltammetric Surface Dealloying. *J. Am. Chem. Soc.* **2007**, *129*, 12624−12625.
(132) Strasser, P.; Koh, S.; Anniyev, T.; Greeley, J.; More, K.; Yu, C.; Liu, Z.; Kaya, S.; Nordlund, D.; Ogasawara, H.; Toney, M. F.; Nilsson, A. Lattice-strain control of the activity in dealloyed core−shell fuel cell catalysts. *Nat. Chem.* **2010**, *2*, 454−460.
(133) Ge, X.; Chen, L.; Kang, J.; Fujita, T.; Hirata, A.; Zhang, W.; Jiang, J.; Chen, M. A Core-Shell Nanoporous Pt-Cu Catalyst with Tunable Composition and High Catalytic Activity. *Adv. Funct. Mater.* **2013**, *23*, 4156−4162.
(134) Tominaka, S.; Hayashi, T.; Nakamura, Y.; Osaka, T. Mesoporous PdCo sponge-like nanostructure synthesized by electrodeposition and dealloying for oxygen reduction reaction. *J. Mater. Chem.* **2010**, *20*, 7175−7182.
(135) Du, C.; Chen, M.; Wang, W.; Yin, G. Nanoporous PdNi Alloy Nanowires As Highly Active Catalysts for the Electro-Oxidation of Formic Acid. *ACS Appl. Mater. Interfaces* **2010**, *3*, 105−109.
(136) Oezaslan, M.; Heggen, M.; Strasser, P. Size-Dependent Morphology of Dealloyed Bimetallic Catalysts: Linking the Nano to the Macro Scale. *J. Am. Chem. Soc.* **2011**, *134*, 514−524.
(137) Li, X.; Chen, Q.; McCue, I.; Snyder, J.; Crozier, P.; Erlebacher, J.; Sieradzki, K. Dealloying of Noble-Metal Alloy Nanoparticles. *Nano Lett.* **2014**, *14*, 2569−2577.
(138) Qiu, H. J.; Xu, H. T.; Li, X.; Wang, J. Q.; Wang, Y. Core-shell-structured nanoporous PtCu with high Cu content and enhanced catalytic performance. *J. Mater. Chem. A* **2015**, *3*, 7939−7944.
(139) Chen, L.; Guo, H.; Fujita, T.; Hirata, A.; Zhang, W.; Inoue, A.; Chen, M. Nanoporous PdNi Bimetallic Catalyst with Enhanced Electrocatalytic Performances for Electro-oxidation and Oxygen Reduction Reactions. *Adv. Funct. Mater.* **2011**, *21*, 4364−4370.
(140) Xu, C.; Liu, Y.; Wang, J.; Geng, H.; Qiu, H. Nanoporous PdCu alloy for formic acid electro-oxidation. *J. Power Sources* **2012**, *199*, 124−131.
(141) Xu, C.; Hao, Q.; Duan, H. Nanoporous PdPt alloy as a highly active electrocatalyst for formic acid oxidation. *J. Mater. Chem. A* **2014**, *2*, 8875−8880.
(142) Wang, R.; Xu, C.; Bi, X.; Ding, Y. Nanoporous surface alloys as highly active and durable oxygen reduction reaction electrocatalysts. *Energy Environ. Sci.* **2012**, *5*, 5281−5286.
(143) Xu, C.; Wang, R.; Chen, M.; Zhang, Y.; Ding, Y. Dealloying to nanoporous Au/Pt alloys and their structure sensitive electrocatalytic properties. *Phys. Chem. Chem. Phys.* **2010**, *12*, 239−246.
(144) Lang, X.-Y.; Han, G.-F.; Xiao, B.-B.; Gu, L.; Yang, Z.-Z.; Wen, Z.; Zhu, Y.-F.; Zhao, M.; Li, J.-C.; Jiang, Q. Mesostructured Intermetallic Compounds of Platinum and Non-Transition Metals for Enhanced Electrocatalysis of Oxygen Reduction reaction. *Adv. Funct. Mater.* **2015**, *25*, 230−237.
(145) Liu, L.; Pippel, E.; Scholz, R.; Goesele, U. Nanoporous Pt-Co Alloy Nanowires: Fabrication, Characterization, and Electrocatalytic Properties. *Nano Lett.* **2009**, *9*, 4352−4358.
(146) Gu, X.; Xu, L.; Tian, F.; Ding, Y. Au-Ag alloy nanoporous nanotubes. *Nano Res.* **2009**, *2*, 386−393.
(147) Wang, D.; Zhao, P.; Li, Y. General preparation for Pt-based alloy nanoporous nanoparticles as potential nanocatalysts. *Sci. Rep.* **2011**, *1*, 37.
(148) Wu, Y.; Wang, D.; Niu, Z.; Chen, P.; Zhou, G.; Li, Y. A Strategy for Designing a Concave Pt−Ni Alloy through Controllable Chemical Etching. *Angew. Chem., Int. Ed.* **2012**, *51*, 12524−12528.
(149) Xiao, S.; Xiao, F.; Hu, Y.; Yuan, S.; Wang, S.; Qian, L.; Liu, Y. Hierarchical Nanoporous Gold-Platinum with Heterogeneous Interfaces for Methanol Electrooxidation. *Sci. Rep.* **2014**, *4*, 4370.
(150) Ding, Y.; Chen, M.; Erlebacher, J. Metallic Mesoporous Nanocomposites for Electrocatalysis. *J. Am. Chem. Soc.* **2004**, *126*, 6876−6877.
(151) Xu, C.; Wang, L.; Wang, R.; Wang, K.; Zhang, Y.; Tian, F.; Ding, Y. Nanotubular Mesoporous Bimetallic Nanostructures with Enhanced Electrocatalytic Performance. *Adv. Mater.* **2009**, *21*, 2165−2169.
(152) Shao, M.; Shoemaker, K.; Peles, A.; Kaneko, K.; Protsailo, L. Pt Monolayer on Porous Pd−Cu Alloys as Oxygen Reduction Electrocatalysts†. *J. Am. Chem. Soc.* **2010**, *132*, 9253−9255.
(153) Wang, T.; Zhuang, J.; Lynch, J.; Chen, O.; Wang, Z.; Wang, X.; LaMontagne, D.; Wu, H.; Wang, Z.; Cao, Y. C. Self-Assembled Colloidal Superparticles from Nanorods. *Science* **2012**, *338*, 358−363.
(154) Rechberger, F.; Heiligtag, F. J.; Süess, M. J.; Niederberger, M. Assembly of $BaTiO_3$ Nanocrystals into Macroscopic Aerogel Monoliths with High Surface Area. *Angew. Chem., Int. Ed.* **2014**, *53*, 6823−6826.
(155) Worsley, M. A.; Pham, T. T.; Yan, A.; Shin, S. J.; Lee, J. R. I.; Bagge-Hansen, M.; Mickelson, W.; Zettl, A. Synthesis and Characterization of Highly Crystalline Graphene Aerogels. *ACS Nano* **2014**, *8*, 11013−11022.
(156) Heiligtag, F. J.; Cheng, W.; de Mendonça, V. R.; Süess, M. J.; Hametner, K.; Günther, D.; Ribeiro, C.; Niederberger, M. Self-Assembly of Metal and Metal Oxide Nanoparticles and Nanowires into a Macroscopic Ternary Aerogel Monolith with Tailored Photocatalytic Properties. *Chem. Mater.* **2014**, *26*, 5576−5584.
(157) Katsoulidis, A. P.; He, J.; Kanatzidis, M. G. Functional Monolithic Polymeric Organic Framework Aerogel as Reducing and Hosting Media for Ag nanoparticles and Application in Capturing of Iodine Vapors. *Chem. Mater.* **2012**, *24*, 1937−1943.
(158) Lesnyak, V.; Voitekhovich, S. V.; Gaponik, P. N.; Gaponik, N.; Eychmüller, A. CdTe Nanocrystals Capped with a Tetrazolyl Analogue of Thioglycolic Acid: Aqueous Synthesis, Characterization, and Metal-Assisted Assembly. *ACS Nano* **2010**, *4*, 4090−4096.
(159) Lesnyak, V.; Wolf, A.; Dubavik, A.; Borchardt, L.; Voitekhovich, S. V.; Gaponik, N.; Kaskel, S.; Eychmüller, A. 3D Assembly of Semiconductor and Metal Nanocrystals: Hybrid CdTe/Au Structures with Controlled Content. *J. Am. Chem. Soc.* **2011**, *133*, 13413−13420.
(160) Gaponik, N.; Herrmann, A.-K.; Eychmüller, A. Colloidal Nanocrystal-Based Gels and Aerogels: Material Aspects and Application Perspectives. *J. Phys. Chem. Lett.* **2011**, *3*, 8−17.
(161) Bigall, N. C.; Herrmann, A.-K.; Vogel, M.; Rose, M.; Simon, P.; Carrillo-Cabrera, W.; Dorfs, D.; Kaskel, S.; Gaponik, N.; Eychmüller, A. Hydrogels and Aerogels from Noble Metal Nanoparticles. *Angew. Chem., Int. Ed.* **2009**, *48*, 9731−9734.
(162) Herrmann, A.-K.; Liu, W.; Gaponik, N.; Bigall, N.-C.; Eychmüller, A. Metal Nanoparticle Aerogels and Their Applications. *ECS Trans.* **2013**, *45*, 149−154.
(163) Liu, W.; Herrmann, A.-K.; Bigall, N. C.; Rodriguez, P.; Wen, D.; Oezaslan, M.; Schmidt, T. J.; Gaponik, N.; Eychmüller, A. Noble Metal Aerogels—Synthesis, Characterization, and Application as Electrocatalysts. *Acc. Chem. Res.* **2015**, *48*, 154−162.
(164) Herrmann, A.-K.; Formanek, P.; Borchardt, L.; Klose, M.; Giebeler, L.; Eckert, J.; Kaskel, S.; Gaponik, N.; Eychmüller, A.

DOI: 10.1021/acs.chemrev.5b00255
Chem. Rev. XXXX, XXX, XXX−XXX

Multimetallic Aerogels by Template-Free Self-Assembly of Au, Ag, Pt, and Pd Nanoparticles. *Chem. Mater.* **2014**, *26*, 1074−1083.
(165) Gao, X.; Esteves, R. J.; Luong, T. T. H.; Jaini, R.; Arachchige, I. U. Oxidation-Induced Self-Assembly of Ag Nanoshells into Transparent and Opaque Ag Hydrogels and Aerogels. *J. Am. Chem. Soc.* **2014**, *136*, 7993−8002.
(166) Ranmohotti, K. G. S.; Gao, X.; Arachchige, I. U. Salt-Mediated Self-Assembly of Metal Nanoshells into Monolithic Aerogel Frameworks. *Chem. Mater.* **2013**, *25*, 3528−3534.
(167) Wen, D.; Herrmann, A.-K.; Borchardt, L.; Simon, F.; Liu, W.; Kaskel, S.; Eychmüller, A. Controlling the Growth of Palladium Aerogels with High-Performance toward Bioelectrocatalytic Oxidation of Glucose. *J. Am. Chem. Soc.* **2014**, *136*, 2727−2730.
(168) Herrmann, A.-K.; Bigall, N. C.; Lu, L.; Eychmüller, A. In *Complex-Shaped Metal Nanoparticles*; Wiley-VCH Verlag GmbH & Co. KGaA: Berlin, 2012; pp 339−359.
(169) Liu, W.; Herrmann, A.-K.; Geiger, D.; Borchardt, L.; Simon, F.; Kaskel, S.; Gaponik, N.; Eychmüller, A. High-Performance Electrocatalysis on Palladium Aerogels. *Angew. Chem., Int. Ed.* **2012**, *51*, 5743−5747.
(170) Wen, D.; Liu, W.; Herrmann, A.-K.; Eychmüller, A. A Membraneless Glucose/O_2 Biofuel Cell Based on Pd Aerogels. *Chem.—Eur. J.* **2014**, *20*, 4380−4385.
(171) Liu, W.; et al. Bimetallic Aerogels: High-Performance Electrocatalysts for the Oxygen Reduction reaction. *Angew. Chem., Int. Ed.* **2013**, *52*, 9849−9852.
(172) Krishna, K. S.; Sandeep, C. S. S.; Philip, R.; Eswaramoorthy, M. Mixing Does the Magic: A Rapid Synthesis of High Surface Area Noble Metal Nanosponges Showing Broadband Nonlinear Optical Response. *ACS Nano* **2010**, *4*, 2681−2688.
(173) Zhu, C.; Guo, S.; Dong, S. Rapid, General Synthesis of PdPt Bimetallic Alloy Nanosponges and Their Enhanced Catalytic Performance for Ethanol/Methanol Electrooxidation in an Alkaline Medium. *Chem.—Eur. J.* **2013**, *19*, 1104−1111.
(174) Zhu, Z.; Zhai, Y.; Zhu, C.; Wang, Z.; Dong, S. Bimetallic alloy nanowires and nanosponges: A comparative study of peroxidase mimetics and as enhanced catalysts for oxygen reduction reaction. *Electrochem. Commun.* **2013**, *36*, 22−25.
(175) (a) Xiao, M.; Feng, L.; Zhu, J.; Liu, C.; Xing, W. Rapid synthesis of a PtRu nano-sponge with different surface compositions and performance evaluation for methanol electrooxidation. *Nanoscale* **2015**, *7*, 9467−9471. (b) Fu, S.; Zhu, C.; Du, D.; Lin, Y. Facile One-Step Synthesis of Three-Dimensional Pd-Ag Bimetallic Alloy Networks and Their Electrocatalytic Activity toward Ethanol Oxidation. *ACS Appl. Mater. Interfaces* **2015**, *7*, 13842−13848.
(176) Zhu, C.; Wen, D.; Oschatz, M.; Holzschuh, M.; Liu, W.; Herrmann, A.-K.; Simon, F.; Kaskel, S.; Eychmüller, A. Kinetically Controlled Synthesis of PdNi Bimetallic Porous Nanostructures with Enhanced Electrocatalytic Activity. *Small* **2015**, *11*, 1430−1434.
(177) Zhu, Z.; Zhai, Y.; Dong, S. Facial Synthesis of PtM (M = Fe, Co, Cu, Ni) Bimetallic Alloy Nanosponges and Their Enhanced Catalysis for Oxygen Reduction reaction. *ACS Appl. Mater. Interfaces* **2014**, *6*, 16721−16726.
(178) Zhu, C.; Wen, D.; Leubner, S.; Oschatz, M.; Liu, W.; Holzschuh, M.; Simon, F.; Kaskel, S.; Eychmueller, A. Nickel cobalt oxide hollow nanosponges as advanced electrocatalysts for the oxygen evolution reaction. *Chem. Commun.* **2015**, *51*, 7851−7854.
(179) Tang, S.; Vongehr, S.; Wang, Y.; Cui, J.; Wang, X.; Meng, X. Versatile synthesis of high surface area multi-metallic nanosponges allowing control over nanostructure and alloying for catalysis and SERS detection. *J. Mater. Chem. A* **2014**, *2*, 3648−3660.
(180) Song, Y.; Garcia, R. M.; Dorin, R. M.; Wang, H.; Qiu, Y.; Coker, E. N.; Steen, W. A.; Miller, J. E.; Shelnutt, J. A. Synthesis of Platinum Nanowire Networks Using a Soft Template. *Nano Lett.* **2007**, *7*, 3650−3655.
(181) Yang, S.; Hong, F.; Wang, L.; Guo, S.; Song, X.; Ding, B.; Yang, Z. Ultrathin Pt-Based Alloy Nanowire Networks: Synthesized by CTAB Assistant Two-Phase Water−Chloroform Micelles. *J. Phys. Chem. C* **2009**, *114*, 203−207.
(182) Xu, Y.; Hou, S.; Liu, Y.; Zhang, Y.; Wang, H.; Zhang, B. Facile one-step room-temperature synthesis of Pt_3Ni nanoparticle networks with improved electro-catalytic properties. *Chem. Commun.* **2012**, *48*, 2665−2667.
(183) Zhang, J.; Xu, Y.; Zhang, B. Facile synthesis of 3D Pd-P nanoparticle networks with enhanced electrocatalytic performance towards formic acid electrooxidation. *Chem. Commun.* **2014**, *50*, 13451−13453.
(184) Gao, X.; Lu, F.; Dong, B.; Liu, Y.; Gao, Y.; Zheng, L. Facile synthesis of gold and gold-based alloy nanowire networks using wormlike micelles as soft templates. *Chem. Commun.* **2015**, *51*, 843−846.
(185) Liu, X.-Y.; Zhang, Y.; Gong, M.-X.; Tang, Y.-W.; Lu, T.-H.; Chen, Y.; Lee, J.-M. Facile synthesis of corallite-like Pt-Pd alloy nanostructures and their enhanced catalytic activity and stability for ethanol oxidation. *J. Mater. Chem. A* **2014**, *2*, 13840−13844.
(186) Liu, X.; Fu, G.; Chen, Y.; Tang, Y.; She, P.; Lu, T. Pt-Pd-Co Trimetallic Alloy Network Nanostructures with Superior Electrocatalytic Activity towards the Oxygen Reduction Reaction. *Chem.—Eur. J.* **2014**, *20*, 585−590.
(187) Zhang, L.; Lu, D.; Chen, Y.; Tang, Y.; Lu, T. Facile synthesis of Pd-Co-P ternary alloy network nanostructures and their enhanced electrocatalytic activity towards hydrazine oxidation. *J. Mater. Chem. A* **2014**, *2*, 1252−1256.
(188) Liu, X.; Xu, G.; Chen, Y.; Lu, T.; Tang, Y.; Xing, W. A Strategy for Fabricating Porous PdNi@Pt Core-shell Nanostructures and Their Enhanced Activity and Durability for the Methanol Electrooxidation. *Sci. Rep.* **2015**, *5*, 7619.
(189) Jin, R.-H.; Yuan, J.-J. Fabrication of silver porous frameworks using poly(ethyleneimine) hydrogel as a soft sacrificial template. *J. Mater. Chem.* **2005**, *15*, 4513−4517.
(190) Walsh, D.; Arcelli, L.; Ikoma, T.; Tanaka, J.; Mann, S. Dextran templating for the synthesis of metallic and metal oxide sponges. *Nat. Mater.* **2003**, *2*, 386−390.
(191) Kim, B.; Hong, S. C.; Jung, S.; Nam, J.; Bang, J.; Kim, S. Novel Synthesis of Porous Silver Nanostructures Using a Starch Template and Their Applications toward Plasmonic Sensors. *ChemPhysChem* **2013**, *14*, 2663−2666.
(192) Lee, M. N.; Mohraz, A. Hierarchically Porous Silver Monoliths from Colloidal Bicontinuous Interfacially Jammed Emulsion Gels. *J. Am. Chem. Soc.* **2011**, *133*, 6945−6947.
(193) Bourret, G. R.; Goulet, P. J. G.; Lennox, R. B. Synthesis of Porous Metallic Monoliths via Chemical Reduction of Au(I) and Ag(I) Nanostructured Sheets. *Chem. Mater.* **2011**, *23*, 4954−4959.
(194) Ressnig, D.; Antonietti, M. Ultrafast Syntheses of Silver Foams from Ag_2NCN: Combustion Synthesis versus Chemical Reduction. *Chem. Mater.* **2014**, *26*, 4064−4067.
(195) Shin, H. C.; Dong, J.; Liu, M. Nanoporous Structures Prepared by an Electrochemical Deposition Process. *Adv. Mater.* **2003**, *15*, 1610−1614.
(196) Shin, H. C.; Liu, M. Three-Dimensional Porous Copper−Tin Alloy Electrodes for Rechargeable Lithium Batteries. *Adv. Funct. Mater.* **2005**, *15*, 582−586.
(197) Cherevko, S.; Chung, C.-H. Direct electrodeposition of nanoporous gold with controlled multimodal pore size distribution. *Electrochem. Commun.* **2011**, *13*, 16−19.
(198) Cherevko, S.; Chung, C.-H. Impact of key deposition parameters on the morphology of silver foams prepared by dynamic hydrogen template deposition. *Electrochim. Acta* **2010**, *55*, 6383−6390.
(199) Ott, A.; Jones, L. A.; Bhargava, S. K. Direct electrodeposition of porous platinum honeycomb structures. *Electrochem. Commun.* **2011**, *13*, 1248−1251.
(200) Cherevko, S.; Kulyk, N.; Chung, C.-H. Nanoporous palladium with sub-10 nm dendrites by electrodeposition for ethanol and ethylene glycol oxidation. *Nanoscale* **2012**, *4*, 103−105.
(201) Liu, J.; Cao, L.; Huang, W.; Li, Z. Direct electrodeposition of PtPd alloy foams comprised of nanodendrites with high electrocatalytic activity for the oxidation of methanol and ethanol. *J. Electroanal. Chem.* **2012**, *686*, 38−45.

DOI: 10.1021/acs.chemrev.5b00255
Chem. Rev. XXXX, XXX, XXX−XXX

(202) Ojani, R.; Hasheminejad, E.; Raoof, J. B. Hydrogen evolution assisted electrodeposition of bimetallic 3D nano/micro-porous PtPd films and their electrocatalytic performance. *Int. J. Hydrogen Energy* **2014**, *39*, 8194−8203.
(203) Xiong, L.; Huang, Y.-X.; Liu, X.-W.; Sheng, G.-P.; Li, W.-W.; Yu, H.-Q. Three-dimensional bimetallic Pd−Cu nanodendrites with superior electrochemical performance for oxygen reduction reaction. *Electrochim. Acta* **2013**, *89*, 24−28.
(204) Yin, J.; Jia, J.; Zhu, L. Macroporous Pt modified glassy carbon electrode: Preparation and electrocatalytic activity for methanol oxidation. *Int. J. Hydrogen Energy* **2008**, *33*, 7444−7447.
(205) Shahbazi, P.; Kiani, A. Nanoporous Ag and Pd foam: Redox induced fabrication using electrochemically deposited nanoporous Cu foam with no need to any additive. *Electrochim. Acta* **2011**, *56*, 9520−9529.
(206) Huang, J.-F. 3-D Nanoporous Pt Electrode Prepared by a 2-D UPD Monolayer Process. *Electroanalysis* **2008**, *20*, 2229−2234.
(207) Nagaraju, D. H.; Lakshminarayanan, V. Electrochemically Grown Mesoporous Gold Film as High Surface Area Material for Electro-Oxidation of Alcohol in Alkaline Medium. *J. Phys. Chem. C* **2009**, *113*, 14922−14926.
(208) Huang, W.; Wang, M.; Zheng, J.; Li, Z. Facile Fabrication of Multifunctional Three-Dimensional Hierarchical Porous Gold Films via Surface Rebuilding. *J. Phys. Chem. C* **2009**, *113*, 1800−1805.
(209) Zhong, G.; Liu, A.; Chen, X.; Wang, K.; Lian, Z.; Liu, Q.; Chen, Y.; Du, M.; Lin, X. Electrochemical biosensor based on nanoporous gold electrode for detection of PML/RARα fusion gene. *Biosens. Bioelectron.* **2011**, *26*, 3812−3817.
(210) Liu, R.; Liu, J.-f.; Jiang, G.-b. Use of Triton X-114 as a weak capping agent for one-pot aqueous phase synthesis of ultrathin noble metal nanowires and a primary study of their electrocatalytic activity. *Chem. Commun.* **2010**, *46*, 7010−7012.
(211) Liu, R.; Liu, J.-f.; Zhou, X.-x.; Sun, M.-T.; Jiang, G.-b. Fabrication of a Au Nanoporous Film by Self-Organization of Networked Ultrathin Nanowires and Its Application as a Surface-Enhanced Raman Scattering Substrate for Single-Molecule Detection. *Anal. Chem.* **2011**, *83*, 9131−9137.
(212) Zhao, X.; Zhang, J.; Wang, L.; Liu, Z.; chen, w. Pd_xCu_{100-x} networks: an active and durable electrocatalyst for ethanol oxidation in alkaline medium. *J. Mater. Chem. A* **2014**, *2*, 20933−20938.
(213) Shi, L.; Wang, A.; Huang, Y.; Chen, X.; Delgado, J. J.; Zhang, T. Facile Synthesis of Ultrathin AuCu Dimetallic Nanowire Networks. *Eur. J. Inorg. Chem.* **2012**, *2012*, 2700−2706.
(214) Peng, Z.; You, H.; Yang, H. Composition-Dependent Formation of Platinum Silver Nanowires. *ACS Nano* **2010**, *4*, 1501−1510.
(215) Yu, X.; Wang, D.; Peng, Q.; Li, Y. Pt−M (M═Cu, Co, Ni, Fe) Nanocrystals: From Small Nanoparticles to Wormlike Nanowires by Oriented Attachment. *Chem.—Eur. J.* **2013**, *19*, 233−239.
(216) He, L.-L.; Zheng, J.-N.; Song, P.; Zhong, S.-X.; Wang, A.-J.; Chen, Z.; Feng, J.-J. Facile synthesis of platinum−gold alloyed string-bead nanochain networks with the assistance of allantoin and their enhanced electrocatalytic performance for oxygen reduction and methanol oxidation reactions. *J. Power Sources* **2015**, *276*, 357−364.
(217) Yu, F.; Zhou, W.; Bellabarba, R. M.; Tooze, R. P. One-step synthesis and shape-control of CuPd nanowire networks. *Nanoscale* **2014**, *6*, 1093−1098.
(218) Hong, W.; Wang, J.; Wang, E. Facile Synthesis of Highly Active PdAu Nanowire Networks as Self-Supported Electrocatalyst for Ethanol Electrooxidation. *ACS Appl. Mater. Interfaces* **2014**, *6*, 9481−9487.
(219) Wang, A.-J.; Lv, J.-J.; Zhou, D.-L.; Weng, X.; Qin, S.-F.; Feng, J.-J. Facile synthesis of ultrathin worm-like Au nanowires for highly active SERS substrates. *New J. Chem.* **2014**, *38*, 3395−3400.
(220) Klajn, R.; Gray, T. P.; Wesson, P. J.; Myers, B. D.; Dravid, V. P.; Smoukov, S. K.; Grzybowski, B. A. Bulk Synthesis and Surface Patterning of Nanoporous Metals and Alloys from Supraspherical Nanoparticle Aggregates. *Adv. Funct. Mater.* **2008**, *18*, 2763−2769.
(221) Wang, L.; Liu, X.; Hu, X.; Song, S.; Fan, C. Unmodified gold nanoparticles as a colorimetric probe for potassium DNA aptamers. *Chem. Commun.* **2006**, 3780−3782.
(222) Liu, Y.; Liu, L.; Guo, R. Br−Induced Facile Fabrication of Spongelike Gold/Amino Acid Nanocomposites and Their Applications in Surface-Enhanced Raman Scattering. *Langmuir* **2010**, *26*, 13479−13485.
(223) Zhang, Z.; Li, H.; Zhang, F.; Wu, Y.; Guo, Z.; Zhou, L.; Li, J. Investigation of Halide-Induced Aggregation of Au Nanoparticles into Spongelike Gold. *Langmuir* **2014**, *30*, 2648−2659.
(224) Qin, G. W.; Liu, J.; Balaji, T.; Xu, X.; Matsunaga, H.; Hakuta, Y.; Zuo, L.; Raveendran, P. A Facile and Template-Free Method to Prepare Mesoporous Gold Sponge and Its Pore Size Control. *J. Phys. Chem. C* **2008**, *112*, 10352−10358.
(225) Zhang, Z.; Wu, Y. Investigation of the $NaBH_4$-Induced Aggregation of Au Nanoparticles. *Langmuir* **2010**, *26*, 9214−9223.
(226) Zhang, Y. X.; Zeng, H. C. Gold Sponges Prepared via Hydrothermally Activated Self-Assembly of Au Nanoparticles. *J. Phys. Chem. C* **2007**, *111*, 6970−6975.
(227) Kim, M.; Jeong, G. H.; Lee, K. Y.; Kwon, K.; Han, S. W. Fabrication of nanoporous superstructures through hierarchical self-assembly of nanoparticles. *J. Mater. Chem.* **2008**, *18*, 2208−2212.
(228) An, K.; Hyeon, T. Synthesis and biomedical applications of hollow nanostructures. *Nano Today* **2009**, *4*, 359−373.
(229) Skrabalak, S. E.; Chen, J.; Sun, Y.; Lu, X.; Au, L.; Cobley, C. M.; Xia, Y. Gold Nanocages: Synthesis, Properties, and Applications. *Acc. Chem. Res.* **2008**, *41*, 1587−1595.
(230) Sun, Y.; Mayers, B. T.; Xia, Y. Template-Engaged Replacement Reaction: A One-Step Approach to the Large-Scale Synthesis of Metal Nanostructures with Hollow Interiors. *Nano Lett.* **2002**, *2*, 481−485.
(231) Xia, X.; Wang, Y.; Ruditskiy, A.; Xia, Y. 25th Anniversary Article: Galvanic Replacement: A Simple and Versatile Route to Hollow Nanostructures with Tunable and Well-Controlled Properties. *Adv. Mater.* **2013**, *25*, 6313−6333.
(232) Liu, Y.; Goebl, J.; Yin, Y. Templated synthesis of nano-structured materials. *Chem. Soc. Rev.* **2013**, *42*, 2610−2653.
(233) Zhang, H.; Jin, M.; Liu, H.; Wang, J.; Kim, M. J.; Yang, D.; Xie, Z.; Liu, J.; Xia, Y. Facile Synthesis of Pd−Pt Alloy Nanocages and Their Enhanced Performance for Preferential Oxidation of CO in Excess Hydrogen. *ACS Nano* **2011**, *5*, 8212−8222.
(234) Alia, S. M.; Yan, Y. S.; Pivovar, B. S. Galvanic displacement as a route to highly active and durable extended surface electrocatalysts. *Catal. Sci. Technol.* **2014**, *4*, 3589−3600.
(235) Gilroy, K. D.; Farzinpour, P.; Sundar, A.; Hughes, R. A.; Neretina, S. Sacrificial Templates for Galvanic Replacement Reactions: Design Criteria for the Synthesis of Pure Pt Nanoshells with a Smooth Surface Morphology. *Chem. Mater.* **2014**, *26*, 3340−3347.
(236) Song, H. M.; Anjum, D. H.; Sougrat, R.; Hedhili, M. N.; Khashab, N. M. Hollow Au@Pd and Au@Pt core-shell nanoparticles as electrocatalysts for ethanol oxidation reactions. *J. Mater. Chem.* **2012**, *22*, 25003−25010.
(237) Wang, C.; Wang, Y.; Xu, L.; Shi, X.; Li, X.; Xu, X.; Sun, H.; Yang, B.; Lin, Q. A Galvanic Replacement Route to Prepare Strongly Fluorescent and Highly Stable Gold Nanodots for Cellular Imaging. *Small* **2013**, *9*, 413−420.
(238) Lu, X.; Au, L.; McLellan, J.; Li, Z.-Y.; Marquez, M.; Xia, Y. Fabrication of Cubic Nanocages and Nanoframes by Dealloying Au/Ag Alloy Nanoboxes with an Aqueous Etchant Based on $Fe(NO_3)_3$ or NH_4OH. *Nano Lett.* **2007**, *7*, 1764−1769.
(239) Chen, Z.; Waje, M.; Li, W.; Yan, Y. Supportless Pt and PtPd nanotubes as electrocatalysts for oxygen-reduction reactions. *Angew. Chem., Int. Ed.* **2007**, *46*, 4060−4063.
(240) Wan, D.; Xia, X.; Wang, Y.; Xia, Y. Robust Synthesis of Gold Cubic Nanoframes through a Combination of Galvanic Replacement, Gold Deposition, and Silver Dealloying. *Small* **2013**, *9*, 3111−3117.
(241) Zhang, G.; Sun, S.; Cai, M.; Zhang, Y.; Li, R.; Sun, X. Porous Dendritic Platinum Nanotubes with Extremely High Activity and Stability for Oxygen Reduction Reaction. *Sci. Rep.* **2013**, *3*, 1526.

DOI: 10.1021/acs.chemrev.5b00255
Chem. Rev. XXXX, XXX, XXX−XXX

(242) Sun, Y.; Xia, Y. Mechanistic Study on the Replacement Reaction between Silver Nanostructures and Chloroauric Acid in Aqueous Medium. *J. Am. Chem. Soc.* **2004**, *126*, 3892−3901.
(243) Sun, Y. G.; Xia, Y. N. Alloying and dealloying processes involved in the preparation of metal nanoshells through a galvanic replacement reaction. *Nano Lett.* **2003**, *3*, 1569−1572.
(244) Chen, J.; Wiley, B.; McLellan, J.; Xiong, Y.; Li, Z.-Y.; Xia, Y. Optical Properties of Pd−Ag and Pt−Ag Nanoboxes Synthesized via Galvanic Replacement Reactions. *Nano Lett.* **2005**, *5*, 2058−2062.
(245) Au, L.; Lu, X.; Xia, Y. A Comparative Study of Galvanic Replacement Reactions Involving Ag Nanocubes and $AuCl_2^-$ or $AuCl_4^-$. *Adv. Mater.* **2008**, *20*, 2517−2522.
(246) Liang, H.-W.; Liu, S.; Gong, J.-Y.; Wang, S.-B.; Wang, L.; Yu, S.-H. Ultrathin Te Nanowires: An Excellent Platform for Controlled Synthesis of Ultrathin Platinum and Palladium Nanowires/Nanotubes with Very High Aspect Ratio. *Adv. Mater.* **2009**, *21*, 1850−1854.
(247) Straney, P. J.; Marbella, L. E.; Andolina, C. M.; Nuhfer, N. T.; Millstone, J. E. Decoupling Mechanisms of Platinum Deposition on Colloidal Gold Nanoparticle Substrates. *J. Am. Chem. Soc.* **2014**, *136*, 7873−7876.
(248) Gao, C.; Lu, Z.; Liu, Y.; Zhang, Q.; Chi, M.; Cheng, Q.; Yin, Y. Highly Stable Silver Nanoplates for Surface Plasmon Resonance Biosensing. *Angew. Chem., Int. Ed.* **2012**, *51*, 5629−5633.
(249) Bi, Y.; Lu, G. Iodide ions control galvanic replacement growth of uniform rhodiumnanotubes at room temperature. *Chem. Commun.* **2008**, 6402−6404.
(250) Lu, Y.; Chen, W. Nanoneedle-Covered Pd−Ag Nanotubes: High Electrocatalytic Activity for Formic Acid Oxidation. *J. Phys. Chem. C* **2010**, *114*, 21190−21200.
(251) Chen, J.; McLellan, J. M.; Siekkinen, A.; Xiong, Y.; Li, Z.-Y.; Xia, Y. Facile Synthesis of Gold−Silver Nanocages with Controllable Pores on the Surface. *J. Am. Chem. Soc.* **2006**, *128*, 14776−14777.
(252) Cobley, C. M.; Xia, Y. Engineering the properties of metal nanostructures via galvanic replacement reactions. *Mater. Sci. Eng., R* **2010**, *70*, 44−62.
(253) Zhang, H.; Jin, M.; Wang, J.; Li, W.; Camargo, P. H. C.; Kim, M. J.; Yang, D.; Xie, Z.; Xia, Y. Synthesis of Pd−Pt Bimetallic Nanocrystals with a Concave Structure through a Bromide-Induced Galvanic Replacement Reaction. *J. Am. Chem. Soc.* **2011**, *133*, 6078−6089.
(254) Fang, Z.; Wang, Y.; Liu, C.; Chen, S.; Sang, W.; Wang, C.; Zeng, J. Rational Design of Metal Nanoframes for Catalysis and Plasmonics. *Small* **2015**, *11*, 2593−2605.
(255) Xia, B. Y.; Wu, H. B.; Wang, X.; Lou, X. W. One-Pot Synthesis of Cubic $PtCu_3$ Nanocages with Enhanced Electrocatalytic Activity for the Methanol Oxidation Reaction. *J. Am. Chem. Soc.* **2012**, *134*, 13934−13937.
(256) Dhavale, V. M.; Kurungot, S. Cu−Pt Nanocage with 3-D Electrocatalytic Surface as an Efficient Oxygen Reduction Electrocatalyst for a Primary Zn−Air Battery. *ACS Catal.* **2015**, *5*, 1445−1452.
(257) Yu, X.; Wang, D.; Peng, Q.; Li, Y. High performance electrocatalyst: Pt-Cu hollow nanocrystals. *Chem. Commun.* **2011**, *47*, 8094−8096.
(258) Ding, J.; Zhu, X.; Bu, L.; Yao, J.; Guo, J.; Guo, S.; Huang, X. Highly open rhombic dodecahedral PtCu nanoframes. *Chem. Commun.* **2015**, *51*, 9722−9725.
(259) Nosheen, F.; Zhang, Z.-C.; Zhuang, J.; Wang, X. One-pot fabrication of single-crystalline octahedral Pt-Cu nanoframes and their enhanced electrocatalytic activity. *Nanoscale* **2013**, *5*, 3660−3663.
(260) Zhang, Z.; Yang, Y.; Nosheen, F.; Wang, P.; Zhang, J.; Zhuang, J.; Wang, X. Fine Tuning of the Structure of Pt−Cu Alloy Nanocrystals by Glycine-Mediated Sequential Reduction Kinetics. *Small* **2013**, *9*, 3063−3069.
(261) Jing, H.; Wang, H. Structural Evolution of Ag−Pd Bimetallic Nanoparticles through Controlled Galvanic Replacement: Effects of Mild Reducing Agents. *Chem. Mater.* **2015**, *27*, 2172−2180.
(262) Yang, Y.; Liu, J.; Fu, Z.-W.; Qin, D. Galvanic Replacement-Free Deposition of Au on Ag for Core−Shell Nanocubes with Enhanced Chemical Stability and SERS Activity. *J. Am. Chem. Soc.* **2014**, *136*, 8153−8156.
(263) Hong, J. W.; Kang, S. W.; Choi, B.-S.; Kim, D.; Lee, S. B.; Han, S. W. Controlled Synthesis of Pd−Pt Alloy Hollow Nanostructures with Enhanced Catalytic Activities for Oxygen Reduction. *ACS Nano* **2012**, *6*, 2410−2419.
(264) Li, C.; Jiang, B.; Imura, M.; Malgras, V.; Yamauchi, Y. Mesoporous Pt hollow cubes with controlled shell thicknesses and investigation of their electrocatalytic performance. *Chem. Commun.* **2014**, *50*, 15337−15340.
(265) Sneed, B. T.; Young, A. P.; Jalalpoor, D.; Golden, M. C.; Mao, S.; Jiang, Y.; Wang, Y.; Tsung, C.-K. Shaped Pd−Ni−Pt Core-Sandwich-Shell Nanoparticles: Influence of Ni Sandwich Layers on Catalytic Electrooxidations. *ACS Nano* **2014**, *8*, 7239−7250.
(266) Shahjamali, M. M.; Bosman, M.; Cao, S.; Huang, X.; Saadat, S.; Martinsson, E.; Aili, D.; Tay, Y. Y.; Liedberg, B.; Loo, S. C. J.; et al. Gold Coating of Silver Nanoprisms. *Adv. Funct. Mater.* **2012**, *22*, 849−854.
(267) Zhang, Q.; Cobley, C. M.; Zeng, J.; Wen, L.-P.; Chen, J.; Xia, Y. Dissolving Ag from Au−Ag Alloy Nanoboxes with H_2O_2: A Method for Both Tailoring the Optical Properties and Measuring the H_2O_2 Concentration. *J. Phys. Chem. C* **2010**, *114*, 6396−6400.
(268) Jang, H.; Min, D.-H. Spherically-Clustered Porous Au−Ag Alloy Nanoparticle Prepared by Partial Inhibition of Galvanic Replacement and Its Application for Efficient Multimodal Therapy. *ACS Nano* **2015**, *9*, 2696−2703.
(269) McEachran, M.; Keogh, D.; Pietrobon, B.; Cathcart, N.; Gourevich, I.; Coombs, N.; Kitaev, V. Ultrathin Gold Nanoframes through Surfactant-Free Templating of Faceted Pentagonal Silver Nanoparticles. *J. Am. Chem. Soc.* **2011**, *133*, 8066−8069.
(270) Zhang, W.; Yang, J.; Lu, X. Tailoring Galvanic Replacement Reaction for the Preparation of Pt/Ag Bimetallic Hollow Nanostructures with Controlled Number of Voids. *ACS Nano* **2012**, *6*, 7397−7405.
(271) Sun, Y.; Wiley, B.; Li, Z.-Y.; Xia, Y. Synthesis and Optical Properties of Nanorattles and Multiple-Walled Nanoshells/Nanotubes Made of Metal Alloys. *J. Am. Chem. Soc.* **2004**, *126*, 9399−9406.
(272) Sun, Y.; Xia, Y. Multiple-Walled Nanotubes Made of Metals. *Adv. Mater.* **2004**, *16*, 264−268.
(273) Mahmoud, M. A.; El-Sayed, M. A. Metallic Double Shell Hollow Nanocages: The Challenges of Their Synthetic Techniques. *Langmuir* **2012**, *28*, 4051−4059.
(274) Mahmoud, M. A.; El-Sayed, M. A. Time Dependence and Signs of the Shift of the Surface Plasmon Resonance Frequency in Nanocages Elucidate the Nanocatalysis Mechanism in Hollow Nanoparticles. *Nano Lett.* **2011**, *11*, 946−953.
(275) Jang, H.-J.; Ham, S.; Acapulco, J. A. I.; Song, Y.; Hong, S.; Shuford, K. L.; Park, S. Fabrication of 2D Au Nanorings with Pt Framework. *J. Am. Chem. Soc.* **2014**, *136*, 17674−17680.
(276) Hu, Y.; Liu, Y.; Li, Z.; Sun, Y. Highly Asymmetric, Interfaced Dimers Made of Au Nanoparticles and Bimetallic Nanoshells: Synthesis and Photo-Enhanced Catalysis. *Adv. Funct. Mater.* **2014**, *24*, 2828−2836.
(277) Ridelman, Y.; Singh, G.; Popovitz-Biro, R.; Wolf, S. G.; Das, S.; Klajn, R. Metallic Nanobowls by Galvanic Replacement Reaction on Heterodimeric Nanoparticles. *Small* **2012**, *8*, 654−660.
(278) Wang, M.; Zhang, W.; Wang, J.; Wexler, D.; Poynton, S. D.; Slade, R. C. T.; Liu, H.; Winther-Jensen, B.; Kerr, R.; Shi, D.; Chen, J. PdNi Hollow Nanoparticles for Improved Electrocatalytic Oxygen Reduction in Alkaline Environments. *ACS Appl. Mater. Interfaces* **2013**, *5*, 12708−12715.
(279) Shan, A.; Chen, Z.; Li, B.; Chen, C.; Wang, R. Monodispersed, ultrathin NiPt hollow nanospheres with tunable diameter and composition via a green chemical synthesis. *J. Mater. Chem. A* **2015**, *3*, 1031−1036.
(280) Ni, W.; Wu, H. B.; Wang, B.; Xu, R.; Lou, X. W. One-Pot Synthesis of Ultra-Light Nickel Nanofoams Composed of Nanowires and Their Transformation into Various Functional Nanofoams. *Small* **2012**, *8*, 3432−3437.

DOI: 10.1021/acs.chemrev.5b00255
Chem. Rev. XXXX, XXX, XXX−XXX

(281) Adams, S.; Thai, D.; Mascona, X.; Schwartzberg, A. M.; Zhang, J. Z. Key Factors Affecting the Reproducibility of Synthesis and Growth Mechanism of Near-Infrared Absorbing Hollow Gold Nanospheres. *Chem. Mater.* **2014**, *26*, 6805−6810.
(282) Vasquez, Y.; Sra, A. K.; Schaak, R. E. One-Pot Synthesis of Hollow Superparamagnetic CoPt Nanospheres. *J. Am. Chem. Soc.* **2005**, *127*, 12504−12505.
(283) Chen, Z.; Ye, S.; Wilson, A. R.; Ha, Y.-C.; Wiley, B. J. Optically transparent hydrogen evolution catalysts made from networks of copper-platinum core-shell nanowires. *Energy Environ. Sci.* **2014**, *7*, 1461−1467.
(284) Mohl, M.; Dobo, D.; Kukovecz, A.; Konya, Z.; Kordas, K.; Wei, J.; Vajtai, R.; Ajayan, P. M. Formation of CuPd and CuPt Bimetallic Nanotubes by Galvanic Replacement Reaction. *J. Phys. Chem. C* **2011**, *115*, 9403−9409.
(285) Li, X.; Liu, H.; Yang, J.; Qiao, S.-Z.; Du, X.-W. Pure gold nanocages by galvanic replacement reaction of magnesium nanoparticles. *RSC Adv.* **2014**, *4*, 1185−1188.
(286) Niu, K.-Y.; Kulinich, S. A.; Yang, J.; Zhu, A. L.; Du, X.-W. Galvanic Replacement Reactions of Active-Metal Nanoparticles. *Chem.—Eur. J.* **2012**, *18*, 4234−4241.
(287) Sasaki, K.; Naohara, H.; Choi, Y.; Cai, Y.; Chen, W.-F.; Liu, P.; Adzic, R. R. Highly stable Pt monolayer on PdAu nanoparticle electrocatalysts for the oxygen reduction reaction. *Nat. Commun.* **2012**, *3*, 1115.
(288) Ghosh, T.; Vukmirovic, M. B.; DiSalvo, F. J.; Adzic, R. R. Intermetallics as Novel Supports for Pt Monolayer O_2 Reduction Electrocatalysts: Potential for Significantly Improving Properties. *J. Am. Chem. Soc.* **2009**, *132*, 906−907.
(289) Zhang, Y.; Ma, C.; Zhu, Y.; Si, R.; Cai, Y.; Wang, J. X.; Adzic, R. R. Hollow core supported Pt monolayer catalysts for oxygen reduction. *Catal. Today* **2013**, *202*, 50−54.
(290) Zhai, Y.; Zhai, J.; Dong, S. Temperature-dependent synthesis of CoPt hollow nanoparticles: from ″nanochain″ to ″nanoring″. *Chem. Commun.* **2010**, *46*, 1500−1502.
(291) Liang, H.-P.; Guo, Y.-G.; Zhang, H.-M.; Hu, J.-S.; Wan, L.-J.; Bai, C.-L. Controllable AuPt bimetallic hollow nanostructures. *Chem. Commun.* **2004**, 1496−1497.
(292) Guo, S.; Dong, S.; Wang, E. Ultralong Pt-on-Pd bimetallic nanowires with nanoporous surface: nanodendritic structure for enhanced electrocatalytic activity. *Chem. Commun.* **2010**, *46*, 1869−1871.
(293) Guo, S.; Dong, S.; Wang, E. Three-Dimensional Pt-on-Pd Bimetallic Nanodendrites Supported on Graphene Nanosheet: Facile Synthesis and Used as an Advanced Nanoelectrocatalyst for Methanol Oxidation. *ACS Nano* **2010**, *4*, 547−555.
(294) Hong, W.; Wang, J.; Wang, E. Dendritic Au/Pt and Au/PtCu Nanowires with Enhanced Electrocatalytic Activity for Methanol Electrooxidation. *Small* **2014**, *10*, 3262−3265.
(295) Zhu, C.; Guo, S.; Dong, S. Facile synthesis of trimetallic AuPtPd alloy nanowires and their catalysis for ethanol electrooxidation. *J. Mater. Chem.* **2012**, *22*, 14851−14855.
(296) Zhu, C.; Guo, S.; Dong, S. PdM (M = Pt, Au) Bimetallic Alloy Nanowires with Enhanced Electrocatalytic Activity for Electrooxidation of Small Molecules. *Adv. Mater.* **2012**, *24*, 2326−2331.
(297) Fang, J.; Lebedkin, S.; Yang, S.; Hahn, H. A new route for the synthesis of polyhedral gold mesocages and shape effect in single-particle surface-enhanced Raman spectroscopy. *Chem. Commun.* **2011**, *47*, 5157−5159.
(298) Ma, A.; Xu, J.; Zhang, X.; Zhang, B.; Wang, D.; Xu, H. Interfacial nanodroplets guided construction of hierarchical Au, Au-Pt, and Au-Pd particles as excellent catalysts. *Sci. Rep.* **2014**, *4*, 4849.
(299) Kim, K. W.; Kim, S. M.; Choi, S.; Kim, J.; Lee, I. S. Electroless Pt Deposition on Mn_3O_4 Nanoparticles via the Galvanic Replacement Process: Electrocatalytic Nanocomposite with Enhanced Performance for Oxygen Reduction Reaction. *ACS Nano* **2012**, *6*, 5122−5129.
(300) Smigelskas, A. D.; Kirkendall, E. O. ZINC DIFFUSION IN ALPHA-BRASS. *Trans. Am. Inst. Min. Metall. Eng.* **1947**, *171*, 130−142.
(301) Yin, Y.; Rioux, R. M.; Erdonmez, C. K.; Hughes, S.; Somorjai, G. A.; Alivisatos, A. P. Formation of Hollow Nanocrystals Through the Nanoscale Kirkendall Effect. *Science* **2004**, *304*, 711−714.
(302) González, E.; Arbiol, J.; Puntes, V. F. Carving at the Nanoscale: Sequential Galvanic Exchange and Kirkendall Growth at Room Temperature. *Science* **2011**, *334*, 1377−1380.
(303) Railsback, J. G.; Johnston-Peck, A. C.; Wang, J.; Tracy, J. B. Size-Dependent Nanoscale Kirkendall Effect During the Oxidation of Nickel Nanoparticles. *ACS Nano* **2010**, *4*, 1913−1920.
(304) Wang, W.; Dahl, M.; Yin, Y. Hollow Nanocrystals through the Nanoscale Kirkendall Effect. *Chem. Mater.* **2012**, *25*, 1179−1189.
(305) Kim, B. Y.; Shim, I.-B.; Araci, Z. O.; Saavedra, S. S.; Monti, O. L. A.; Armstrong, N. R.; Sahoo, R.; Srivastava, D. N.; Pyun, J. Synthesis and Colloidal Polymerization of Ferromagnetic Au−Co Nanoparticles into Au−Co_3O_4 Nanowires. *J. Am. Chem. Soc.* **2010**, *132*, 3234−3235.
(306) Sun, Y.; Xia, Y. Shape-Controlled Synthesis of Gold and Silver Nanoparticles. *Science* **2002**, *298*, 2176−2179.
(307) Jiang, Z.; Zhang, Q.; Zong, C.; Liu, B.-J.; Ren, B.; Xie, Z.; Zheng, L. Cu-Au alloy nanotubes with five-fold twinned structure and their application in surface-enhanced Raman scattering. *J. Mater. Chem.* **2012**, *22*, 18192−18197.
(308) Ren, M.; Chen, J.; Li, Y.; Zhang, H.; Zou, Z.; Li, X.; Yang, H. Lattice contracted Pd-hollow nanocrystals: Synthesis, structure and electrocatalysis for formic acid oxidation. *J. Power Sources* **2014**, *246*, 32−38.
(309) Han, L.; Liu, H.; Cui, P.; Peng, Z.; Zhang, S.; Yang, J. Alloy Cu_3Pt nanoframes through the structure evolution in Cu-Pt nanoparticles with a core-shell construction. *Sci. Rep.* **2014**, *4*, 6414.
(310) Yang, J.; Qi, L.; Lu, C.; Ma, J.; Cheng, H. Morphosynthesis of Rhombododecahedral Silver Cages by Self-Assembly Coupled with Precursor Crystal Templating. *Angew. Chem., Int. Ed.* **2005**, *44*, 598−603.
(311) Ben Moshe, A.; Markovich, G. Synthesis of Single Crystal Hollow Silver Nanoparticles in a Fast Reaction-Diffusion Process. *Chem. Mater.* **2011**, *23*, 1239−1245.
(312) Wang, L.; Yamauchi, Y. Metallic Nanocages: Synthesis of Bimetallic Pt−Pd Hollow Nanoparticles with Dendritic Shells by Selective Chemical Etching. *J. Am. Chem. Soc.* **2013**, *135*, 16762−16765.
(313) Bai, F.; Sun, Z.; Wu, H.; Haddad, R. E.; Xiao, X.; Fan, H. Templated Photocatalytic Synthesis of Well-Defined Platinum Hollow Nanostructures with Enhanced Catalytic Performance for Methanol Oxidation. *Nano Lett.* **2011**, *11*, 3759−3762.
(314) Liu, H.; Ye, F.; Yao, Q.; Cao, H.; Xie, J.; Lee, J. Y.; Yang, J. Stellated Ag-Pt bimetallic nanoparticles: An effective platform for catalytic activity tuning. *Sci. Rep.* **2014**, *4*, 3969.
(315) Yang, M.; Cai, Q.; Liu, C.; Wu, R.; Sun, D.; Chen, Y.; Tang, Y.; Lu, T. Monodispersed hollow platinum nanospheres: facile synthesis and their enhanced electrocatalysis for methanol oxidation. *J. Mater. Chem. A* **2014**, *2*, 13738−13743.
(316) Ding, L.-X.; Wang, A.-L.; Li, G.-R.; Liu, Z.-Q.; Zhao, W.-X.; Su, C.-Y.; Tong, Y.-X. Porous Pt-Ni-P Composite Nanotube Arrays: Highly Electroactive and Durable Catalysts for Methanol Electrooxidation. *J. Am. Chem. Soc.* **2012**, *134*, 5730−5733.
(317) Choi, B.-S.; Lee, Y. W.; Kang, S. W.; Hong, J. W.; Kim, J.; Park, I.; Han, S. W. Multimetallic Alloy Nanotubes with Nanoporous Framework. *ACS Nano* **2012**, *6*, 5659−5667.
(318) Xiong, Y.; Wiley, B.; Chen, J.; Li, Z.-Y.; Yin, Y.; Xia, Y. Corrosion-Based Synthesis of Single-Crystal Pd Nanoboxes and Nanocages and Their Surface Plasmon Properties. *Angew. Chem., Int. Ed.* **2005**, *44*, 7913−7917.
(319) Liu, X.; Li, X.; Wang, D.; Yu, R.; Cui, Y.; Peng, Q.; Li, Y. Palladium/tin bimetallic single-crystalline hollow nanospheres. *Chem. Commun.* **2012**, *48*, 1683−1685.
(320) Dong, R.; Liu, W.; Hao, J. Soft Vesicles in the Synthesis of Hard Materials. *Acc. Chem. Res.* **2012**, *45*, 504−513.
(321) Zhang, L. X.; Li, P. C.; Liu, X. H.; Du, L. W.; Wang, E. K. The Effect of Template Phase on the Structures of As-Synthesized Silica

DOI: 10.1021/acs.chemrev.5b00255
Chem. Rev. XXXX, XXX, XXX−XXX

Nanoparticles with Fragile Didodecyldimethylammonium Bromide Vesicles as Templates. *Adv. Mater.* **2007**, *19*, 4279−4283.
(322) Buchold, D. H. M.; Feldmann, C. Nanoscale γ-AlO(OH) Hollow Spheres: Synthesis and Container-Type Functionality. *Nano Lett.* **2007**, *7*, 3489−3492.
(323) Wang, J.; Shah, Z. H.; Zhang, S.; Lu, R. Silica-based nanocomposites via reverse microemulsions: classifications, preparations, and applications. *Nanoscale* **2014**, *6*, 4418−4437.
(324) Zimmermann, C.; Feldmann, C.; Wanner, M.; Gerthsen, D. Nanoscale Gold Hollow Spheres Through a Microemulsion Approach. *Small* **2007**, *3*, 1347−1349.
(325) Bastakoti, B. P.; Li, Y.; Kimura, T.; Yamauchi, Y. Asymmetric Block Copolymers for Supramolecular Templating of Inorganic Nanospace Materials. *Small* **2015**, *11*, 1992−2002.
(326) Pang, X.; Zhao, L.; Han, W.; Xin, X.; Lin, Z. A general and robust strategy for the synthesis of nearly monodisperse colloidal nanocrystals. *Nat. Nanotechnol.* **2013**, *8*, 426−431.
(327) Liu, Q.; Liu, H.; Han, M.; Zhu, J.; Liang, Y.; Xu, Z.; Song, Y. Nanometer-Sized Nickel Hollow Spheres. *Adv. Mater.* **2005**, *17*, 1995−1999.
(328) Bastakoti, B. P.; Inuoe, M.; Yusa, S.-i.; Liao, S.-H.; Wu, K. C. W.; Nakashima, K.; Yamauchi, Y. A block copolymer micelle template for synthesis of hollow calcium phosphate nanospheres with excellent biocompatibility. *Chem. Commun.* **2012**, *48*, 6532−6534.
(329) Zhang, X.; Li, D. Metal-Compound-Induced Vesicles as Efficient Directors for Rapid Synthesis of Hollow Alloy Spheres. *Angew. Chem., Int. Ed.* **2006**, *45*, 5971−5974.
(330) Zhang, D.; Qi, L.; Ma, J.; Cheng, H. Synthesis of Submicrometer-Sized Hollow Silver Spheres in Mixed Polymer−Surfactant Solutions. *Adv. Mater.* **2002**, *14*, 1499−1502.
(331) Sasidharan, M.; Nakashima, K. Core−Shell−Corona Polymeric Micelles as a Versatile Template for Synthesis of Inorganic Hollow Nanospheres. *Acc. Chem. Res.* **2013**, *47*, 157−167.
(332) Sasidharan, M.; Gunawardhana, N.; Inoue, M.; Yusa, S.-i.; Yoshio, M.; Nakashima, K. La_2O_3 hollow nanospheres for high performance lithium-ion rechargeable batteries. *Chem. Commun.* **2012**, *48*, 3200−3202.
(333) Koh, H.-D.; Park, S.; Russell, T. P. Fabrication of Pt/Au Concentric Spheres from Triblock Copolymer. *ACS Nano* **2010**, *4*, 1124−1130.
(334) Sasidharan, M.; Chenrayan, S.; Kumari, V.; Bhaumik, A. Dual role of micelles as templates and reducing agent for the fabrication of catalytically active hollow silver nanospheres. *Chem. Commun.* **2014**, *51*, 733−736.
(335) Song, Y.; Garcia, R. M.; Dorin, R. M.; Wang, H.; Qiu, Y.; Shelnutt, J. A. Synthesis of Platinum Nanocages by Using Liposomes Containing Photocatalyst Molecules. *Angew. Chem., Int. Ed.* **2006**, *45*, 8126−8130.
(336) Zhou, Y. Lipid Nanotubes as Scaffold Toward Construction of One-Dimensional Nanostructures. *Sci. Adv. Mater.* **2010**, *2*, 359−364.
(337) Zhou, Y.; Shimizu, T. Lipid Nanotubes: A Unique Template To Create Diverse One-Dimensional Nanostructures. *Chem. Mater.* **2008**, *20*, 625−633.
(338) Matsui, H.; Pan, S.; Gologan, B.; Jonas, S. H. Bolaamphiphile Nanotube-Templated Metallized Wires. *J. Phys. Chem. B* **2000**, *104*, 9576−9579.
(339) Ji, Q.; Kamiya, S.; Jung, J.-H.; Shimizu, T. Self-assembly of glycolipids on silica nanotube templates yielding hybrid nanotubes with concentric organic and inorganic layers. *J. Mater. Chem.* **2005**, *15*, 743−748.
(340) Wang, Y.; Ma, S.; Su, Y.; Han, X. Palladium Nanotubes Formed by Lipid Tubule Templating and Their Application in Ethanol Electrocatalysis. *Chem.—Eur. J.* **2015**, *21*, 6084−6089.
(341) Yang, L.; Hu, C.; Wang, J.; Yang, Z.; Guo, Y.; Bai, Z.; Wang, K. Facile synthesis of hollow palladium/copper alloyed nanocubes for formic acid oxidation. *Chem. Commun.* **2011**, *47*, 8581−8583.
(342) Choi, B.-S.; Kim, S. M.; Gong, J.; Lee, Y. W.; Kang, S. W.; Lee, H.-S.; Park, J. Y.; Han, S. W. One-Pot Self-Templating Synthesis of Pt Hollow Nanostructures and Their Catalytic Properties for CO Oxidation. *Chem.—Eur. J.* **2014**, *20*, 11669−11674.
(343) Lim, B.; Xia, Y. N. Metal Nanocrystals with Highly Branched Morphologies. *Angew. Chem., Int. Ed.* **2011**, *50*, 76−85.
(344) Lim, B.; Jiang, M.; Yu, T.; Camargo, P. C.; Xia, Y. Nucleation and growth mechanisms for Pd-Pt bimetallic nanodendrites and their electrocatalytic properties. *Nano Res.* **2010**, *3*, 69−80.
(345) Wang, F.; Li, C.; Sun, L.-D.; Xu, C.-H.; Wang, J.; Yu, J. C.; Yan, C.-H. Porous Single-Crystalline Palladium Nanoparticles with High Catalytic Activities. *Angew. Chem., Int. Ed.* **2012**, *51*, 4872−4876.
(346) Wang, L.; Wang, H.; Nemoto, Y.; Yamauchi, Y. Rapid and Efficient Synthesis of Platinum Nanodendrites with High Surface Area by Chemical Reduction with Formic Acid. *Chem. Mater.* **2010**, *22*, 2835−2841.
(347) Wang, J.; Zhang, X.-B.; Wang, Z.-L.; Wang, L.-M.; Xing, W.; Liu, X. One-step and rapid synthesis of "clean" and monodisperse dendritic Pt nanoparticles and their high performance toward methanol oxidation and p-nitrophenol reduction. *Nanoscale* **2012**, *4*, 1549−1552.
(348) Sun, S. H.; Yang, D. Q.; Villers, D.; Zhang, G. X.; Sacher, E.; Dodelet, J. P. Template- and Surfactant-free Room Temperature Synthesis of Self-Assembled 3D Pt Nanoflowers from Single-Crystal Nanowires. *Adv. Mater.* **2008**, *20*, 571−574.
(349) Gao, Q.; Gao, M.-R.; Liu, J.-W.; Chen, M.-Y.; Cui, C.-H.; Li, H.-H.; Yu, S.-H. One-pot synthesis of branched palladium nanodendrites with superior electrocatalytic performance. *Nanoscale* **2013**, *5*, 3202−3207.
(350) Watt, J.; Cheong, S.; Toney, M. F.; Ingham, B.; Cookson, J.; Bishop, P. T.; Tilley, R. D. Ultrafast Growth of Highly Branched Palladium Nanostructures for Catalysis. *ACS Nano* **2009**, *4*, 396−402.
(351) Cheng, L.; Ma, C.; Yang, G.; You, H.; Fang, J. Hierarchical silver mesoparticles with tunable surface topographies for highly sensitive surface-enhanced Raman spectroscopy. *J. Mater. Chem. A* **2014**, *2*, 4534−4542.
(352) Ren, W.; Guo, S.; Dong, S.; Wang, E. A Simple Route for the Synthesis of Morphology-Controlled and SERS-Active Ag Dendrites with Near-Infrared Absorption. *J. Phys. Chem. C* **2011**, *115*, 10315−10320.
(353) Nehl, C. L.; Liao, H.; Hafner, J. H. Optical Properties of Star-Shaped Gold Nanoparticles. *Nano Lett.* **2006**, *6*, 683−688.
(354) Lee, Y.; Park, T. G. Facile Fabrication of Branched Gold Nanoparticles by Reductive Hydroxyphenol Derivatives. *Langmuir* **2011**, *27*, 2965−2971.
(355) Wang, L.; Yamauchi, Y. Controlled Aqueous Solution Synthesis of Platinum−Palladium Alloy Nanodendrites with Various Compositions Using Amphiphilic Triblock Copolymers. *Chem.—Asian J.* **2010**, *5*, 2493−2498.
(356) Zhou, Y.; Wang, D.; Li, Y. Pd and Au@Pd nanodendrites: a one-pot synthesis and their superior catalytic properties. *Chem. Commun.* **2014**, *50*, 6141−6144.
(357) Tzitzios, V.; Niarchos, D.; Gjoka, M.; Boukos, N.; Petridis, D. Synthesis and Characterization of 3D CoPt Nanostructures. *J. Am. Chem. Soc.* **2005**, *127*, 13756−13757.
(358) Guo, S.; Li, J.; Dong, S.; Wang, E. Three-Dimensional Pt-on-Au Bimetallic Dendritic Nanoparticle: One-Step, High-Yield Synthesis and Its Bifunctional Plasmonic and Catalytic Properties. *J. Phys. Chem. C* **2010**, *114*, 15337−15342.
(359) Hong, W.; Shang, C.; Wang, J.; Wang, E. Synthesis of dendritic PdAu nanoparticles with enhanced electrocatalytic activity. *Electrochem. Commun.* **2014**, *48*, 65−68.
(360) Cai, Z.; Kuang, Y.; Qi, X.; Wang, P.; Zhang, Y.; Zhang, Z.; Sun, X. Ultrathin branched PtFe and PtRuFe nanodendrites with enhanced electrocatalytic activity. *J. Mater. Chem. A* **2014**, *3*, 1182−1187.
(361) Wang, W.; Wang, D.; Liu, X.; Peng, Q.; Li, Y. Pt-Ni nanodendrites with high hydrogenation activity. *Chem. Commun.* **2013**, *49*, 2903−2905.
(362) Nosheen, F.; Zhang, Z.; Xiang, G.; Xu, B.; Yang, Y.; Saleem, F.; Xu, X.; Zhang, J.; Wang, X. Three-dimensional hierarchical Pt-Cu superstructures. *Nano Res.* **2014**, 1−7.

DOI: 10.1021/acs.chemrev.5b00255
Chem. Rev. XXXX, XXX, XXX−XXX

(363) Tan, Y.; Fan, J.; Chen, G.; Zheng, N.; Xie, Q. Au/Pt and Au/Pt_3Ni nanowires as self-supported electrocatalysts with high activity and durability for oxygen reduction. *Chem. Commun.* **2011**, *47*, 11624−11626.
(364) Mohanty, A.; Garg, N.; Jin, R. A Universal Approach to the Synthesis of Noble Metal Nanodendrites and Their Catalytic Properties. *Angew. Chem., Int. Ed.* **2010**, *49*, 4962−4966.
(365) Song, Y.; Yang, Y.; Medforth, C. J.; Pereira, E.; Singh, A. K.; Xu, H.; Jiang, Y.; Brinker, C. J.; van Swol, F.; Shelnutt, J. A. Controlled Synthesis of 2-D and 3-D Dendritic Platinum Nanostructures. *J. Am. Chem. Soc.* **2003**, *126*, 635−645.
(366) Lacroix, L.-M.; Gatel, C.; Arenal, R.; Garcia, C.; Lachaize, S.; Blon, T.; Warot-Fonrose, B.; Snoeck, E.; Chaudret, B.; Viau, G. Tuning Complex Shapes in Platinum Nanoparticles: From Cubic Dendrites to Fivefold Stars. *Angew. Chem., Int. Ed.* **2012**, *51*, 4690−4694.
(367) Huang, X.; Li, Y.; Chen, Y.; Zhou, E.; Xu, Y.; Zhou, H.; Duan, X.; Huang, Y. Palladium-Based Nanostructures with Highly Porous Features and Perpendicular Pore Channels as Enhanced Organic Catalysts. *Angew. Chem., Int. Ed.* **2013**, *52*, 2520−2524.
(368) Teng, X.; Liang, X.; Maksimuk, S.; Yang, H. Synthesis of Porous Platinum Nanoparticles. *Small* **2006**, *2*, 249−253.
(369) Wang, L.; Yamauchi, Y. Facile Synthesis of Three-Dimensional Dendritic Platinum Nanoelectrocatalyst. *Chem. Mater.* **2009**, *21*, 3562−3569.
(370) Peng, Z.; Yang, H. Designer platinum nanoparticles: Control of shape, composition in alloy, nanostructure and electrocatalytic property. *Nano Today* **2009**, *4*, 143−164.
(371) Feng, Y.; Liu, H.; Yang, J. Bimetallic nanodendrites via selective overgrowth of noble metals on multiply twinned Au seeds. *J. Mater. Chem. A* **2014**, *2*, 6130−6137.
(372) Hao, Y.; Yang, Y.; Hong, L.; Yuan, J.; Niu, L.; Gui, Y. Facile Preparation of Ultralong Dendritic PtIrTe Nanotubes and Their High Electrocatalytic Activity on Methanol Oxidation. *ACS Appl. Mater. Interfaces* **2014**, *6*, 21986−21994.
(373) Mahmoud; Tabor, C. E.; El-Sayed, M. A.; Ding, Y.; Wang, Z. L. A New Catalytically Active Colloidal Platinum Nanocatalyst: The Multiarmed Nanostar Single Crystal. *J. Am. Chem. Soc.* **2008**, *130*, 4590−4591.
(374) Lim, B.; Jiang, M.; Camargo, P. H. C.; Cho, E. C.; Tao, J.; Lu, X.; Zhu, Y.; Xia, Y. Pd-Pt Bimetallic Nanodendrites with High Activity for Oxygen Reduction. *Science* **2009**, *324*, 1302−1305.
(375) Peng, Z.; Yang, H. Synthesis and Oxygen Reduction Electrocatalytic Property of Pt-on-Pd Bimetallic Heteronanostructures. *J. Am. Chem. Soc.* **2009**, *131*, 7542−7543.
(376) DeSantis, C. J.; Peverly, A. A.; Peters, D. G.; Skrabalak, S. E. Octopods versus Concave Nanocrystals: Control of Morphology by Manipulating the Kinetics of Seeded Growth via Co-Reduction. *Nano Lett.* **2011**, *11*, 2164−2168.
(377) DeSantis, C. J.; Skrabalak, S. E. Core Values: Elucidating the Role of Seed Structure in the Synthesis of Symmetrically Branched Nanocrystals. *J. Am. Chem. Soc.* **2013**, *135*, 10−13.
(378) Weiner, R. G.; DeSantis, C. J.; Cardoso, M. B. T.; Skrabalak, S. E. Diffusion and Seed Shape: Intertwined Parameters in the Synthesis of Branched Metal Nanostructures. *ACS Nano* **2014**, *8*, 8625−8635.
(379) Weiner, R. G.; Skrabalak, S. E. Metal Dendrimers: Synthesis of Hierarchically Stellated Nanocrystals by Sequential Seed-Directed Overgrowth. *Angew. Chem., Int. Ed.* **2014**, *54*, 1181−1184.
(380) Yu, Y.; Zhang, Q.; Xie, J.; Lee, J. Y. Engineering the architectural diversity of heterogeneous metallic nanocrystals. *Nat. Commun.* **2013**, *4*, 1454.
(381) Wang, L.; Yamauchi, Y. Block Copolymer Mediated Synthesis of Dendritic Platinum Nanoparticles. *J. Am. Chem. Soc.* **2009**, *131*, 9152−9153.
(382) Wang, L.; Nemoto, Y.; Yamauchi, Y. Direct Synthesis of Spatially-Controlled Pt-on-Pd Bimetallic Nanodendrites with Superior Electrocatalytic Activity. *J. Am. Chem. Soc.* **2011**, *133*, 9674−9677.
(383) Wang, L.; Yamauchi, Y. Autoprogrammed Synthesis of Triple-Layered Au@Pd@Pt Core−Shell Nanoparticles Consisting of a Au@Pd Bimetallic Core and Nanoporous Pt Shell. *J. Am. Chem. Soc.* **2010**, *132*, 13636−13638.
(384) Wang, L.; Yamauchi, Y. Strategic Synthesis of Trimetallic Au@Pd@Pt Core−Shell Nanoparticles from Poly(vinylpyrrolidone)-Based Aqueous Solution toward Highly Active Electrocatalysts. *Chem. Mater.* **2011**, *23*, 2457−2465.
(385) Xia, B. Y.; Ng, W. T.; Wu, H. B.; Wang, X.; Lou, X. W. Self-Supported Interconnected Pt Nanoassemblies as Highly Stable Electrocatalysts for Low-Temperature Fuel Cells. *Angew. Chem., Int. Ed.* **2012**, *124*, 7325−7328.
(386) Xia, B. Y.; Wu, H. B.; Li, N.; Yan, Y.; Lou, X. W.; Wang, X. One-Pot Synthesis of Pt−Co Alloy Nanowire Assemblies with Tunable Composition and Enhanced Electrocatalytic Properties. *Angew. Chem., Int. Ed.* **2015**, *54*, 3797−3801.
(387) Chen, S.; Su, H.; Wang, Y.; Wu, W.; Zeng, J. Size-Controlled Synthesis of Platinum−Copper Hierarchical Trigonal Bipyramid Nanoframes. *Angew. Chem., Int. Ed.* **2014**, *54*, 108−113.
(388) Kuang, Y.; Cai, Z.; Zhang, Y.; He, D.; Yan, X.; Bi, Y.; Li, Y.; Li, Z.; Sun, X. Ultrathin Dendritic Pt_3Cu Triangular Pyramid Caps with Enhanced Electrocatalytic Activity. *ACS Appl. Mater. Interfaces* **2014**, *6*, 17748−17752.
(389) Teng, X.; Maksimuk, S.; Frommer, S.; Yang, H. Three-Dimensional PtRu Nanostructures. *Chem. Mater.* **2006**, *19*, 36−41.
(390) Viswanath, B.; Patra, S.; Munichandraiah, N.; Ravishankar, N. Nanoporous Pt with High Surface Area by Reaction-Limited Aggregation of Nanoparticles. *Langmuir* **2009**, *25*, 3115−3121.
(391) Zhang, Q.; Liu, S.-J.; Yu, S.-H. Recent advances in oriented attachment growth and synthesis of functional materials: concept, evidence, mechanism, and future. *J. Mater. Chem.* **2009**, *19*, 191−207.
(392) You, H.; Yang, S.; Ding, B.; Yang, H. Synthesis of colloidal metal and metal alloy nanoparticles for electrochemical energy applications. *Chem. Soc. Rev.* **2013**, *42*, 2880−2904.
(393) Ortiz, N.; Skrabalak, S. E. Manipulating Local Ligand Environments for the Controlled Nucleation of Metal Nanoparticles and their Assembly into Nanodendrites. *Angew. Chem., Int. Ed.* **2012**, *51*, 11757−11761.
(394) Jung, N.; Chung, D. Y.; Ryu, J.; Yoo, S. J.; Sung, Y.-E. Pt-based nanoarchitecture and catalyst design for fuel cell applications. *Nano Today* **2014**, *9*, 433−456.
(395) Bianchini, C.; Shen, P. K. Palladium-Based Electrocatalysts for Alcohol Oxidation in Half Cells and in Direct Alcohol Fuel Cells. *Chem. Rev.* **2009**, *109*, 4183−4206.
(396) Shao, Y.; Kou, R.; Wang, J.; Viswanathan, V. V.; Kwak, J. H.; Liu, J.; Wang, Y.; Lin, Y. The influence of the electrochemical stressing (potential step and potential-static holding) on the degradation of polymer electrolyte membrane fuel cell electrocatalysts. *J. Power Sources* **2008**, *185*, 280−286.
(397) Shao, Y.; Liu, J.; Wang, Y.; Lin, Y. Novel catalyst support materials for PEM fuel cells: current status and future prospects. *J. Mater. Chem.* **2009**, *19*, 46−59.
(398) Zhang, S.; Shao, Y.; Yin, G.; Lin, Y. Recent progress in nanostructured electrocatalysts for PEM fuel cells. *J. Mater. Chem. A* **2013**, *1*, 4631−4641.
(399) Cui, C.-H.; Yu, S.-H. Engineering Interface and Surface of Noble Metal Nanoparticle Nanotubes toward Enhanced Catalytic Activity for Fuel Cell Applications. *Acc. Chem. Res.* **2013**, *46*, 1427−1437.
(400) Zhang, H.; Jin, M.; Xia, Y. Enhancing the catalytic and electrocatalytic properties of Pt-based catalysts by forming bimetallic nanocrystals with Pd. *Chem. Soc. Rev.* **2012**, *41*, 8035−8049.
(401) Guo, S.; Dong, S.; Wang, E. Constructing Carbon Nanotube/Pt Nanoparticle Hybrids Using an Imidazolium-Salt-Based Ionic Liquid as a Linker. *Adv. Mater.* **2010**, *22*, 1269−1272.
(402) Xia, B. Y.; Wu, H. B.; Yan, Y.; Lou, X. W.; Wang, X. Ultrathin and Ultralong Single-Crystal Platinum Nanowire Assemblies with Highly Stable Electrocatalytic Activity. *J. Am. Chem. Soc.* **2013**, *135*, 9480−9485.

DOI: 10.1021/acs.chemrev.5b00255
Chem. Rev. XXXX, XXX, XXX−XXX

(403) Zuo, Y.; Cai, K.; Wu, L.; Li, T.; Lv, Z.; Liu, J.; Shao, K.; Han, H. Spiny-porous platinum nanotubes with enhanced electrocatalytic activity for methanol oxidation. *J. Mater. Chem. A* **2015**, *3*, 1388−1391.
(404) Rauber, M.; Alber, I.; Müller, S.; Neumann, R.; Picht, O.; Roth, C.; Schökel, A.; Toimil-Molares, M. E.; Ensinger, W. Highly-Ordered Supportless Three-Dimensional Nanowire Networks with Tunable Complexity and Interwire Connectivity for Device Integration. *Nano Lett.* **2011**, *11*, 2304−2310.
(405) Alia, S. M.; Zhang, G.; Kisailus, D.; Li, D.; Gu, S.; Jensen, K.; Yan, Y. Porous Platinum Nanotubes for Oxygen Reduction and Methanol Oxidation Reactions. *Adv. Funct. Mater.* **2010**, *20*, 3742−3746.
(406) Zhang, C.; Yang, H.; Sun, T.; Shan, N.; Chen, J.; Xu, L.; Yan, Y. Synthesis of three-dimensionally ordered macro-/mesoporous Pt with high electrocatalytic activity by a dual-templating approach. *J. Power Sources* **2014**, *245*, 579−582.
(407) Gong, M.; Fu, G.; Chen, Y.; Tang, Y.; Lu, T. Autocatalysis and Selective Oxidative Etching Induced Synthesis of Platinum−Copper Bimetallic Alloy Nanodendrites Electrocatalysts. *ACS Appl. Mater. Interfaces* **2014**, *6*, 7301−7308.
(408) Ding, L.-X.; Li, G.-R.; Wang, Z.-L.; Liu, Z.-Q.; Liu, H.; Tong, Y.-X. Porous Ni@Pt Core-Shell Nanotube Array Electrocatalyst with High Activity and Stability for Methanol Oxidation. *Chem.—Eur. J.* **2012**, *18*, 8386−8391.
(409) Cui, C.-H.; Li, H.-H.; Yu, S.-H. Large scale restructuring of porous Pt-Ni nanoparticle tubes for methanol oxidation: A highly reactive, stable, and restorable fuel cell catalyst. *Chem. Sci.* **2011**, *2*, 1611−1614.
(410) Wang, A.-L.; Xu, H.; Feng, J.-X.; Ding, L.-X.; Tong, Y.-X.; Li, G.-R. Design of Pd/PANI/Pd Sandwich-Structured Nanotube Array Catalysts with Special Shape Effects and Synergistic Effects for Ethanol Electrooxidation. *J. Am. Chem. Soc.* **2013**, *135*, 10703−10709.
(411) Antolini, E. Catalysts for direct ethanol fuel cells. *J. Power Sources* **2007**, *170*, 1−12.
(412) Guo, S.; Dong, S.; Wang, E. Pt/Pd bimetallic nanotubes with petal-like surfaces for enhanced catalytic activity and stability towards ethanol electrooxidation. *Energy Environ. Sci.* **2010**, *3*, 1307−1310.
(413) Wu, H.; Li, H.; Zhai, Y.; Xu, X.; Jin, Y. Facile Synthesis of Free-Standing Pd-Based Nanomembranes with Enhanced Catalytic Performance for Methanol/Ethanol Oxidation. *Adv. Mater.* **2012**, *24*, 1594−1597.
(414) Lv, J.-J.; Zheng, J.-N.; Li, S.-S.; Chen, L.-L.; Wang, A.-J.; Feng, J.-J. Facile synthesis of Pt-Pd nanodendrites and their superior electrocatalytic activity. *J. Mater. Chem. A* **2014**, *2*, 4384−4390.
(415) Lv, J.-J.; Mei, L.-P.; weng, x.; Wang, A.-J.; Chen, L.-L.; Liu, X.-F.; Feng, J.-J. Facile synthesis of three-dimensional Pt-Pd alloyed multipods with enhanced electrocatalytic activity and stability for ethylene glycol oxidation. *Nanoscale* **2015**, *7*, 5699−5705.
(416) Wang, A.-L.; He, X.-J.; Lu, X.-F.; Xu, H.; Tong, Y.-X.; Li, G.-R. Palladium−Cobalt Nanotube Arrays Supported on Carbon Fiber Cloth as High-Performance Flexible Electrocatalysts for Ethanol Oxidation. *Angew. Chem., Int. Ed.* **2015**, *54*, 3669−3673.
(417) Hong, W.; Wang, J.; Wang, E. Synthesis of porous PdAg nanoparticles with enhanced electrocatalytic activity. *Electrochem. Commun.* **2014**, *40*, 63−66.
(418) Antolini, E. Palladium in fuel cell catalysis. *Energy Environ. Sci.* **2009**, *2*, 915−931.
(419) Yu, X.; Pickup, P. G. Recent advances in direct formic acid fuel cells (DFAFC). *J. Power Sources* **2008**, *182*, 124−132.
(420) Zhang, S.; Shao, Y.; Yin, G.; Lin, Y. Facile synthesis of PtAu alloy nanoparticles with high activity for formic acid oxidation. *J. Power Sources* **2010**, *195*, 1103−1106.
(421) Zhang, S.; Shao, Y.; Yin, G.; Lin, Y. Electrostatic Self-Assembly of a Pt-around-Au Nanocomposite with High Activity towards Formic Acid Oxidation. *Angew. Chem., Int. Ed.* **2010**, *49*, 2211−2214.
(422) Zhang, S.; Shao, Y.; Liao, H.-g.; Liu, J.; Aksay, I. A.; Yin, G.; Lin, Y. Graphene Decorated with PtAu Alloy Nanoparticles: Facile Synthesis and Promising Application for Formic Acid Oxidation. *Chem. Mater.* **2011**, *23*, 1079−1081.
(423) Chen, D.; Cui, P.; He, H.; Liu, H.; Yang, J. Highly catalytic hollow palladium nanoparticles derived from silver@silver−palladium core−shell nanostructures for the oxidation of formic acid. *J. Power Sources* **2014**, *272*, 152−159.
(424) Adams, B. D.; Asmussen, R. M.; Ostrom, C. K.; Chen, A. Synthesis and Comparative Study of Nanoporous Palladium-Based Bimetallic Catalysts for Formic Acid Oxidation. *J. Phys. Chem. C* **2014**, *118*, 29903−29910.
(425) Gong, M.; Li, F.; Yao, Z.; Zhang, S.; Dong, J.; Chen, Y.; Tang, Y. Highly active and durable platinum-lead bimetallic alloy nanoflowers for formic acid electrooxidation. *Nanoscale* **2015**, *7*, 4894−4899.
(426) Debe, M. K. Electrocatalyst approaches and challenges for automotive fuel cells. *Nature* **2012**, *486*, 43−51.
(427) Zhu, C.; Dong, S. Recent progress in graphene-based nanomaterials as advanced electrocatalysts towards oxygen reduction reaction. *Nanoscale* **2013**, *5*, 1753−1767.
(428) Wu, J.; Yang, H. Platinum-Based Oxygen Reduction Electrocatalysts. *Acc. Chem. Res.* **2013**, *46*, 1848−1857.
(429) Chung, H. T.; Won, J. H.; Zelenay, P. Active and stable carbon nanotube/nanoparticle composite electrocatalyst for oxygen reduction. *Nat. Commun.* **2013**, *4*, 1922.
(430) van der Vliet, D. F.; Wang, C.; Tripkovic, D.; Strmcnik, D.; Zhang, X. F.; Debe, M. K.; Atanasoski, R. T.; Markovic, N. M.; Stamenkovic, V. R. Mesostructured thin films as electrocatalysts with tunable composition and surface morphology. *Nat. Mater.* **2012**, *11*, 1051−1058.
(431) Guo, S.; Li, D.; Zhu, H.; Zhang, S.; Markovic, N. M.; Stamenkovic, V. R.; Sun, S. FePt and CoPt Nanowires as Efficient Catalysts for the Oxygen Reduction Reaction. *Angew. Chem., Int. Ed.* **2013**, *52*, 3465−3468.
(432) Zhang, J.; Yang, H.; Fang, J.; Zou, S. Synthesis and Oxygen Reduction Activity of Shape-Controlled Pt_3Ni Nanopolyhedra. *Nano Lett.* **2010**, *10*, 638−644.
(433) Guo, S.; Zhang, S.; Su, D.; Sun, S. Seed-Mediated Synthesis of Core/Shell FePtM/FePt (M = Pd, Au) Nanowires and Their Electrocatalysis for Oxygen Reduction Reaction. *J. Am. Chem. Soc.* **2013**, *135*, 13879−13884.
(434) Guo, S.; Zhang, X.; Zhu, W.; He, K.; Su, D.; Mendoza-Garcia, A.; Ho, S. F.; Lu, G.; Sun, S. Nanocatalyst Superior to Pt for Oxygen Reduction Reactions: The Case of Core/Shell Ag(Au)/CuPd Nanoparticles. *J. Am. Chem. Soc.* **2014**, *136*, 15026−15033.
(435) Kou, R.; Shao, Y.; Mei, D.; Nie, Z.; Wang, D.; Wang, C.; Viswanathan, V. V.; Park, S.; Aksay, I. A.; Lin, Y.; et al. Stabilization of Electrocatalytic Metal Nanoparticles at Metal−Metal Oxide−Graphene Triple Junction Points. *J. Am. Chem. Soc.* **2011**, *133*, 2541−2547.
(436) Guo, S.; Sun, S. FePt Nanoparticles Assembled on Graphene as Enhanced Catalyst for Oxygen Reduction Reaction. *J. Am. Chem. Soc.* **2012**, *134*, 2492−2495.
(437) Wang, H.-H.; Zhou, Z.-Y.; Yuan, Q.; Tian, N.; Sun, S.-G. Pt nanoparticle netlike-assembly as highly durable and highly active electrocatalyst for oxygen reduction reaction. *Chem. Commun.* **2011**, *47*, 3407−3409.
(438) Sun, S.; Zhang, G.; Geng, D.; Chen, Y.; Li, R.; Cai, M.; Sun, X. A Highly Durable Platinum Nanocatalyst for Proton Exchange Membrane Fuel Cells: Multiarmed Starlike Nanowire Single Crystal. *Angew. Chem., Int. Ed.* **2011**, *50*, 422−426.
(439) Koenigsmann, C.; Zhou, W.-p.; Adzic, R. R.; Sutter, E.; Wong, S. S. Size-Dependent Enhancement of Electrocatalytic Performance in Relatively Defect-Free, Processed Ultrathin Platinum Nanowires. *Nano Lett.* **2010**, *10*, 2806−2811.
(440) Stamenkovic, V. R.; Fowler, B.; Mun, B. S.; Wang, G.; Ross, P. N.; Lucas, C. A.; Marković, N. M. Improved Oxygen Reduction Activity on $Pt_3Ni(111)$ via Increased Surface Site Availability. *Science* **2007**, *315*, 493−497.
(441) GreeleyJ; Stephens, I. E. L.; Bondarenko, A. S.; Johansson, T. P.; Hansen, H. A.; Jaramillo, T. F.; RossmeislJ; ChorkendorffI;

DOI: 10.1021/acs.chemrev.5b00255
Chem. Rev. XXXX, XXX, XXX−XXX

Nørskov, J. K. Alloys of platinum and early transition metals as oxygen reduction electrocatalysts. *Nat. Chem.* **2009**, *1*, 552−556.
(442) Zhang, C.; Sandorf, W.; Peng, Z. Octahedral Pt_2CuNi Uniform Alloy Nanoparticle Catalyst with High Activity and Promising Stability for Oxygen Reduction Reaction. *ACS Catal.* **2015**, 2296−2300.
(443) Wu, J.; Zhang, J.; Peng, Z.; Yang, S.; Wagner, F. T.; Yang, H. Truncated Octahedral Pt_3Ni Oxygen Reduction Reaction Electrocatalysts. *J. Am. Chem. Soc.* **2010**, *132*, 4984−4985.
(444) Zheng, J.-N.; He, L.-L.; Chen, C.; Wang, A.-J.; Ma, K.-F.; Feng, J.-J. One-pot synthesis of platinum3cobalt nanoflowers with enhanced oxygen reduction and methanol oxidation. *J. Power Sources* **2014**, *268*, 744−751.
(445) Wu, J.; Gross, A.; Yang, H. Shape and Composition-Controlled Platinum Alloy Nanocrystals Using Carbon Monoxide as Reducing Agent. *Nano Lett.* **2011**, *11*, 798−802.
(446) Huang, X.; Zhu, E.; Chen, Y.; Li, Y.; Chiu, C.-Y.; Xu, Y.; Lin, Z.; Duan, X.; Huang, Y. A Facile Strategy to Pt_3Ni Nanocrystals with Highly Porous Features as an Enhanced Oxygen Reduction Reaction Catalyst. *Adv. Mater.* **2013**, *25*, 2974−2979.
(447) Liu, L.; Pippel, E. Low-Platinum-Content Quaternary PtCuCoNi Nanotubes with Markedly Enhanced Oxygen Reduction Activity. *Angew. Chem., Int. Ed.* **2011**, *50*, 2729−2733.
(448) Lu, Y.; Jiang, Y.; Chen, W. PtPd porous nanorods with enhanced electrocatalytic activity and durability for oxygen reduction reaction. *Nano Energy* **2013**, *2*, 836−844.
(449) Fu, G.; Wu, K.; Lin, J.; Tang, Y.; Chen, Y.; Zhou, Y.; Lu, T. One-Pot Water-Based Synthesis of Pt−Pd Alloy Nanoflowers and Their Superior Electrocatalytic Activity for the Oxygen Reduction Reaction and Remarkable Methanol-Tolerant Ability in Acid Media. *J. Phys. Chem. C* **2013**, *117*, 9826−9834.
(450) Guo, S.; Zhang, S.; Sun, S. Tuning Nanoparticle Catalysis for the Oxygen Reduction Reaction. *Angew. Chem., Int. Ed.* **2013**, *52*, 8526−8544.
(451) Liao, H.; Hou, Y. Liquid-Phase Templateless Synthesis of Pt-on-$Pd_{0.85}Bi_{0.15}$ Nanowires and PtPdBi Porous Nanoparticles with Superior Electrocatalytic Activity. *Chem. Mater.* **2013**, *25*, 457−465.
(452) Qiu, H. J.; Xu, H.-T.; Liu, L.; Wang, Y. Correlation of the structure and applications of dealloyed nanoporous metals in catalysis and energy conversion/storage. *Nanoscale* **2015**, *7*, 386−400.
(453) Xu, C.; Zhang, H.; Hao, Q.; Duan, H. A Hierarchical Nanoporous PtCu Alloy as an Oxygen-Reduction Reaction Electrocatalyst with High Activity and Durability. *ChemPlusChem* **2014**, *79*, 107−113.
(454) Liu, X.-J.; Cui, C.-H.; Li, H.-H.; Lei, Y.; Zhuang, T.-T.; Sun, M.; Arshad, M. N.; Albar, H. A. H. M.; Sobahi, T.; Yu, S.-H. Hollow ternary PtPdCu nanoparticles: a superior and durable cathodic electrocatalyst. *Chem. Sci.* **2015**, *6*, 3038−3043.
(455) Wang, C.; et al. Design and Synthesis of Bimetallic Electrocatalyst with Multilayered Pt-Skin Surfaces. *J. Am. Chem. Soc.* **2011**, *133*, 14396−14403.
(456) Shui, J.-l.; Chen, C.; Li, J. C. M. Evolution of Nanoporous Pt−Fe Alloy Nanowires by Dealloying and their Catalytic Property for Oxygen Reduction Reaction. *Adv. Funct. Mater.* **2011**, *21*, 3357−3362.
(457) Gan, L.; Heggen, M.; O'Malley, R.; Theobald, B.; Strasser, P. Understanding and Controlling Nanoporosity Formation for Improving the Stability of Bimetallic Fuel Cell Catalysts. *Nano Lett.* **2013**, *13*, 1131−1138.
(458) Chen, C.; Kang, Y.; Huo, Z.; Zhu, Z.; Huang, W.; Xin, H. L.; Snyder, J. D.; Li, D.; Herron, J. A.; Mavrikakis, M.; et al. Highly Crystalline Multimetallic Nanoframes with Three-Dimensional Electrocatalytic Surfaces. *Science* **2014**, *343*, 1339−1343.
(459) Snyder, J.; Fujita, T.; Chen, M. W.; Erlebacher, J. Oxygen reduction in nanoporous metal−ionic liquid composite electrocatalysts. *Nat. Mater.* **2010**, *9*, 904−907.
(460) Zhu, C.; Yang, G.; Li, H.; Du, D.; Lin, Y. Electrochemical Sensors and Biosensors Based on Nanomaterials and Nanostructures. *Anal. Chem.* **2014**, *87*, 230−249.
(461) Zhu, C.; Dong, S. Energetic Graphene-Based Electrochemical Analytical Devices in Nucleic Acid, Protein and Cancer Diagnostics and Detection. *Electroanalysis* **2014**, *26*, 14−29.
(462) Walcarius, A.; Minteer, S. D.; Wang, J.; Lin, Y.; Merkoci, A. Nanomaterials for bio-functionalized electrodes: recent trends. *J. Mater. Chem. B* **2013**, *1*, 4878−4908.
(463) Lei, J.; Ju, H. Signal amplification using functional nanomaterials for biosensing. *Chem. Soc. Rev.* **2012**, *41*, 2122−2134.
(464) Du, D.; Zou, Z.; Shin, Y.; Wang, J.; Wu, H.; Engelhard, M. H.; Liu, J.; Aksay, I. A.; Lin, Y. Sensitive Immunosensor for Cancer Biomarker Based on Dual Signal Amplification Strategy of Graphene Sheets and Multienzyme Functionalized Carbon Nanospheres. *Anal. Chem.* **2010**, *82*, 2989−2995.
(465) Ghanem, M. A. Electrocatalytic activity and simultaneous determination of catechol and hydroquinone at mesoporous platinum electrode. *Electrochem. Commun.* **2007**, *9*, 2501−2506.
(466) Evans, S. A. G.; Elliott, J. M.; Andrews, L. M.; Bartlett, P. N.; Doyle, P. J.; Denuault, G. Detection of Hydrogen Peroxide at Mesoporous Platinum Microelectrodes. *Anal. Chem.* **2002**, *74*, 1322−1326.
(467) Liu, L.; Scholz, R.; Pippel, E.; Gosele, U. Microstructure, electrocatalytic and sensing properties of nanoporous $Pt_{46}Ni_{54}$ alloy nanowires fabricated by mild dealloying. *J. Mater. Chem.* **2010**, *20*, 5621−5627.
(468) Ke, X.; Xu, Y.; Yu, C.; Zhao, J.; Cui, G.; Higgins, D.; Li, Q.; Wu, G. Nanoporous gold on three-dimensional nickel foam: An efficient hybrid electrode for hydrogen peroxide electroreduction in acid media. *J. Power Sources* **2014**, *269*, 461−465.
(469) Huan, T. N.; Ganesh, T.; Kim, K. S.; Kim, S.; Han, S.-H.; Chung, H. A three-dimensional gold nanodendrite network porous structure and its application for an electrochemical sensing. *Biosens. Bioelectron.* **2011**, *27*, 183−186.
(470) Chen, C.; Xie, Q.; Yang, D.; Xiao, H.; Fu, Y.; Tan, Y.; Yao, S. Recent advances in electrochemical glucose biosensors: a review. *RSC Adv.* **2013**, *3*, 4473−4491.
(471) Meng, L.; Jin, J.; Yang, G.; Lu, T.; Zhang, H.; Cai, C. Nonenzymatic Electrochemical Detection of Glucose Based on Palladium−Single-Walled Carbon Nanotube Hybrid Nanostructures. *Anal. Chem.* **2009**, *81*, 7271−7280.
(472) Cao, X.; Wang, N.; Jia, S.; Shao, Y. Detection of Glucose Based on Bimetallic PtCu Nanochains Modified Electrodes. *Anal. Chem.* **2013**, *85*, 5040−5046.
(473) Zhang, Y.; Xu, F.; Sun, Y.; Guo, C.; Cui, K.; Shi, Y.; Wen, Z.; Li, Z. Seed-Mediated Synthesis of Au Nanocages and Their Electrocatalytic Activity towards Glucose Oxidation. *Chem.—Eur. J.* **2010**, *16*, 9248−9256.
(474) Chou, C.-H.; Chen, J.-C.; Tai, C.-C.; Sun, I. W.; Zen, J.-M. A Nonenzymatic Glucose Sensor Using Nanoporous Platinum Electrodes Prepared by Electrochemical Alloying/Dealloying in a Water-Insensitive Zinc Chloride-1-Ethyl-3-Methylimidazolium Chloride Ionic Liquid. *Electroanalysis* **2008**, *20*, 771−775.
(475) Shen, Q.; Jiang, L.; Zhang, H.; Min, Q.; Hou, W.; Zhu, J.-J. Three-dimensional Dendritic Pt Nanostructures: Sonoelectrochemical Synthesis and Electrochemical Applications. *J. Phys. Chem. C* **2008**, *112*, 16385−16392.
(476) Niu, X.; Lan, M.; Chen, C.; Zhao, H. Nonenzymatic electrochemical glucose sensor based on novel Pt−Pd nanoflakes. *Talanta* **2012**, *99*, 1062−1067.
(477) Wang, Y.; Shao, Y.; Matson, D. W.; Li, J.; Lin, Y. Nitrogen-Doped Graphene and Its Application in Electrochemical Biosensing. *ACS Nano* **2010**, *4*, 1790−1798.
(478) Zhai, D.; Liu, B.; Shi, Y.; Pan, L.; Wang, Y.; Li, W.; Zhang, R.; Yu, G. Highly Sensitive Glucose Sensor Based on Pt Nanoparticle/Polyaniline Hydrogel Heterostructures. *ACS Nano* **2013**, *7*, 3540−3546.
(479) Szamocki, R.; Reculusa, S.; Ravaine, S.; Bartlett, P. N.; Kuhn, A.; Hempelmann, R. Tailored Mesostructuring and Biofunctionalization of Gold for Increased Electroactivity. *Angew. Chem., Int. Ed.* **2006**, *45*, 1317−1321.

DOI: 10.1021/acs.chemrev.5b00255
Chem. Rev. XXXX, XXX, XXX−XXX

(480) Gamero, M.; Pariente, F.; Lorenzo, E.; Alonso, C. Nanostructured rough gold electrodes for the development of lactate oxidase-based biosensors. *Biosens. Bioelectron.* **2010**, *25*, 2038−2044.
(481) Chen, L. Y.; Fujita, T.; Chen, M. W. Biofunctionalized nanoporous gold for electrochemical biosensors. *Electrochim. Acta* **2012**, *67*, 1−5.
(482) Qiu, H.; Xue, L.; Ji, G.; Zhou, G.; Huang, X.; Qu, Y.; Gao, P. Enzyme-modified nanoporous gold-based electrochemical biosensors. *Biosens. Bioelectron.* **2009**, *24*, 3014−3018.
(483) Xu, C.; Liu, Y.; Su, F.; Liu, A.; Qiu, H. Nanoporous PtAg and PtCu alloys with hollow ligaments for enhanced electrocatalysis and glucose biosensing. *Biosens. Bioelectron.* **2011**, *27*, 160−166.
(484) Ahangar, L. E.; Mehrgardi, M. A. Nanoporous gold electrode as a platform for the construction of an electrochemical DNA hybridization biosensor. *Biosens. Bioelectron.* **2012**, *38*, 252−257.
(485) Chen, X.; Wang, Y.; Zhou, J.; Yan, W.; Li, X.; Zhu, J.-J. Electrochemical Impedance Immunosensor Based on Three-Dimensionally Ordered Macroporous Gold Film. *Anal. Chem.* **2008**, *80*, 2133−2140.
(486) Zheng, T.; Zhang, Q.; Feng, S.; Zhu, J.-J.; Wang, Q.; Wang, H. Robust Nonenzymatic Hybrid Nanoelectrocatalysts for Signal Amplification toward Ultrasensitive Electrochemical Cytosensing. *J. Am. Chem. Soc.* **2014**, *136*, 2288−2291.

DOI: 10.1021/acs.chemrev.5b00255
Chem. Rev. XXXX, XXX, XXX−XXX